LATTICE SOLITONS
IN CUBIC-QUINTIC MEDIA

Ph.D. THESIS

İzzet GÖKSEL

Department of Mathematical Engineering

Mathematical Engineering Programme

JULY 2017

ISTANBUL TECHNICAL UNIVERSITY ★ GRADUATE SCHOOL OF SCIENCE ENGINEERING AND TECHNOLOGY

**LATTICE SOLITONS
IN CUBIC-QUINTIC MEDIA**

Ph.D. THESIS

İzzet GÖKSEL
(509112074)

Department of Mathematical Engineering

Mathematical Engineering Programme

Thesis Advisor: Assoc. Prof. Dr. İlkay BAKIRTAŞ AKAR
Co-advisor: Prof. Dr. Nalan ANTAR

JULY 2017

İSTANBUL TEKNİK ÜNİVERSİTESİ ★ FEN BİLİMLERİ ENSTİTÜSÜ

KÜBİK-KUİNTİK ORTAMLARDA
KAFES SOLİTONLARI

DOKTORA TEZİ

İzzet GÖKSEL
(509112074)

Matematik Mühendisliği Anabilim Dalı

Matematik Mühendisliği Programı

Tez Danışmanı: Doç. Dr. İlkay BAKIRTAŞ AKAR
Eş Danışman: Prof. Dr. Nalan ANTAR

TEMMUZ 2017

İzzet GÖKSEL, a Ph.D. student of ITU Graduate School of Science Engineering and Technology 509112074 successfully defended the thesis entitled "LATTICE SOLITONS IN CUBIC-QUINTIC MEDIA", which he prepared after fulfilling the requirements specified in the associated legislations, before the jury whose signatures are below.

Thesis Advisor :	**Assoc. Prof. Dr. İlkay BAKIRTAŞ AKAR** Istanbul Technical University	....
Co-advisor :	**Prof. Dr. Nalan ANTAR** Istanbul Technical University	....
Jury Members :	**Prof. Dr. Mevlüt TEYMÜR** Istanbul Technical University	....
	Prof. Dr. Hilmi DEMİRAY Işık University	....
	Assis. Prof. Dr. Cihan BAYINDIR Işık University	....
	Assoc. Prof. Dr. Semra AHMETOLAN Istanbul Technical University	....
	Assis. Prof. Dr. Güler GAYGUSUZOĞLU Namık Kemal University	....

Date of Submission : 30 June 2017
Date of Defense : 13 July 2017

To my sister Gözde,

FOREWORD

First and foremost, I would like to express my gratitude to Assoc. Prof. Dr. İlkay Bakırtaş Akar and Prof. Dr. Nalan Antar for they are my teachers, advisors, colleagues and maybe most importantly someone like family. In the course of my graduate studies, we have studied together, worked together, travelled together and above all, academically grown together. This thesis is the outcome of our hard work.

Besides my advisors, I would like to individually thank all my jury members for their time, attention and guidance. I have learned a lot from them; in particular, during my thesis progress report presentations.

I wish to send my greetings to Assoc. Prof. Dr. Boaz Ilan for the research and teaching opportunity at the University of California during the last year of my graduate studies. I am glad for our scientific connection across the globe.

I would also like to thank my colleague Mahmut Bağcı for his collaboration. I guess, we have mastered solitons during our concurrent graduate studies under the supervision of our common advisors.

I am tempted to thank everyone who has shared their knowledge with me.

Last but not least, I wish to thank my family for their love and support.

I dedicate this thesis to my sister Gözde.

July 2017 İzzet GÖKSEL
(Engineer)

TABLE OF CONTENTS

ABBREVIATIONS

(1+1)D   **:** One Plus One Dimensional
(2+1)D   **:** Two Plus One Dimensional
1D   **:** One Dimensional
2D   **:** Two Dimensional
CQNLS   **:** Cubic-Quintic Nonlinear Schrödinger
Eq.   **:** Equation
IC   **:** Initial Condition
NLS   **:** Nonlinear Schrödinger
ODE   **:** Ordinary Differential Equation
PDE   **:** Partial Differential Equation
$\mathcal{PT}$ **:** Parity-Time

LATTICE SOLITONS
IN CUBIC-QUINTIC MEDIA

SUMMARY

Solitons are localized nonlinear waves and occur in many branches of physics. Their properties have provided fundamental understanding of complex nonlinear systems. There has been considerable interest in studying solitons in lattices that can be generated in nonlinear optical materials. In nonlinear optics, the propagation of electromagnetic waves in photorefractive materials with intrinsic nonlinear resonance can be modelled by the nonlinear Schrödinger (NLS) equation containing both cubic and quintic terms. Recently, particular attention is drawn to nonlinear waves in parity-time ($\mathcal{PT}$) symmetric potentials.

In this thesis, the existence and stability properties of optical solitons on periodic and certain $\mathcal{PT}$-symmetric lattices are investigated. The governing equation for the physical model is the cubic-quintic nonlinear Schrödinger (CQNLS) equation with an external potential:

$$iu_z + \Delta u + \alpha |u|^2 u + \beta |u|^4 u + Vu = 0 . \tag{1}$$

Here, u corresponds to the complex-valued, slowly varying amplitude of the electric field in the x (or xy) plane propagating in the z-direction, Δu corresponds to diffraction, V is an external optical potential (i.e. lattice), α and β are coefficients of the cubic and quintic nonlinearities, respectively.

First, solutions to the CQNLS equation with two dimensional periodic potential V_N for $N = 4$

$$V_N(x,y) = \frac{V_0}{N^2} \left| \sum_{n=0}^{N-1} e^{i\left(x\cos\frac{2\pi n}{N} + y\cos\frac{2\pi n}{N}\right)} \right|^2 , \tag{2}$$

one dimensional $\mathcal{PT}$-symmetric potential

$$V_{\mathcal{PT}}(x) = V(x) + iW(x) = [V_0 \operatorname{sech}^2(x) + V_1 \operatorname{sech}^4(x)] + i[W_0 \operatorname{sech}(x)\tanh(x)] \tag{3}$$

and two dimensional $\mathcal{PT}$-symmetric potential

$$
\begin{aligned}
V_{\mathcal{PT}}(x,y) &= V(x,y) + iW(x,y) \\
&= \{V_0 \operatorname{sech}^2(x)\operatorname{sech}^2(y) + V_1 \operatorname{sech}^4(x)\operatorname{sech}^4(y) \\
&\quad + V_2[\operatorname{sech}^2(x) + \operatorname{sech}^2(y) - \operatorname{sech}^2(x)\operatorname{sech}^2(y)]\} \\
&\quad + i\{W_0[\operatorname{sech}(x)\tanh(x) + \operatorname{sech}(y)\tanh(y)]\}
\end{aligned}
\tag{4}
$$

are obtained analytically whenever possible. Then, numerical solutions are calculated by means of the 'Spectral Renormalization Method' or 'Pseudo-Spectral Renormalization Method'. It is observed that the numerical solutions are in good agreement with the analytical solutions.

Next, the stability properties of the obtained solitons are investigated. Linear stability analysis is conducted by linear spectrum analysis and linear evolution, whereas nonlinear stability analysis is conducted by nonlinear evolution. A split-step Fourier method is used for both evolutions.

KÜBİK-KUİNTİK ORTAMLARDA
KAFES SOLİTONLARI

ÖZET

Solitonlar; doğrusal olmayan dalga yayılımı, biyolojik sistemler ve doğrusal olmayan optik gibi matematiğin uygulama bulduğu alanlarda ortaya konulan modellerin çözümlerinde elde edilen kararlı yapılar olarak karşımıza çıkarlar. Bulundukları sistemdeki doğrusalsızlığın (nonlineerliğin) ve ayrılmanın (dispersiyonun) dengelenmesiyle oluşan bu dalgalar - solitonlar - ilerlerken kendi yapılarını korurlar ve birbirleriyle olan etkileşimleri elastiktir.

Schrödinger denklemi, dalga-parçacık ikiliği gibi kuantum etkilerinin geçerli olduğu, atom ve atom altı parçacıklardan oluşan kuantum sistemlerdeki fiziksel sistemin zamana bağlı değişimini tarif eden bir matematiksel denklemdir. İsmini denklemi ortaya koymuş olan ve bu alandaki çalışmalarından ötürü Nobel Fizik Ödülü'ne layık görülen Erwin Schrödinger'den alan bu diferansiyel denklem, klasik mekanikteki Newton'un İkinci Yasası'nın kuantum mekaniğindeki karşılığı olarak düşünülebilir.

Doğrusal olmayan Schrödinger (NLS) denklemi ise, Schrödinger denkleminin teorik fizikteki doğrusal olmayan çeşididir ve optik kablolarda veya dalga kılavuzlarında ışığın yayılması gibi doğrusal olmayan, ayırgan (dispersif) ortamlarda yavaşça değişim gösteren tek renkli (monokromatik) dalgaların ilerlemesini betimleyen evrensel bir denklemdir.

Hem üçüncü dereceden (kübik) hem de beşinci dereceden (kuintik) doğrusal olmayan terim içeren Schrödinger (CQNLS) denklemi, birçok fiziksel durumu betimler ve özellikle de optikte karşımıza çıkar. Doğrusal olmayan optikte CQNLS denklemi, elektromanyetik dalganın ışık kıran (fotorefraktif) maddelerde yayılımını betimler. Kübik-kuintik doğrusalsızlığın nedeni madde içindeki öz rezonanstır.

İki boyutlu kübik NLS denkleminin soliton tipi çözümlerinin patladığı yani çözümün genliğinin, sonlu zamanda ya da mesafede sınırsızca büyümeye başladığı bilinmektedir. Fiziksel problemlerin çözümünde en temel sorunlardan biri çözümlerin kararlılığıdır. Optik problemlerinde bu, veri iletiminin uzun mesafelere sağlıklı olarak yapılabilmesi bağlamında önem taşır. Son on yılda literatürde, iki boyutlu NLS denkleminin çözümlerinin patlamasını engelleyecek yöntemler tartışılmaktadır. Gösterilmiştir ki, NLS denklemine eklenen bir potansiyel terimi, ki bu fiziksel ortamda düzeneğe eklenecek olan bir kafes (latis) ile karşılamaktadır, belli parametreler rejiminde dalga tipi çözümün kararlı hale gelmesini mümkün kılmaktadır. Bunun yanı sıra, sisteme eklenen potansiyel, dalganın biçiminde, genliğinde ve iletim süresinde değişiklikler yapabilmektedir. Dolayısıyla, fiziksel sistem düzeneğinde çeşitli yollarla oluşturulabilen kafeslerin optik problemlerinin çözümünde ve çözümlerin kararlılığı ve yapısının ayarlanması bağlamında önemli uygulama alanları vardır. Her ne kadar tek boyutlu NLS denkleminin çözümleri kararlı olsa da tek boyutlu çözümlerin yapısı ve özellikleri de iki boyutta olduğu gibi, sisteme eklenecek olan kafesler ile ayarlanabilir.

Bu kafesler laboratuvar ortamında lazer ışınlarının birbiriyle etkileştirilmesi veya düzeneğe eklenecek olan kristal ya da yarı kristaller ile oluşturulmaktadır.

Bu tezde, kübik-kuintik doğrusalsızlık barındıran ortamlarda temel kafes solitonların varlığı ve özellikleri incelenmiştir. Bu amaçla ele alınan fiziksel model, aşağıdaki CQNLS denklemidir:

$$iu_z + \Delta u + \alpha |u|^2 u + \beta |u|^4 u + V u = 0 . \tag{5}$$

Burada u karmaşık değerli fonksiyonu, x (veya xy) düzleminde olup z ekseni boyunca yayılan alanın yavaşça değişen genliğine, Δu kırınıma, V ise dış potansiyele (yani kafese) karşılık gelmektedir. α ve β sırasıyla kübik ve kuintik doğrusalsızlık katsayılarıdır ve bunların pozitif olması odaklanmaya, negatif olması ise odaktan sapmaya karşılık gelmektedir.

Tezde ilk olarak, gerekli fiziksel altyapı oluşturulup Maxwell denklemlerinden yola çıkılarak kullanılacak esas denklem olan CQNLS denklemi türetilmiştir. Ardından temelini kuantum mekaniğinden alan parite-zaman ($\mathcal{PT}$) simetrisi kavramı açıklanmıştır.

Kuantum mekaniğinde bir sistemin toplam enerjisi Hamiltonyen operatörüyle ifade edilebilir. Hermisyen olmadıkları halde, $\mathcal{PT}$ simetrisine sahip bazı Hamiltonyenlerin de tüm özdeğerlerinin gerçel olabildiği gösterilmiştir. Bu açıdan, $\mathcal{PT}$ simetrisi son zamanlardaki araştırmalarda sıkça yer almaktadır.

Tezde, $N = 4$'e karşı gelen

$$V_N(x,y) = \frac{V_0}{N^2} \left| \sum_{n=0}^{N-1} e^{i\left(x\cos\frac{2\pi n}{N} + y\cos\frac{2\pi n}{N}\right)} \right|^2 \tag{6}$$

2 boyutlu periyodik potansiyel,

$$V_{\mathcal{PT}}(x) = V(x) + iW(x) = [V_0 \operatorname{sech}^2(x) + V_1 \operatorname{sech}^4(x)] + i[W_0 \operatorname{sech}(x)\tanh(x)] \tag{7}$$

ile tanımlanan $\mathcal{PT}$ simetrisine sahip 1 boyutlu potansiyel ve

$$\begin{aligned} V_{\mathcal{PT}}(x,y) &= V(x,y) + iW(x,y) \\ &= \{V_0 \operatorname{sech}^2(x)\operatorname{sech}^2(y) + V_1 \operatorname{sech}^4(x)\operatorname{sech}^4(y) \\ &\quad + V_2[\operatorname{sech}^2(x) + \operatorname{sech}^2(y) - \operatorname{sech}^2(x)\operatorname{sech}^2(y)]\} \\ &\quad + i\{W_0[\operatorname{sech}(x)\tanh(x) + \operatorname{sech}(y)\tanh(y)]\} \end{aligned} \tag{8}$$

ile tanımlanan $\mathcal{PT}$ simetrisine sahip 2 boyutlu potansiyel ele alınmıştır. Burada V_i ($i = 0,1,2$) ve W_0 katsayıları potansiyellerin sırasıyla gerçel ve karmaşık kısımlarının derinliklerini temsil etmektedir.

Son potansiyelin özel (kasıtlı) olarak bu şekilde seçilmesiyle; tek başına integre edilebilir olmayan (2+1) boyutlu CQNLS denkleminin, bu potansiyel altında analitik çözümleri elde edilebilmiştir.

Ayrıca yapılan çalışmada, doğada kristallerin yukarıdaki matematik modellemenin aksine tam simetrik olmadıklarından, yani atomik boyutta da olsa bazı kusurlar içerebileceklerinden, kafes yapısındaki bu kusurları modelleyen bir yapı da kullanılmıştır.

Analitik çözüm elde edilemeyen durumlarda, tez kapsamında geliştirilmiş olan 'Spektral Yeniden Normalleştirme' ve 'Sözde Spektral Yeniden Normalleştirme' yöntemleri kullanılarak sayısal çözümler aranmıştır. Temelde bir Fourier yinelemesi olan bu yöntemlerde, çözümler $u = fe^{i\mu z}$ dönüşümü sonrası Fourier uzayında gerçekleştirilen bir özyinelemenin yakınsamasıyla elde edilmektedir.

Tezde sırasıyla potansiyelsiz (1+1) boyutlu CQNLS denkleminin $\mu > 0$ yayılma sabiti olmak üzere

$$u(x,z) = \frac{2\sqrt{\mu}}{\sqrt{\alpha + \left(\sqrt{\alpha^2 + \frac{16}{3}\beta\mu}\right)\cosh(2\sqrt{\mu}x)}} \, e^{i\mu z} \tag{9}$$

yapısındaki, $\mathcal{PT}$ simetrisine sahip potansiyelli (1+1) boyutlu CQNLS denkleminin

$$u(x,z) = \sqrt{\frac{2 - V_0 + \frac{W_0^2}{9}}{\alpha}} \, \text{sech}(x) \exp\left(i\left[z + \frac{W_0}{3}\arctan(\sinh(x))\right]\right) \tag{10}$$

yapısındaki ve $\mathcal{PT}$ simetrisine sahip potansiyelli (2+1) boyutlu CQNLS denkleminin

$$u(x,y,z) = \sqrt{\frac{2 - V_0 + \frac{W_0^2}{9}}{\alpha}} \, \text{sech}(x)\,\text{sech}(y)$$
$$\exp\left(i\left\{2z + \frac{W_0}{3}\left[\arctan(\sinh(x)) + \arctan(\sinh(y))\right]\right\}\right) \tag{11}$$

yapısındaki analitik çözümleri elde edilmiştir.

Öte yandan potansiyelsiz (1+1) boyutlu CQNLS denkleminin, $\mathcal{PT}$ simetrisine sahip potansiyelli (1+1) boyutlu CQNLS denkleminin, potansiyelsiz (2+1) boyutlu CQNLS denkleminin, periyodik potansiyelli (2+1) boyutlu CQNLS denkleminin, $\mathcal{PT}$ simetrisine sahip potansiyelli (2+1) boyutlu CQNLS denkleminin, $\mathcal{PT}$ simetrisine sahip ancak kusur içeren potansiyelli (2+1) boyutlu CQNLS denkleminin ve son olarak da $\mathcal{PT}$ simetrisine sahip ancak kusur içeren potansiyelli (2+1) boyutlu kübik doyurulabilir NLS denkleminin çözümleri yukarıda bahsedilen sayısal yöntemlerle elde edilmiştir.

Elde edilen sayısal çözümlerle analitik çözümlerin uyum sağladığı görülmüştür.

Sonrasında, elde edilen solitonların kararlılıkları incelenmiştir. Doğrusal kararlılık için, probleme karşılık gelen doğrusallaştırılmış operatörün özdeğerlerinin incelendiği doğrusal spektrum analizi ve küçük bir sarsım (pertürbasyon) ile birlikte çözümün doğrusallaştırılıp ilerletilmesinin incelendiği doğrusal evrim analizi yapılmıştır. Doğrusal olmayan kararlılık için ise küçük bir sarsım ile birlikte çözümün ilerletilmesinin incelendiği doğrusal olmayan evrim analizi yapılmıştır. Her iki evrim analizi için de parçalı-adımlı (split-step) Fourier yöntemi geliştirilip kullanılmıştır. Bazı durumlarda ise elde edilen solitonların güçleri (enerjileri) hesaplanıp bunların değişiminden yola çıkılarak kararlılık hakkında yorumlar yapılmıştır.

1. INTRODUCTION

In the last decade, optical solitons have become essential for studying solitons' interactions and most of the progress on soliton phenomena owes them as complicated experiments can be conducted with ease in a laboratory environment that offers precise control over almost every parameter. Furthermore, the ability to sample the waves directly as they propagate and the availability of numerous material systems that are fully characterized by a set of simple equations result in a field in which theory and experiments make rapid progress.

Solitons are localized nonlinear waves and occur in many branches of physics [1]. Their properties have provided fundamental understanding of complex nonlinear systems [2]. There has been considerable interest in studying solitons in lattices that can be generated in nonlinear optical materials [3]. In periodic lattices, solitons can typically form when their propagation constant is within certain regions, so-called gaps. Recently, particular attention is drawn to nonlinear waves in complex potentials, especially the so-called parity-time ($\mathcal{PT}$) symmetric potentials [4]. $\mathcal{PT}$-symmetric systems have been realized in optical models governed by nonlinear Schrödinger (NLS) type equations and on top of that, analytical solutions were obtained for the one dimensional case [5].

In optics, the propagation distance z takes place of the time variable t of quantum mechanics. In this regard, NLS type equations are used to model $\mathcal{PT}$-symmetric structures [6]. In nonlinear optics, the propagation of electromagnetic waves in photorefractive materials with intrinsic nonlinear resonance can be modelled by the NLS equation containing both cubic and quintic terms [7]. Cubic-quintic nonlinear Schrödinger (CQNLS) equation with external real potentials is studied in [8] and it is reported that it may stabilize solitons that are unstable in free space. Recently, one dimensional CQNLS equation with a trapping potential represented by a delta-function is investigated by means of the rigorous theory of orbital stability of Hamiltonian

systems [9]. In [10], two-dimensional solitons in a coupled model which combines the cubic-quintic nonlinearity and $\mathcal{PT}$-symmetry were reported.

Localized solitary waves, or shortly solitons, form in nonlinear media as a result of the balance between the self-trapping and linear diffraction [11]. Optical solitons on $\mathcal{PT}$-symmetric lattices have been widely studied [12]. However, most of the studies focus on one-dimensional cases (e.g. [13]) or investigate only the cubic nonlinearity (e.g. [14]).

Numerous theoretical studies deal with periodic or perfectly symmetric potentials. In real life however, atomic crystals can have various irregularities such as defects and dislocations [15]. In general, when the lattice periodicity is slightly perturbed, the band-gap structure and soliton properties also become slightly perturbed, hence solitons are expected to exist much the same in the perfectly periodic case.

In an optical fiber, the cubic nonlinearity typically generates the classic NLS equation. Nevertheless, a Kerr nonlinearity cannot sufficiently represent the field-induced change in the refractive index in case of short pulses and a high pulse power. In these circumstances, a saturation term is introduced which leads to the saturable NLS equation. [16] The cubic-saturable NLS equation has many applications in nonlinear optics and its exact bright and dark soliton solutions are obtained in the one dimensional (1D) case [17].

1.1 Purpose of Thesis

In this thesis, the existence and stability of optical solitons on periodic and certain type of $\mathcal{PT}$-symmetric lattices will be investigated. The governing equation for the physical model is the CQNLS equation with an external potential:

$$iu_z + \Delta u + \alpha|u|^2 u + \beta|u|^4 u + Vu = 0 . \qquad (1.1)$$

In optics, u corresponds to the complex-valued, slowly varying amplitude of the electric field in the x or xy-plane propagating in the z-direction, Δu corresponds to diffraction, V is an external optical potential, α and β are real constants.

The solution to the CQNLS equation above with an external potential will be obtained analytically whenever possible; then, numerically by spectral methods. As the external

potential V, the following periodic and $\mathcal{PT}$-symmetric lattices will be considered:

$$V_N(x,y) = \frac{V_0}{N^2} \left| \sum_{n=0}^{N-1} e^{i\left(x\cos\frac{2\pi n}{N} + y\cos\frac{2\pi n}{N}\right)} \right|^2 ,$$

$$V_{\mathcal{PT}}(x) = V(x) + iW(x)$$

$$= [V_0 \operatorname{sech}^2(x) + V_1 \operatorname{sech}^4(x)] + i[W_0 \operatorname{sech}(x)\tanh(x)] ,$$

$$V_{\mathcal{PT}}(x,y) = V(x,y) + iW(x,y) \tag{1.2}$$

$$= \{V_0 \operatorname{sech}^2(x)\operatorname{sech}^2(y) + V_1 \operatorname{sech}^4(x)\operatorname{sech}^4(y)$$

$$+ V_2[\operatorname{sech}^2(x) + \operatorname{sech}^2(y) - \operatorname{sech}^2(x)\operatorname{sech}^2(y)]\}$$

$$+ i\{W_0[\operatorname{sech}(x)\tanh(x) + \operatorname{sech}(y)\tanh(y)]\} .$$

For the solution of the CQNLS equation, a fixed-point spectral computational method will be employed which uses the ansatz $u(\boldsymbol{x},z) = f(\boldsymbol{x})e^{i\mu z}$ where μ is the propagation constant (eigenvalue) and solves it iteratively in the Fourier space.

To study the effect of the cubic-saturable nonlinearities and potential defects on the existence and stability properties of lattice solitons on the maximum of the $\mathcal{PT}$-symmetric potential, another physical model is used. The propagation of a light beam along the z-axis of the medium composed from alternating domains with cubic and saturable nonlinearities is described by the following (2+1) dimensional NLS equation with an external $\mathcal{PT}$-symmetric potential:

$$iu_z + \Delta u + \frac{|u|^2 u}{1 + s|u|^2} + V_{\mathcal{PT}} u = 0 , \tag{1.3}$$

where $u = u(x,y,z)$ is the envelope proportional to the electric field, z is the propagation distance, $\Delta u = u_{xx} + u_{yy}$ corresponds to diffraction, s is the saturation coefficient [18] and $V_{\mathcal{PT}}(x,y)$ is the external potential. It is to be noted that $s = 0$ represents a Kerr medium. To investigate different cubic-saturable media, we will let the saturation parameter s vary between 0 and 1.

For the solution of the cubic-saturable NLS equation, a pseudo-spectral method will be introduced.

Then, the numerical existence of fundamental solitons on the periodic and $\mathcal{PT}$-symmetric lattices will be shown and the band-gap structures will be found for varying parameters.

Finally, the linear and nonlinear stability properties of the solitons will be investigated.

1.2 Literature Review

Solitons arise as the solutions of a widespread class of weakly nonlinear dispersive partial differential equations (PDEs) describing physical systems. [19]

In optics, the term soliton (also called an optical mode) is used to refer to any optical field that does not change during propagation due to a delicate balance between nonlinear and linear effects in the medium.

A crystal is a structure arranged in an orderly repeating pattern extending in all three spatial dimensions. Patterns are located upon the points of a lattice, which is an array of points repeating periodically in three dimensions. A structure that is ordered but non-periodic (i.e. lacks any translational symmetry) is called a quasicrystal. The Penrose is a quasicrystal, for instance and has a rotational symmetry. [20]

Recently, Freedman et al. observed solitons in Penrose and other quasicrystal lattices generated by the optical induction method [21].

The Fourier transform of a continuous, smooth and absolutely integrable function is explained in detail in [22].

Although higher dimensional NLS models are not integrable, they possess stationary solutions which are unstable on propagation. Maybe the most fascinating issue related to the higher dimensional NLS is that for a wide range of initial conditions, the system evolution shows collapse [23]. Wave collapse occurs where the solution tends to infinity in finite time (distance). Collapse was theoretically predicted for the (2+1)D NLS equation back in the 1960's [24]. It is known that there exist solutions which have a singularity in finite time and are extremely sensitive to the addition of small perturbations to the equation and there has been much interest in the determination of the structure of this singularity [25, 26]. In another study ([27]), the existence and nonlinear stability properties of the fundamental Penrose lattice solitons for $N = 7$ are investigated and some Penrose-7 solitons are found to be unstable depending on the location, eigenvalue and potential depth.

Optical spatial solitons and their interactions in Kerr and saturable media have been elucidated in detail in [28]. In [29], the numerical existence of an optical lattice soliton

in saturable media is demonstrated by means of the Spectral Renormalization Method. Numerical existence of vortex solitons are also reported in saturable media in [30]. It is well known that the nonlinear saturation suppresses the collapse of the fundamental solitons in two and three dimensions [31, 32].

Spectral Renormalization Method is essentially a Fourier iteration method. The idea of this method was proposed by Petviashvili in [33]. Later, this method is improved by Ablowitz et al. and applied to (2+1)D NLS equation [34].

In [35], Vakhitov and Kolokolov proved a necessary condition for the linear stability of the soliton $f(x, \mu)$. Key analytical results on nonlinear stability were obtained in [36, 37]. They proved that the necessary conditions for nonlinear stability are the slope and the spectral condition. Furthermore, it is well known that a necessary condition for collapse in the two dimensional (2D) cubic NLS equation is that the power of the beam exceeds the critical power $P_c \approx 11.7$ [38].

The fundamental solitons of the NLS equation can become unstable in two ways: focusing instability and drift instability [39].

(1+1)D CQNLS equation is investigated and solved in [40–43].

Existence of localized modes supported by the $\mathcal{PT}$-symmetric nonlinear lattices is reported in [44].

1.3 Hypothesis

Properties of the (1+1)D cubic NLS equation are well-known. There are also studies about the (1+1)D CQNLS equation and (2+1)D cubic NLS equation. Yet, not much is known about the (2+1)D CQNLS equation, let alone with an external $\mathcal{PT}$-symmetric potential.

We expect to obtain numerical solutions for all the cases which will be investigated in this thesis. These numerical solutions are supposed to agree with their analytical counterparts, provided that they exist.

We hypothesize that the obtained solitons would not be stable in most cases, especially by the presence of a defect in the potential or quintic nonlinearity.

2. DERIVATION OF THE CQNLS EQUATION

To begin with, here are some preliminaries from electromagnetics. [45, 46]

Permeability μ:

The electromagnetic permeability, denoted by μ, is the measure of the ability of a material to support the formation of a magnetic field within itself.

Vacuum permeability μ_0:

The magnetic constant μ_0, commonly called the vacuum permeability or permeability of free space, is a baseline physical constant, which is the value of magnetic permeability in a classical vacuum. Its value is exactly defined by

$$\mu_0 = 4\pi \cdot 10^{-7} \frac{N}{A^2} = 4\pi \cdot 10^{-7} \frac{kg \cdot m}{A^2 s^2} \ . \tag{2.1}$$

Relative permeability μ_r:

The relative permeability, denoted by μ_r, is the ratio of the permeability of a specific medium to the permeability of free space:

$$\mu_r = \frac{\mu}{\mu_0} \ . \tag{2.2}$$

Permittivity ε:

The electromagnetic permittivity, denoted by ε, is the measure of the resistance that is encountered when forming an electric field in a medium.

Vacuum permittivity ε_0:

The electric constant ε_0, commonly called the vacuum permittivity or permittivity of free space, is a baseline physical constant, which is the value of the absolute dielectric permittivity of classical vacuum. Its value is defined by

$$\begin{aligned} \varepsilon_0 &= \frac{1}{\mu_0 c_0{}^2} \\ &= \frac{1}{4\pi \cdot 10^{-7} \frac{N}{A^2} \cdot \left(2.99792458 \cdot 10^8 \frac{m}{s}\right)^2} = \frac{1}{35950207150\pi \frac{kg \cdot m^2}{A^2 s^4} m} \\ &\approx 8.8542 \cdot 10^{-12} \frac{F}{m} \end{aligned} \tag{2.3}$$

where c_0 is the speed of light in free space (vacuum).

Relative permittivity ε_r:

The relative permeability, denoted by ε_r, is the ratio of the permittivity of a specific medium to the permittivity of free space:

$$\varepsilon_r = \frac{\varepsilon}{\varepsilon_0} \; . \tag{2.4}$$

Refractive index n:

The refractive index of an optical medium, denoted by n, is a dimensionless number that describes how light or any other radiation, propagates through that medium. The refractive index of electromagnetic radiation is given by

$$n = \sqrt{\varepsilon_r \mu_r} \; . \tag{2.5}$$

Substituting Eq. (2.2), (2.3) and (2.4) in Eq. (2.5) gives

$$n = \sqrt{\varepsilon_r \mu_r} = \sqrt{\frac{\varepsilon}{\varepsilon_0} \cdot \frac{\mu}{\mu_0}} = \sqrt{\varepsilon \mu c_0^2} = \sqrt{\varepsilon \mu}\, c_0 \; . \tag{2.6}$$

Wavenumber k:

The wavenumber k, also called the angular or circular wavenumber, is the number of wavelengths per 2π units of distance:

$$k = \frac{2\pi}{\lambda} = \frac{2\pi f}{v} = \frac{\omega}{v} \; , \tag{2.7}$$

where f is the frequency, ω is the angular frequency and v is the speed of the wave. If a wave at the speed of light in vacuum is considered, then its wavenumber is given by

$$k_0 = \frac{\omega}{c_0} \; . \tag{2.8}$$

Electric field $\vec{E}$:

The electric field, denoted by $\vec{E}$, is a vector field. The field vector at a given point is defined as the force vector per unit charge that would be exerted on a stationary test charge at that point. An electric field is generated by electric charge, as well as by a time-varying magnetic field. The SI units of this field are newtons per coulomb (N/C) or equivalently, volts per meter (V/m), which in terms of SI base units are $kg \cdot m/(A \cdot s^3)$.

Electric displacement field $\vec{D}$:

The electric displacement field, denoted by $\vec{D}$, is a vector field that accounts for the effects of free and bound charge within materials. The SI units of this field are coulombs per square meter (C/m^2), which in terms of SI base units are $A \cdot s/m^2$. For a linear, homogeneous and isotropic medium, the electric displacement field and the electric field are proportional:

$$\vec{D} = \varepsilon \vec{E} \ . \tag{2.9}$$

Electric charge density ρ:

The electric charge density ρ is the amount of electric charge per unit volume of space and is given by the differential

$$\rho = \frac{dQ}{dV} \ , \tag{2.10}$$

where Q is the electric charge. The SI units of the electric charge density are coulombs per cubic meter (C/m^3), which in terms of SI base units are $A \cdot s/m^3$. If ρ is constant, then $Q = \rho V$; if not

$$Q = \iiint\limits_{V} \rho dV \ . \tag{2.11}$$

Magnetic field $\vec{H}$:

The magnetic field, denoted by $\vec{H}$, is a vector field that gives at any given point the magnetic field strength. The SI units of this field are amperes per meter (A/m).

Magnetic displacement field $\vec{B}$:

The magnetic displacement field, denoted by $\vec{B}$, is a vector field that gives at any given point the magnetic flux density. The SI units of this field are teslas (T), which in terms of SI base units are $kg/(A \cdot s^2)$. For a linear, homogeneous and isotropic medium, the magnetic displacement field and the magnetic field are proportional:

$$\vec{B} = \mu \vec{H} \ . \tag{2.12}$$

Electric current density J:

The electric current density, denoted by J, is the electric current per unit area and is given by the limit

$$J = \lim_{A \to 0} \frac{I(A)}{A} \ . \tag{2.13}$$

9

The SI units of the electric current density are amperes per square meter (A/m^2).

Gauss' Law (Maxwell's First Equation):

Gauss' Law for a D-field states that the net outward normal electric displacement field flux through any closed surface is equal to the free electric charge enclosed within that closed surface:

$$\Phi_D = \oiint_S \vec{D} \cdot \vec{n}\, dS = Q_{free} . \tag{2.14}$$

Substituting Eq. (2.11) in Eq. (2.14) gives

$$\oiint_S \vec{D} \cdot \vec{n}\, dS = \iiint_V \rho_{free} dV . \tag{2.15}$$

By the Divergence Theorem, Eq. (2.15) is equivalent to

$$\iiint_V \vec{\nabla} \cdot \vec{D}\, dV = \iiint_V \rho_{free} dV , \tag{2.16}$$

which yields the differential form:

$$\vec{\nabla} \cdot \vec{D} = \rho_{free} . \tag{2.17}$$

If the medium is charge-free, then $\rho_{free} = 0$ and

$$\vec{\nabla} \cdot \vec{D} = 0 . \tag{2.18}$$

Substituting Eq. (2.9) in Eq. (2.18) gives

$$0 = \vec{\nabla} \cdot \vec{D} = \vec{\nabla} \cdot (\varepsilon \vec{E}) = \vec{\nabla \varepsilon} \cdot \vec{E} + \varepsilon \left(\vec{\nabla} \cdot \vec{E} \right) . \tag{2.19}$$

It follows from Eq. (2.19), that

$$\vec{\nabla} \cdot \vec{E} = \frac{\vec{\nabla \varepsilon} \cdot \vec{E}}{-\varepsilon} . \tag{2.20}$$

Faraday's Law of Induction (Maxwell's Third Equation):

Maxwell–Faraday equation states that a time-varying magnetic field is always accompanied by a spatially-varying, non-conservative electric field and vice versa:

$$\vec{\nabla} \times \vec{E} = -\frac{\partial \vec{B}}{\partial t} \tag{2.21}$$

Assuming that the field is monochromatic and harmonic, $\vec{B}$ can be written as

$$\vec{B}(x,y,z,t) = \vec{B}(x,y,z)\, e^{-i\omega t} . \tag{2.22}$$

10

Substituting Eq. (2.22) in Eq. (2.21) gives

$$\vec{\nabla} \times \vec{E} = -\vec{B}(x,y,z) \, e^{-i\omega t}(-i\omega) = i\omega \vec{B} \tag{2.23}$$

Ampère's Circuital Law with Maxwell's Correction (Maxwell's Fourth Equation):

Ampère's Law with Maxwell's correction states that magnetic fields can be generated in two ways: by electrical current ("Ampère's Circuital Law") and by changing electric fields ("Maxwell's Correction"):

$$\vec{\nabla} \times \vec{H} = \vec{J} + \frac{\partial \vec{D}}{\partial t} . \tag{2.24}$$

Substituting Eq. (2.9) in Eq. (2.24) gives

$$\vec{\nabla} \times \vec{H} = \vec{J} + \varepsilon \frac{\partial \vec{E}}{\partial t} . \tag{2.25}$$

If the medium is charge-free, then $\vec{J} = \vec{0}$ and Eq. (2.25) becomes

$$\vec{\nabla} \times \vec{H} = \varepsilon \frac{\partial \vec{E}}{\partial t} . \tag{2.26}$$

Assuming that the field is monochromatic and harmonic, $\vec{E}$ can be written as

$$\vec{E}(x,y,z,t) = \vec{E}(x,y,z) \, e^{-i\omega t} . \tag{2.27}$$

Substituting Eq. (2.27) in Eq. (2.26) gives

$$\vec{\nabla} \times \vec{H} = \varepsilon \vec{E}(x,y,z) \, e^{-i\omega t}(-i\omega) = -i\varepsilon\omega \vec{E} . \tag{2.28}$$

Now, let us proceed to derive the CQNLS equation. Substituting Eq. (2.12) in Eq. (2.23) gives

$$\vec{\nabla} \times \vec{E} = i\mu\omega \vec{H} . \tag{2.29}$$

Taking the rotational of the both sides of Eq. (2.29) yields

$$\vec{\nabla} \times \left(\vec{\nabla} \times \vec{E} \right) = \vec{\nabla} \times \left(i\mu\omega \vec{H} \right) . \tag{2.30}$$

Expanding Eq. (2.30) results in

$$\vec{\nabla} \left(\vec{\nabla} \cdot \vec{E} \right) - \Delta \vec{E} = i\mu\omega \left(\vec{\nabla} \times \vec{H} \right) . \tag{2.31}$$

Substituting Eq. (2.20) and (2.28) in Eq. (2.31) gives

$$\vec{\nabla} \left(\frac{\vec{\nabla\varepsilon} \cdot \vec{E}}{-\varepsilon} \right) - \Delta \vec{E} = \varepsilon\mu\omega^2 \vec{E} . \tag{2.32}$$

11

Supposing that ε changes little over a single optical wavelength, the first term in Eq. (2.32) can be neglected:

$$-\Delta \vec{E} = \varepsilon \mu c_0{}^2 \frac{\omega^2}{c_0{}^2} \vec{E} \ . \tag{2.33}$$

Substituting Eq. (2.6) and (2.8) in Eq. (2.33) gives the *Helmholtz equation*:

$$\Delta \vec{E} + (k_0 n)^2 \vec{E} = 0 \ . \tag{2.34}$$

Polarizing the electric field along one transverse axis makes the Helmholtz equation scalar. Hence, $\vec{E}$ will be replaced by E in Eq. (2.34). This scalar approximation is satisfied if n does not vary strongly in the medium, which is the case in many applications in nonlinear optics. Consider the refractive index as the sum of a constant index and a small variation

$$n = n_0 + \Delta n \qquad , \qquad \Delta n \ll n_0 \tag{2.35}$$

and the electric field as a slowly varying wave envelope along the propagation direction z

$$E(x,y,z) = u(x,y,z) \, e^{ik_0 n_0 z} \ . \tag{2.36}$$

[47] Then,

$$
\begin{aligned}
n^2 &= n_0{}^2 + (\Delta n)^2 + 2n_0 \Delta n \approx n_0{}^2 + 2n_0 \Delta n \\
E_{xx} &= u_{xx} \, e^{ik_0 n_0 z} \\
E_{yy} &= u_{yy} \, e^{ik_0 n_0 z} \\
E_z &= (u_z + ik_0 n_0 u) \, e^{ik_0 n_0 z} \\
E_{zz} &= \left(u_{zz} + 2ik_0 n_0 u_z - k_0{}^2 n_0{}^2 u\right) e^{ik_0 n_0 z} \\
\Delta E &= E_{xx} + E_{yy} + E_{zz} = \left(u_{xx} + u_{yy} + u_{zz} + 2ik_0 n_0 u_z - k_0{}^2 n_0{}^2 u\right) e^{ik_0 n_0 z} \ .
\end{aligned}
\tag{2.37}
$$

Using Eq. (2.37) in the scalar form of Eq. (2.34) yields

$$\left(u_{xx} + u_{yy} + u_{zz} + 2ik_0 n_0 u_z + 2k_0{}^2 n_0 \Delta n \ u\right) e^{ik_0 n_0 z} = 0 \ . \tag{2.38}$$

Omitting the small term u_{zz} and multiplying Eq. (2.38) by $e^{-ik_0 n_0 z}$ gives

$$2ik_0 n_0 u_z + u_{xx} + u_{yy} + 2k_0{}^2 n_0 \Delta n \ u = 0 \ . \tag{2.39}$$

Introducing the change of variable

$$\tilde{z} = \frac{z}{2k_0 n_0} \tag{2.40}$$

12

and using

$$u_z = u_{\tilde{z}} \cdot \tilde{z}_z = \frac{u_{\tilde{z}}}{2k_0 n_0} \tag{2.41}$$

in Eq. (2.39) yields

$$iu_{\tilde{z}} + u_{xx} + u_{yy} + 2k_0^2 n_0 \Delta n \, u = 0 \; . \tag{2.42}$$

In a non-Kerr, nonlinear medium, $\Delta n = f(|u|^2)$. [48] By taking

$$f(|u|^2) = \frac{1}{2k_0^2 n_0} \left(\alpha |u|^2 + \beta |u|^4 \right) \tag{2.43}$$

and dropping the tilde from $\tilde{z}$ for convenience, the CQNLS equation is obtained:

$$iu_z + u_{xx} + u_{yy} + \alpha |u|^2 u + \beta |u|^4 u = 0 \; . \tag{2.44}$$

On the other hand, taking

$$f(|u|^2) = \frac{1}{2k_0^2 n_0} \left(\frac{|u|^2}{1 + s|u|^2} \right) \tag{2.45}$$

and dropping the tilde yields the cubic-saturable NLS equation:

$$iu_z + u_{xx} + u_{yy} + \frac{|u|^2 u}{1 + s|u|^2} = 0 \; . \tag{2.46}$$

3. OPTICAL LATTICES

Optical lattices are formed by the interference of counter-propagating laser beams, creating a spatially periodic polarization pattern. The resulting potentials can be modelled mathematically. For instance, the potential

$$V_N(x,y) = \frac{V_0}{N^2} \left| \sum_{n=0}^{N-1} e^{i\left(x\cos\frac{2\pi n}{N} + y\cos\frac{2\pi n}{N}\right)} \right|^2 \tag{3.1}$$

for $N = 4$ yields a periodic lattice which corresponds to a 2D crystal structure. [18] Its contour image, contour plot and cross section are displayed in Figure 3.1.

3.1 $\mathcal{PT}$-Symmetry

Any measurement of a physical observable in our universe obviously yields a real quantity. In quantum mechanics, observables correspond to eigenvalues of operators. Hence, the reality requires all the eigenvalues of operators to be real.

Consider the Hamiltonian operator $\widehat{H}$ which is the sum of the kinetic energy operator $\widehat{T}$ and potential energy operator $\widehat{V}$:

$$\widehat{H} = \widehat{T} + \widehat{V} = \frac{\widehat{p}^2}{2m} + \widehat{V}(\widehat{x}) \tag{3.2}$$

where $\widehat{p}$ is the momentum operator, m is the mass and $\widehat{x}$ is the position operator.

Real eigenvalues of (3.2) correspond to a real energy spectrum. To guarantee a real spectrum, it was postulated that all observables corresponded to eigenvalues of Hermitian (i.e. self adjoint) operators by recalling the result from linear algebra that Hermitian matrices have all real spectra. In fact, a Hermitian Hamiltonian ensures a real energy spectrum. However, Bender et al. investigated non-Hermitian Hamiltonians and found out that many of them have entirely real spectra provided that they have the so-called parity-time symmetry property [49]. Furthermore, they showed in many cases a threshold value above which the spectrum becomes complex. This threshold is the boundary between the $\mathcal{PT}$-symmetric and broken symmetry phases and in literature, the transition is referred to as spontaneous $\mathcal{PT}$-symmetry breaking.
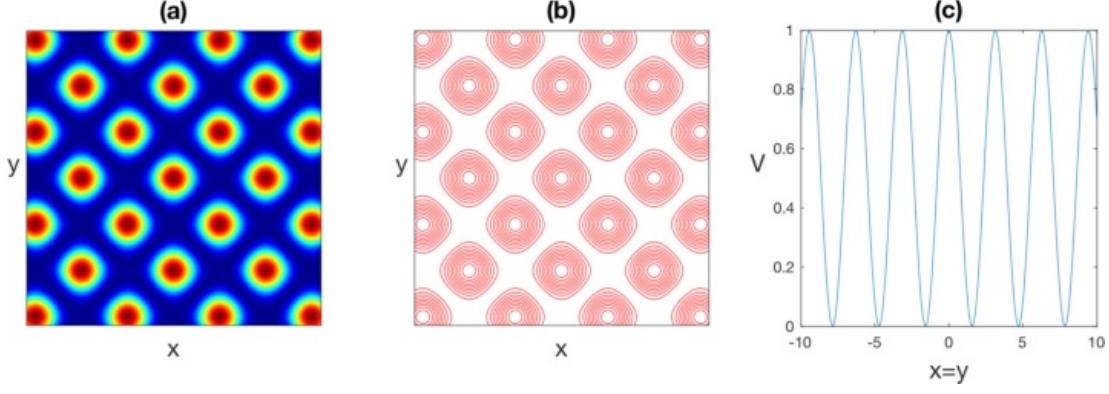
Figure 3.1 : (a) Contour image, (b) Contour plot, (c) Cross section of the potential in Eq. (3.1) with $V_0 = 1$.

$\mathcal{PT}$-symmetry is defined by means of the parity operator $\widehat{\mathcal{P}}$ and time (reversal) operator $\widehat{\mathcal{T}}$ whose actions are given as follows:

$$
\begin{aligned}
&\widehat{\mathcal{P}}: \; \widehat{p} \to -\widehat{p}, \widehat{x} \to -\widehat{x} && (\mathcal{P}(a\psi + b\phi))(\mathbf{x}) = a\psi(-\mathbf{x}) + b\phi(-\mathbf{x}) \\
&\widehat{\mathcal{T}}: \; \widehat{p} \to -\widehat{p}, \widehat{x} \to \widehat{x}, i \to -i && (\mathcal{T}(a\psi + b\phi))(\mathbf{x}) = a^*\psi^*(\mathbf{x}) + b^*\phi^*(\mathbf{x})
\end{aligned}
\tag{3.3}
$$

where the raised asterisk (*) denotes the complex conjugate [50, 51]. A Hamiltonian is said to be $\mathcal{PT}$-symmetric if it has the same eigenfunctions as the $\mathcal{PT}$ operator and satisfies the commutativity

$$
\widehat{\mathcal{P}}\widehat{\mathcal{T}}\widehat{H} = \widehat{H}\widehat{\mathcal{P}}\widehat{\mathcal{T}} \; .
\tag{3.4}
$$

On one hand,

$$
\begin{aligned}
(\mathcal{PT}H)(f(\mathbf{x},t)) &= (\mathcal{PT})\left(\frac{p^2}{2m}f(\mathbf{x},t) + V(\mathbf{x})f(\mathbf{x},t) \right) \\
&= \mathcal{P}\left(\frac{(-p)^2}{2m}f^*(\mathbf{x},t) + V^*(\mathbf{x})f^*(\mathbf{x},t) \right) \\
&= \frac{p^2}{2m}f^*(-\mathbf{x},t) + V^*(-\mathbf{x})f^*(-\mathbf{x},t)
\end{aligned}
\tag{3.5}
$$

and on the other hand,

$$
\begin{aligned}
(H\mathcal{PT})(f(\mathbf{x},t)) &= (H\mathcal{P})(f^*(\mathbf{x},t)) \\
&= H(f^*(-\mathbf{x},t)) \\
&= \frac{p^2}{2m}f^*(-\mathbf{x},t) + V(\mathbf{x})f^*(-\mathbf{x},t) \; .
\end{aligned}
\tag{3.6}
$$

One speaks of broken $\mathcal{PT}$-symmetry if Eq. (3.4) is satisfied but the same eigenfunctions are not shared. $\mathcal{PT}$-symmetric structures have been realized in optical models governed by NLS type equations by which the propagation distance z replaces

time in quantum mechanics [6]. The necessary (but not sufficient) condition in Eq. (3.4) implies

$$
\left.
\begin{aligned}
\widehat{H}\widehat{\mathcal{P}}\widehat{\mathcal{T}} &= \frac{\widehat{p}^2}{2m} + V(\boldsymbol{x}) \\[2ex]
\widehat{\mathcal{P}}\widehat{\mathcal{T}}\widehat{H} &= \frac{\widehat{p}^2}{2m} + V^*(-\boldsymbol{x})
\end{aligned}
\right\} \Rightarrow V(\boldsymbol{x}) = V^*(-\boldsymbol{x}).
\tag{3.7}
$$

Consider the complex potential

$$
V_{\mathcal{PT}}(\boldsymbol{x}) = V(\boldsymbol{x}) + iW(\boldsymbol{x})
\tag{3.8}
$$

where $V, W \in \mathbb{R}^n$. As

$$
V_{\mathcal{PT}}{}^*(-\boldsymbol{x}) = V^*(-\boldsymbol{x}) - iW^*(-\boldsymbol{x}) = V(-\boldsymbol{x}) - iW(-\boldsymbol{x}),
\tag{3.9}
$$

the real part of the potential, $V(\boldsymbol{x})$ must be an even function and the complex part of the potential, $W(\boldsymbol{x})$ must be an odd function so that Eq. (3.7) holds [52].

3.2 $\mathcal{PT}$-Symmetric Lattices

In this thesis, we will consider the following 1D $\mathcal{PT}$-symmetric potential

$$
V_{\mathcal{PT}}(x) = V(x) + iW(x) = [V_0 \operatorname{sech}^2(x) + V_1 \operatorname{sech}^4(x)] + i[W_0 \operatorname{sech}(x)\tanh(x)]
\tag{3.10}
$$

and 2D $\mathcal{PT}$-symmetric potential

$$
\begin{aligned}
V_{\mathcal{PT}}(x,y) &= V(x,y) + iW(x,y) \\
&= \{V_0 \operatorname{sech}^2(x)\operatorname{sech}^2(y) + V_1 \operatorname{sech}^4(x)\operatorname{sech}^4(y) \\
&\quad + V_2[\operatorname{sech}^2(x) + \operatorname{sech}^2(y) - \operatorname{sech}^2(x)\operatorname{sech}^2(y)]\} \\
&\quad + i\{W_0[\operatorname{sech}(x)\tanh(x) + \operatorname{sech}(y)\tanh(y)]\}
\end{aligned}
\tag{3.11}
$$

where V_i $(i = 0, 1, 2)$ and W_0 represent the depths of the real and imaginary parts of the potentials, respectively. Note that for both potentials, V is an even, real-valued function and W is an odd, real-valued function.

In Figure 3.2 and 3.3, contour plots and cross sections of the 1D and 2D $\mathcal{PT}$-symmetric potentials are displayed, respectively.

The potential in Eq. (3.10) can be seen as an extension of the so-called complexified Scarf II potential [53]

$$
[V_0 \operatorname{sech}^2(x)] + i[W_0 \operatorname{sech}(x)\tanh(x)]
\tag{3.12}
$$
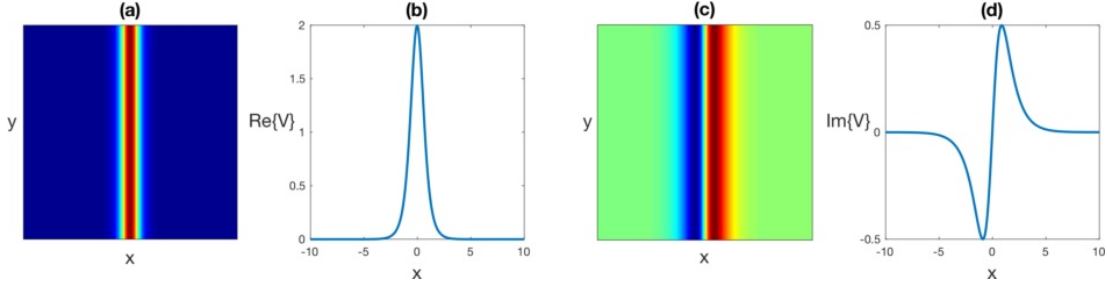
Figure 3.2 : (a) Real part, (b) Cross section of the real part, (c) Imaginary part, (d) Cross section of the imaginary part of the potential in Eq. (3.10) with $V_0 = V_1 = W_0 = 1$.
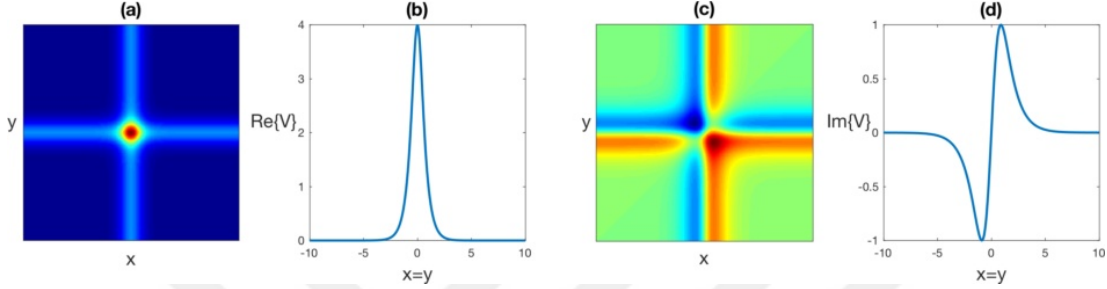
Figure 3.3 : (a) Real part, (b) Cross section of the real part, (c) Imaginary part, (d) Cross section of the imaginary part of the potential in Eq. (3.11) with $V_0 = 2, V_1 = V_2 = W_0 = 1$.

for a Kerr medium to a cubic-quintic nonlinear medium whereas the potential in Eq. (3.11) can be regarded as an extension of the 2D Scarff $\mathcal{PT}$-symmetric potential [14]

$$[V_0 \operatorname{sech}^2(x) \operatorname{sech}^2(y)] + i[W_0 \operatorname{sech}(x) \tanh(x) \operatorname{sech}^2(y)] \tag{3.13}$$

for Kerr medium (i.e. $\beta = 0$) to a cubic-quintic nonlinear medium. Both potentials are particularly of interest due to their physical significance [54]. Furthermore, they will conveniently provide analytical solutions which will be obtained in Section 6.2.1 and 7.3.1.

3.3 $\mathcal{PT}$-Symmetric Lattices with Defects

So far, we have assumed that the $\mathcal{PT}$-symmetric optical lattices we will use, are perfect, i.e. they can be represented precisely with our mathematical model. In reality, crystals are neither ideal nor infinitely large. These deviations from the ideal structure are called lattice defects.

Before we introduce the defects, let us consider the following 2D lattice

$$V_{\mathcal{PT}}^0(x,y) = V^0(x,y) + iW(x,y) = V_0 |2\cos(x) + 2\cos(y)|^2 + iW_0 [\sin(2x) + \sin(2y)] ,$$

$$\tag{3.14}$$
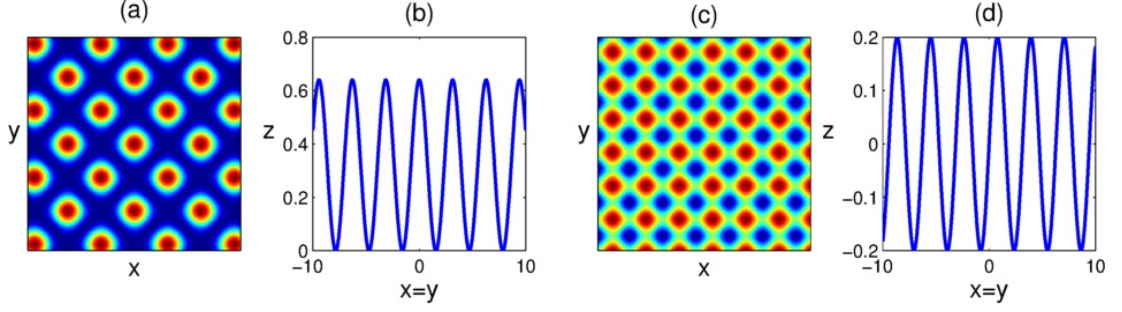
Figure 3.4 : (a) Real part, (b) Cross section of the real part, (c) Imaginary part, (d) Cross section of the imaginary part of the potential in Eq. (3.14) with $V_0 = 0.04$ and $W_0 = 0.1$.

which satisfies the necessary condition for $\mathcal{PT}$-symmetry $V_{\mathcal{PT}}(x,y) = V_{\mathcal{PT}}{}^*(-x,-y)$ as $V^0(x,y)$ is an even, real-valued function and $W(x,y)$ is an odd, real-valued function. Indeed,

$$V^0(-x,-y) = V_0 |2\cos(-x) + 2\cos(-y)|^2 = V_0 |2\cos(x) + 2\cos(y)|^2 = V^0(x,y)$$

$$W(-x,-y) = W_0 [\sin(-2x) + \sin(-2y)] = W_0 [-\sin(2x) - \sin(2y)] = -W(x,y) .$$

$$(3.15)$$

The real and imaginary parts of the potential in Eq. (3.14) with $V_0 = 0.04$ and $W_0 = 0.1$ are depicted in Figure 3.4(a) and 3.4(c); and their diagonal cross sections are plotted in Figure 3.4(b) and 3.4(d), respectively. As it can been seen from these figures, the potential is completely symmetric.

By means of a phase function given by

$$\theta(x,y) = \arctan\left(\frac{y-\pi}{x}\right) \pm \arctan\left(\frac{y+\pi}{x}\right)$$

$$(3.16)$$

[55], one can engender a positive or negative defect on the lattice in the following way:

$$\begin{aligned} V_{\mathcal{PT}}(x,y) &= V(x,y) + iW(x,y) \\ &= V_0 \left|2\cos(x) + 2\cos(y) + e^{i\theta(x,y)}\right|^2 + iW_0 [\sin(2x) + \sin(2y)] . \end{aligned}$$

$$(3.17)$$

First, consider the plus sign in Eq. (3.16) which will create the positive defect.

$$\begin{aligned} V_{\mathcal{PT}}^+(x,y) = &V_0 \left|2\cos(x) + 2\cos(y) + \exp\left(i\left[\arctan\left(\frac{y-\pi}{x}\right) + \arctan\left(\frac{y+\pi}{x}\right)\right]\right)\right|^2 \\ &+ iW_0 [\sin(2x) + \sin(2y)] \end{aligned}$$

$$(3.18)$$
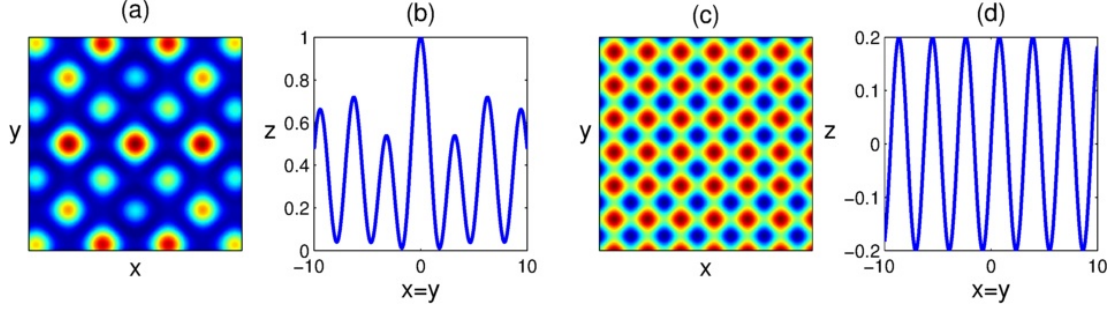
Figure 3.5 : (a) Real part, (b) Cross section of the real part, (c) Imaginary part, (d) Cross section of the imaginary part of the potential in Eq. (3.18) with $V_0 = 0.04$ and $W_0 = 0.1$.

is also $\mathcal{PT}$-symmetric as $V^+(x,y)$ is an even, real-valued function and $W(x,y)$ is an odd, real-valued function. Indeed,

$$
\begin{aligned}
&V^+(-x,-y) \\
&= V_0 \left| 2\cos(-x) + 2\cos(-y) + \exp\left(i\left[\arctan\left(\frac{-y-\pi}{-x} \right) + \arctan\left(\frac{-y+\pi}{-x} \right) \right] \right) \right|^2 \\
&= V_0 \left| 2\cos(x) + 2\cos(y) + \exp\left(i\left[\arctan\left(\frac{y+\pi}{x} \right) + \arctan\left(\frac{y-\pi}{x} \right) \right] \right) \right|^2 \\
&= V_0 \left| 2\cos(x) + 2\cos(y) + \exp\left(i\left[\arctan\left(\frac{y-\pi}{x} \right) + \arctan\left(\frac{y+\pi}{x} \right) \right] \right) \right|^2 \\
&= V^+(x,y) .
\end{aligned}
$$

$$(3.19)$$

The real and imaginary parts of the $\mathcal{PT}$-symmetric potential in Eq. (3.18) with a positive defect, $V_0 = 0.04$ and $W_0 = 0.1$ are depicted in Figure 3.5(a) and 3.5(c); and their diagonal cross sections are plotted in Figure 3.5(b) and 3.5(d), respectively. As it can been seen from these figures, the real part of the potential is not symmetric anymore; moreover, it has a global maximum at the center instead of a local one.

Then, consider the minus sign in Eq. (3.16) which will create the negative defect.

$$
\begin{aligned}
V_{\mathcal{PT}}^-(x,y) = &V_0 \left| 2\cos(x) + 2\cos(y) + \exp\left(i\left[\arctan\left(\frac{y-\pi}{x} \right) - \arctan\left(\frac{y+\pi}{x} \right) \right] \right) \right|^2 \\
&+ iW_0 \left[\sin(2x) + \sin(2y) \right]
\end{aligned}
$$

$$(3.20)$$

is also $\mathcal{PT}$-symmetric as $V^-(x,y)$ is an even, real-valued function and $W(x,y)$ is an odd, real-valued function. Indeed,

$$V^-(-x,-y)$$

$$= V_0 \left| 2\cos(-x) + 2\cos(-y) + \exp\left(i\left[\arctan\left(\frac{-y-\pi}{-x} \right) - \arctan\left(\frac{-y+\pi}{-x} \right) \right] \right) \right|^2$$

$$= V_0 \left| 2\cos(x) + 2\cos(y) + \exp\left(i\left[\arctan\left(\frac{y+\pi}{x} \right) - \arctan\left(\frac{y-\pi}{x} \right) \right] \right) \right|^2$$

$$= V_0 \left| 2\cos(x) + 2\cos(y) + \cos\left(\arctan\left(\frac{y+\pi}{x} \right) - \arctan\left(\frac{y-\pi}{x} \right) \right) \right.$$

$$\left. + i\sin\left(\arctan\left(\frac{y+\pi}{x} \right) - \arctan\left(\frac{y-\pi}{x} \right) \right) \right|^2$$

$$= V_0 \left| 2\cos(x) + 2\cos(y) + \cos\left(\arctan\left(\frac{y-\pi}{x} \right) - \arctan\left(\frac{y+\pi}{x} \right) \right) \right.$$

$$\left. - i\sin\left(\arctan\left(\frac{y-\pi}{x} \right) - \arctan\left(\frac{y+\pi}{x} \right) \right) \right|^2$$

$$= V_0 \left[2\cos(x) + 2\cos(y) + \cos\left(\arctan\left(\frac{y-\pi}{x} \right) - \arctan\left(\frac{y+\pi}{x} \right) \right) \right.$$

$$\left. - i\sin\left(\arctan\left(\frac{y-\pi}{x} \right) - \arctan\left(\frac{y+\pi}{x} \right) \right) \right]$$

$$\cdot \left[2\cos(x) + 2\cos(y) + \cos\left(\arctan\left(\frac{y-\pi}{x} \right) - \arctan\left(\frac{y+\pi}{x} \right) \right) \right.$$

$$\left. + i\sin\left(\arctan\left(\frac{y-\pi}{x} \right) - \arctan\left(\frac{y+\pi}{x} \right) \right) \right]$$

$$= V_0 \left[2\cos(x) + 2\cos(y) + \cos\left(\arctan\left(\frac{y-\pi}{x} \right) - \arctan\left(\frac{y+\pi}{x} \right) \right) \right.$$

$$\left. + i\sin\left(\arctan\left(\frac{y-\pi}{x} \right) - \arctan\left(\frac{y+\pi}{x} \right) \right) \right]$$

$$\cdot \left[2\cos(x) + 2\cos(y) + \cos\left(\arctan\left(\frac{y-\pi}{x} \right) - \arctan\left(\frac{y+\pi}{x} \right) \right) \right.$$

$$\left. - i\sin\left(\arctan\left(\frac{y-\pi}{x} \right) - \arctan\left(\frac{y+\pi}{x} \right) \right) \right]$$

$$= V_0 \left| 2\cos(x) + 2\cos(y) + \cos\left(\arctan\left(\frac{y-\pi}{x} \right) - \arctan\left(\frac{y+\pi}{x} \right) \right) \right.$$

$$\left. + i\sin\left(\arctan\left(\frac{y-\pi}{x} \right) - \arctan\left(\frac{y+\pi}{x} \right) \right) \right|^2$$

$$= V_0 \left| 2\cos(x) + 2\cos(y) + \exp\left(i\left[\arctan\left(\frac{y-\pi}{x} \right) - \arctan\left(\frac{y+\pi}{x} \right) \right] \right) \right|^2$$

$$= V^-(x,y) .$$

$$(3.21)$$

The real and imaginary parts of the $\mathcal{PT}$-symmetric potential in Eq. (3.20) with a negative defect, $V_0 = 0.04$ and $W_0 = 0.1$ are depicted in Figure 3.6(a) and 3.6(c); and
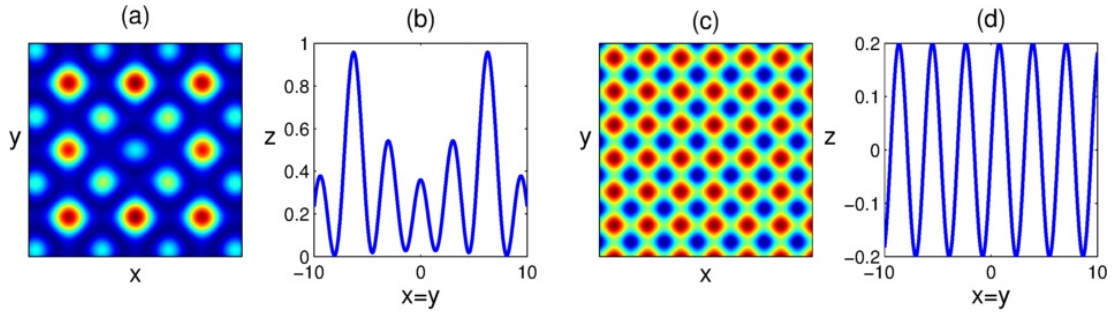
Figure 3.6 : (a) Real part, (b) Cross section of the real part, (c) Imaginary part, (d) Cross section of the imaginary part of the potential in Eq. (3.20) with $V_0 = 0.04$ and $W_0 = 0.1$.

their diagonal cross sections are plotted in Figure 3.6(b) and 3.6(d), respectively. As it can been seen from these figures, the real part of the potential is not symmetric anymore; moreover, it has a local maximum at the center but of smaller value.

4. SPECTRAL METHODS

In this chapter, the main numerical methods, that are used in this thesis to obtain soliton solutions, will be explained.

4.1 Spectral Renormalization Method

Spectral Renormalization Method is basically a Fourier iteration method proposed by Petviashvili in [33]. Later, this method is improved by Ablowitz et al. and applied to NLS equation [34]. Here, the method is modified so that it can be applied to the (2+1)D CQNLS equation.

Numeric solutions to Eq. (1.1) with a $\mathcal{PT}$-symmetric potential $V_{\mathcal{PT}} = V + iW$ are sought by means of the above mentioned method. As we are looking for soliton solutions, we use the ansatz $u(x,y,z) = f(x,y)e^{i\mu z}$, where $\lim\limits_{(x,y) \to \pm\infty} f(x,y) = 0$ and the propagation constant $\mu > 0$, in Eq. (1.1) which gives

$$-\mu f + f_{xx} + f_{yy} + \alpha|f|^2 f + \beta|f|^4 f + (V + iW)f = 0 . \tag{4.1}$$

After applying Fourier transformation ($\mathcal{F}$), one obtains

$$\hat{f} = \frac{\alpha\mathcal{F}(|f|^2 f) + \beta\mathcal{F}(|f|^4 f) + \mathcal{F}((V + iW)f)}{\mu + k_x^2 + k_y^2} , \tag{4.2}$$

where k_x and k_y are the corresponding Fourier transform variables. This equation could be indexed and utilized as an iteration to find f, but the scheme does not converge. Nonetheless, introducing a new field variable $f(x,y) = \lambda w(x,y)$ with $\lambda \in \mathbb{R}^+$ gives

$$\hat{w} = \frac{\alpha\lambda^2\mathcal{F}(|w|^2 w) + \beta\lambda^4\mathcal{F}(|w|^4 w) + \mathcal{F}((V + iW)w)}{\mu + k_x^2 + k_y^2} . \tag{4.3}$$

When indexed, Eq. (4.3) can be utilized in an iterative method in order to find w. For this purpose, $\hat{w}$ can be calculated using the following iteration scheme:

$$\hat{w}_{n+1} = \frac{\alpha\lambda^2\mathcal{F}(|w_n|^2 w_n) + \beta\lambda^4\mathcal{F}(|w_n|^4 w_n) + \mathcal{F}((V + iW)w_n)}{\mu + k_x^2 + k_y^2} , \quad n \in \mathbb{N} \tag{4.4}$$

with the initial condition taken as a Gaussian type function $w_0 = e^{-x^2 - y^2}$ and where the convergence criterions are $|\hat{w}_n - \hat{w}_{n-1}| < 10^{-12}$ and that the obtained numerical solution satisfies Eq. (1.1) with an absolute error less than 10^{-6}.

However, λ is unknown and hence must be calculated for each iteration. After multiplying Eq. (4.3) by $(\mu + k_x^2 + k_y^2)\hat{w}^*$ and integrating over the entire space, one gets

$$\lambda^4 \int\limits_{-\infty}^{\infty}\int\limits_{-\infty}^{\infty} \beta \mathcal{F}(|w|^4 w)\hat{w}^* d\boldsymbol{k} + \lambda^2 \int\limits_{-\infty}^{\infty}\int\limits_{-\infty}^{\infty} \alpha \mathcal{F}(|w|^2 w)\hat{w}^* d\boldsymbol{k}$$
$$+ \int\limits_{-\infty}^{\infty}\int\limits_{-\infty}^{\infty} [\mathcal{F}((V+iW)w) - (\mu + k_x^2 + k_y^2)\hat{w}]\hat{w}^* d\boldsymbol{k} = 0 \ . \tag{4.5}$$

This is nothing but a fourth degree polynomial of the form $P(\lambda) = a\lambda^4 + b\lambda^2 + c = 0$, from which λ can easily be solved analytically by employing the following formula:

$$\lambda_{1;2}^2 = \frac{-b \pm \sqrt{b^2 - 4ac}}{2a} \tag{4.6}$$

where

$$a = \beta \int\limits_{-\infty}^{\infty}\int\limits_{-\infty}^{\infty} \mathcal{F}(|w|^4 w)\hat{w}^* d\boldsymbol{k} \ ,$$

$$b = \alpha \int\limits_{-\infty}^{\infty}\int\limits_{-\infty}^{\infty} \mathcal{F}(|w|^2 w)\hat{w}^* d\boldsymbol{k} \ , \tag{4.7}$$

$$c = \int\limits_{-\infty}^{\infty}\int\limits_{-\infty}^{\infty} [\mathcal{F}((V+iW)w) - (\mu + k_x^2)\hat{w}]\hat{w}^* d\boldsymbol{k} \ .$$

Once convergence is reached, the desired soliton is $f(x,y) = \lambda \mathcal{F}^{-1}(\hat{w})$.

This method is configured in a similar manner so that it can be applied to the (1+1)D CQNLS equation, in the absence of the second spatial coordinate y. Furthermore, V and W can be taken as zero, when working without a potential.

4.2 Pseudo-Spectral Renormalization Method

The idea of the Spectral Renormalization Method is to transform the governing equation into Fourier space and determine a convergence factor in order to get a convergent fixed-point iteration method. This method is successful if the governing equation contains nonlinearity with constant homogeneity. However, many physical systems have nonlinearities with different homogeneities such as cubic-saturable nonlinearity.

The convergence factor (λ) in the Spectral Renormalization Method for the CQNLS equation can be directly calculated from the governing equation. However, the

convergence factor for the cubic-saturable case cannot be explicitly obtained from the governing equation, hence a standard nonlinear algebraic solver should be used in order to calculate it at each iteration. To overcome this issue, we introduce the Pseudo-Spectral Renormalization Method [56] where the convergence factor can be explicitly obtained even in the cubic-saturable case.

The idea behind the Pseudo-Spectral Renormalization Method is simple, yet it is a very successful method, especially owing to its speed and accuracy. This method can be applied to any nonlinear system for computing self-localized solitons.

To describe the method, we begin by considering the cubic saturable NLS equation given by Eq. (1.3). Localized wave solutions $u(x,y,z) = f(x,y)e^{i\mu z}$ satisfy

$$-\mu f + f_{xx} + f_{yy} + \frac{|f|^2 f}{1 + s|f|^2} + V_{\mathcal{PT}} f = 0 \,. \tag{4.8}$$

This is a nonlinear eigenvalue problem for f and $\mu > 0$ that is supplemented with the boundary condition $\lim_{(x,y)\to\pm\infty} f(x,y) = 0$. By applying the Fourier transform to the linear part and taking its inverse Fourier transform, one gets

$$-\mathcal{F}^{-1}\{(\mu + k_x^2 + k_y^2)\hat{f}\} + \frac{|f|^2 f}{1 + s|f|^2} + V_{\mathcal{PT}} f = 0 \,. \tag{4.9}$$

In order to get a convergent iteration scheme, define a new variable as $f(x,y) = \lambda w(x,y)$ where $\lambda \neq 0$ is to be determined. Then, w satisfies

$$-\mathcal{F}^{-1}\{(\mu + k_x^2 + k_y^2)\hat{w}\} + \frac{|\lambda|^2 |w|^2 w}{1 + s|\lambda|^2 |w|^2} + V_{\mathcal{PT}} w = 0 \,. \tag{4.10}$$

Multiplying by the denominator and grouping yields

$$|\lambda|^2 |w|^2 \left[(1 + s\,V_{\mathcal{PT}})w - s\,\mathcal{F}^{-1}\{(\mu + k_x^2 + k_y^2)\hat{w}\}\right] = \mathcal{F}^{-1}\{(\mu + k_x^2 + k_y^2)\hat{w}\} - V_{\mathcal{PT}} w. \tag{4.11}$$

By multiplying by the complex conjugate of w, i.e. by w^* and integrating over the entire space, the explicit expression of the convergence factor is found as

$$|\lambda|^2 = \frac{\int\limits_{-\infty}^{\infty}\int\limits_{-\infty}^{\infty} \left(\mathcal{F}^{-1}\{(\mu + k_x^2 + k_y^2)\hat{w}\} - V_{\mathcal{PT}} w\right) w^* dx dy}{\int\limits_{-\infty}^{\infty}\int\limits_{-\infty}^{\infty} \left[(1 + s\,V_{\mathcal{PT}})w - s\,\mathcal{F}^{-1}\{(\mu + k_x^2 + k_y^2)\hat{w}\}\right]|w|^2 w^* dx dy} \,. \tag{4.12}$$

Solving for the first w in Eq. (4.10) yields

$$w = \mathcal{F}^{-1}\left[\frac{1}{(\mu + k_x^2 + k_y^2)}\mathcal{F}\left(\frac{|\lambda|^2 |w|^2 w}{1 + s|\lambda|^2 |w|^2} + V_{\mathcal{PT}} w\right)\right] \,. \tag{4.13}$$

w can be obtained by iterating Eq. (4.13) as

$$w_{n+1} = \mathcal{F}^{-1}\left[\frac{1}{(\mu + k_x^2 + k_y^2)}\mathcal{F}\left(\frac{|\lambda_n|^2|w_n|^2 w_n}{1 + s|\lambda_n|^2|w_n|^2} + V_{\mathcal{PT}}w_n\right)\right], \ n \in \mathbb{N} \qquad (4.14)$$

with the initial condition chosen as a Gaussian type function $w_0 = e^{-x^2-y^2}$. λ_0 is taken as 1 and the other λ_n are calculated by Eq. (4.12). The iteration continues until $|w_n - w_{n-1}| < 10^{-12}$ and the obtained numerical solution $f_n = \lambda_n w_n$ satisfies Eq. (4.8) with an absolute error less than 10^{-12}. Convergence is usually obtained quickly when the mode is strongly localized in the gap.

5. STABILITY ANALYSIS

Obtaining a soliton is usually not enough, especially if it suffers from collapse or blows up in finite time. Thus, it is of great importance to analyze the stability of the obtained solitons. In this chapter, it will be explained how the linear and nonlinear stability properties of the obtained solitons are analyzed.

5.1 Split-Step Method

The split-step method is a numerical method, in which the equation is split into two pieces and integrated consecutively to obtain the numerical solution at the next step.

The method will be first explained and illustrated for linear equations and then for nonlinear equations.

5.1.1 Split-Step Method for Linear Equations

Consider a linear PDE for $u(x,y,z)$ which can be written as

$$u_z = (L+M)u \tag{5.1}$$

where L and M are linear operators independent of z. The exact solution of Eq. (5.1) at $z = h$ can be formally written as

$$u(x,y,h) = e^{h(L+M)}u(x,y,0) \tag{5.2}$$

where h is the step size in z-direction. On the other hand, the formal solutions of the two split equations

$$\begin{aligned} u_z &= Lu \\ u_z &= Mu \end{aligned} \tag{5.3}$$

at $z = h$ can be written as

$$\begin{aligned} u(x,y,h) &= e^{hL}u(x,y,0) \\ u(x,y,h) &= e^{hM}u(x,y,0) \ , \end{aligned} \tag{5.4}$$

27

respectively. If the original equation (5.1) is hard or even impossible to solve but the split equations (5.3) are easily solvable, then the solution of the original equation can be approximated by consecutive splits

$$e^{h(L+M)} \approx e^{b_n hM} e^{a_n hL} e^{b_{n-1} hM} e^{a_{n-1} hL} \dots e^{b_1 hM} e^{a_1 hL} \qquad (5.5)$$

where a_i and b_i $(i = 1\dots n)$ are constant coefficients of the splitting scheme which determine the order of the method. If the difference between the right and left side of Eq. (5.5) is of order $O(h^{n+1})$, then the method is of nth order (accurate in z).

Taking $a_1 = b_1 = 1$ and all the other coefficients zero, yields the following first order splitting scheme

$$e^{h(L+M)} \approx e^{hM} e^{hL} \qquad (5.6)$$

as the difference between

$$
\begin{aligned}
e^{hM} e^{hL} &= \left(1 + hM + \frac{1}{2} h^2 M^2 + O(h^3)\right) \left(1 + hL + \frac{1}{2} h^2 L^2 + O(h^3)\right) \\
&= 1 + hL + \frac{1}{2} h^2 L^2 + hM + h^2 ML + \frac{1}{2} h^2 M^2 + O(h^3) \\
&= 1 + hL + hM + \frac{1}{2} h^2 L^2 + \frac{1}{2} h^2 M^2 + h^2 ML + O(h^3)
\end{aligned}
\qquad (5.7)
$$

and

$$
\begin{aligned}
e^{h(L+M)} &= 1 + h(L+M) + \frac{1}{2} h^2 (L+M)^2 + O(h^3) \\
&= 1 + hL + hM + \frac{1}{2} h^2 L^2 + \frac{1}{2} h^2 LM + \frac{1}{2} h^2 ML + \frac{1}{2} h^2 M^2 + O(h^3)
\end{aligned}
\qquad (5.8)
$$

is

$$\frac{1}{2} h^2 (ML - LM) = O(h^2) . \qquad (5.9)$$

Taking $a_1 = a_2 = \frac{1}{2}$, $b_1 = 1$ and all the other coefficients zero, yields the following second order splitting scheme

$$e^{h(L+M)} \approx e^{\frac{1}{2} hL} e^{hM} e^{\frac{1}{2} hL} \qquad (5.10)$$

as the difference between

$$e^{\frac{1}{2}hL}e^{hM}e^{\frac{1}{2}hL}$$

$$= \left(1 + \frac{1}{2}hL + \frac{1}{8}h^2L^2 + \frac{1}{48}h^3L^3 + O(h^4)\right) \cdot \left(1 + hM + \frac{1}{2}h^2M^2 + \frac{1}{6}h^3M^3 + O(h^4)\right)$$

$$\cdot \left(1 + \frac{1}{2}hL + \frac{1}{8}h^2L^2 + \frac{1}{48}h^3L^3 + O(h^4)\right)$$

$$= \left(\begin{aligned} &1 + hM + \frac{1}{2}h^2M^2 + \frac{1}{6}h^3M^3 + \frac{1}{2}hL + \frac{1}{2}h^2LM + \frac{1}{4}h^3LM^2 + \frac{1}{8}h^2L^2 \\ &+ \frac{1}{8}h^3L^2M + \frac{1}{48}h^3L^3 + O(h^4) \end{aligned}\right)$$

$$\cdot \left(1 + \frac{1}{2}hL + \frac{1}{8}h^2L^2 + \frac{1}{48}h^3L^3 + O(h^4)\right)$$

$$= 1 + \frac{1}{2}hL + \frac{1}{8}h^2L^2 + \frac{1}{48}h^3L^3 + hM + \frac{1}{2}h^2ML + \frac{1}{8}h^3ML^2 + \frac{1}{2}h^2M^2 + \frac{1}{4}h^3M^2L$$

$$+ \frac{1}{6}h^3M^3 + \frac{1}{2}hL + \frac{1}{4}h^2L^2 + \frac{1}{16}h^3L^3 + \frac{1}{2}h^2LM + \frac{1}{4}h^3LML + \frac{1}{4}h^3LM^2$$

$$+ \frac{1}{8}h^2L^2 + \frac{1}{16}h^3L^3 + \frac{1}{8}h^3L^2M + \frac{1}{48}h^3L^3 + O(h^4)$$

$$= 1 + h(L+M) + \frac{1}{2}h^2(L^2 + LM + ML + M^2)$$

$$+ h^3\left(\frac{1}{6}L^3 + \frac{1}{8}L^2M + \frac{1}{4}LML + \frac{1}{8}ML^2 + \frac{1}{4}M^2L + \frac{1}{4}LM^2 + \frac{1}{6}M^3\right) + O(h^4)$$

$$\tag{5.11}$$

and

$$e^{h(L+M)} = 1 + h(L+M) + \frac{1}{2}h^2(L+M)^2 + \frac{1}{6}h^3(L+M)^3 + O(h^4)$$

$$= 1 + h(L+M) + \frac{1}{2}h^2(L^2 + LM + ML + M^2)$$

$$+ \frac{1}{6}h^3(L^3 + L^2M + LML + LM^2 + ML^2 + MLM + M^2L + M^3) + O(h^4)$$

$$\tag{5.12}$$

is

$$h^3\left(-\frac{1}{24}L^2M + \frac{1}{12}LML - \frac{1}{24}ML^2 + \frac{1}{12}M^2L - \frac{1}{6}MLM + \frac{1}{12}LM^2\right) = O(h^3). \tag{5.13}$$

In the literature, the latter splitting is known as *Strang splitting* named after Gilbert Strang [57].

Note that the differences found in Eq. (5.9) and (5.13) are

$$\frac{1}{2}h^2(ML - LM) = \frac{1}{2}[hM, hL] \tag{5.14}$$

29

and

$$h^3(-\frac{1}{24}L^2M + \frac{1}{12}LML - \frac{1}{24}ML^2 + \frac{1}{12}M^2L - \frac{1}{6}MLM + \frac{1}{12}LM^2)$$

$$= \frac{h^3}{12}(M^2L - 2MLM + LM^2) - \frac{h^3}{24}(L^2M - 2LML + ML^2) \qquad (5.15)$$

$$= \frac{h^3}{12}[M,[M,L]] - \frac{h^3}{24}[L,[L,M]] = \frac{1}{12}[hM,[hM,hL]] - \frac{1}{24}[hL,[hL,hM]]$$

respectively, where $[\ \cdot\ ,\ \cdot\ ]$ is the Lie bracket. These could have been also derived using the Baker–Campbell–Hausdorff formula [58]

$$\ln(e^X e^Y) = X + Y + \frac{1}{2}[X,Y] + \frac{1}{12}([X,[X,Y]] + [Y,[Y,X]]) + ... \qquad (5.16)$$

Higher order schemes can be constructed by taking symmetric product of lower order schemes with the help of this formula. A fourth order split-step scheme is given for instance by taking

$$a_1 = a_4 = \frac{c}{2}\ ,\ a_2 = a_3 = \frac{1-c}{2}\ ,\ b_1 = b_3 = c\ ,\ b_2 = 1 - 2c \text{ where } c = \frac{1}{2 - \sqrt[3]{2}} \qquad (5.17)$$

and all the other coefficients zero. Owing to its high order, this fourth order split-step scheme will be utilized in our stability analysis.

Below, split-step method using Strang splitting will be illustrated with a simple linear example.

Consider the problem $u_z = 3u$ with the initial condition $u(0) = 1$. It can be easily found that its exact solution is $u(z) = e^{3z}$. Consider the splitting $u_z = u + 2u$, i.e. $L = 1$ and $M = 2$.

1. Solving $u_z = u$ with $u(0) = 1$ yields $u(z) = e^z$. Advancing half step gives $u(\frac{1}{2}h) = e^{\frac{1}{2}h}$.

2. Solving $u_z = 2u$ with $u(0) = e^{\frac{1}{2}h}$ yields $u(z) = e^{\frac{1}{2}h}e^{2z}$. Advancing one step gives $u(h) = e^{\frac{1}{2}h}e^{2h} = e^{\frac{5}{2}h}$.

3. Solving $u_z = u$ with $u(0) = e^{\frac{5}{2}h}$ yields $u(z) = e^{\frac{5}{2}h}e^z$. Advancing half step gives $u(\frac{1}{2}h) = e^{\frac{5}{2}h}e^{\frac{1}{2}h} = e^{3h}$.

That is, after one iteration of Strang splitting, one obtains $u(h) = e^{3h}$. As L and M were commutative operators in this example, the splitting yielded the exact solution.

5.1.2 Split-Step Method for Nonlinear Equations

Consider a nonlinear PDE for $u(x, y, z)$ which can be written as

$$u_z = (M + N)u \tag{5.18}$$

where M and N are operators independent of z and at least one of them, say N is nonlinear. A common practice in the literature is to use the split-step schemes developed for the linear equations also for the nonlinear ones. Their use is trivial, however their order is not. In his book, Yang verifies that each of the three schemes given in the previous section have the same order in the nonlinear case [47].

Below, split-step method using Strang splitting will be illustrated with a simple nonlinear example.

Consider the problem $u_z = u^2 - u$ with the initial condition $u(0) = 0.8$. It can be easily found that its exact solution is $u(z) = \dfrac{4}{e^z + 4}$.

Let $M = -u$ and $N = u^2$.

1. Solving $u_z = -u$ with $u(0) = 0.8$ yields $u(z) = 0.8e^{-z}$. Advancing half step gives $u(\frac{1}{2}h) = 0.8e^{-\frac{1}{2}h}$.

2. Solving $u_z = u^2$ with $u(0) = 0.8e^{-\frac{1}{2}h}$ yields $u(z) = \dfrac{4}{5e^{\frac{1}{2}h} - 4z}$. Advancing one step gives $u(h) = \dfrac{4}{5e^{\frac{1}{2}h} - 4h}$.

3. Solving $u_z = -u$ with $u(0) = \dfrac{4}{5e^{\frac{1}{2}h} - 4h}$ yields $u(z) = \dfrac{4e^{-z}}{5e^{\frac{1}{2}h} - 4h}$. Advancing half step gives $u(\frac{1}{2}h) = \dfrac{4}{5e^h - 4he^{\frac{1}{2}h}}$.

That is, after one iteration of Strang splitting, one obtains $u(z) = \dfrac{4}{5e^z - 4ze^{\frac{1}{2}z}}$.

Conversely, let $M = u^2$ and $N = -u$.

1. Solving $u_z = u^2$ with $u(0) = 0.8$ yields $u(z) = \dfrac{4}{5 - 4z}$. Advancing half step gives $u(\frac{1}{2}h) = \dfrac{4}{5 - 2h}$.

2. Solving $u_z = -u$ with $u(0) = \dfrac{4}{5 - 2h}$ yields $u(z) = \dfrac{4e^{-z}}{5 - 2h}$. Advancing one step gives $u(h) = \dfrac{4e^{-h}}{5 - 2h}$.
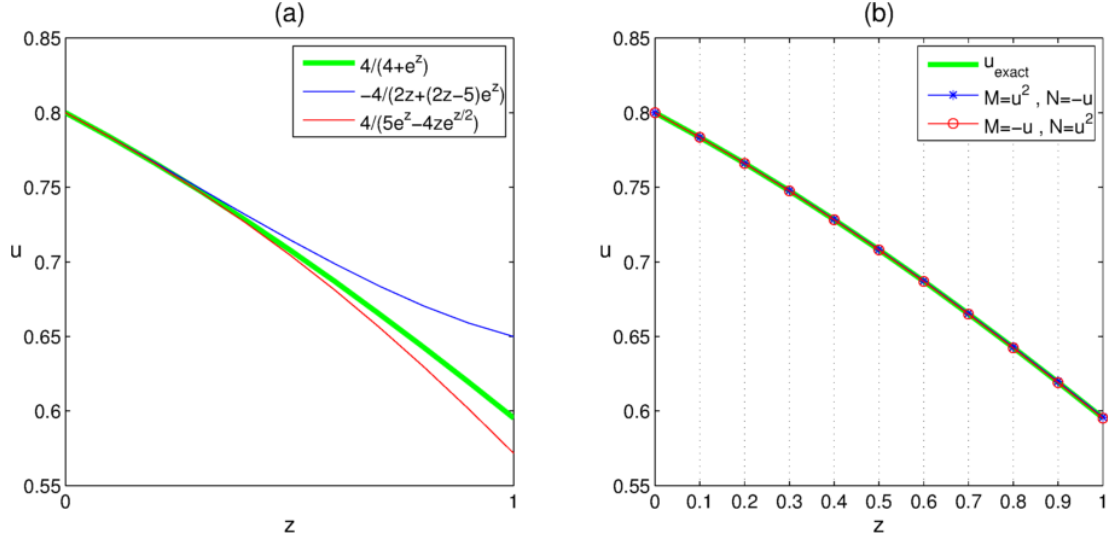
Figure 5.1 : Exact solution of the equation $u_z = u^2 - u$ in comparison with the numerical solutions obtained by means of split-step method using Strang splitting with step size (a) $h = 1$ and (b) $h = 0.1$.

3. Solving $u_z = u^2$ with $u(0) = \dfrac{4e^{-h}}{5 - 2h}$ yields $u(z) = \dfrac{-4}{4z + (2h - 5)e^h}$. Advancing half step gives $u(\tfrac{1}{2}h) = \dfrac{-4}{2h + (2h - 5)e^h}$.

That is, after one iteration of Strang splitting, one obtains $u(z) = \dfrac{-4}{2z + (2z - 5)e^z}$.

The three different equations obtained for $u(z)$ are plotted for the interval $[0; 1]$ in Figure 5.1(a). As it can be seen from the graph, numerical solutions are only valid in a small neighborhood of the initial value. Thus, the step size is chosen as $h = 0.1$ and the calculations above are repeated ten times in order to reach the solution at $z = 1$. The resulting graph is seen in Figure 5.1(b) where the numerical solutions are very close to the exact solution.

5.2 Nonlinear Stability

A soliton is considered nonlinearly stable if it conserves its shape, location and maximum amplitude during direct simulations. To study their nonlinear stability, obtained solitons are computed over a long distance. For this purpose, split-step Fourier method is employed to advance in z.

The split-step Fourier method is a pseudo-spectral numerical method for solving nonlinear PDEs like the NLS equation due to its easy implementation and speed compared to other methods, notably finite difference methods [59]. It is actually

32

a split-step method whose linear step is taken in the frequency domain while the nonlinear step is taken in the time domain. The name comes from the Fourier and inverse Fourier transforms which are necessary for going back and forth between these domains.

Consider Eq. (1.1) which can be rewritten as

$$u_z = i(\partial_{xx} + \partial_{yy})u + i(\alpha|u|^2 + \beta|u|^4 + V_{\mathcal{PT}})u \tag{5.19}$$

and hence can be split as in Eq. (5.18) with the linear operator $M = i(\partial_{xx} + \partial_{yy})$ and the nonlinear operator $N = i(\alpha|u|^2 + \beta|u|^4 + V_{\mathcal{PT}})$.

The linear step $u_z = Mu$ is solved by means of Fourier transform. Taking the Fourier transform of both sides of

$$u_z = i(\partial_{xx} + \partial_{yy})u \tag{5.20}$$

gives

$$\hat{u}_z = i\left((-ik_x)^2 + (-ik_y)^2\right)\hat{u} = -i(k_x{}^2 + k_y{}^2)\hat{u} . \tag{5.21}$$

This is nothing but an ordinary differential equation (ODE) of $\hat{u}$ and its exact solution is given by

$$\hat{u} = \hat{C}_1 e^{-i(k_x{}^2 + k_y{}^2)z} \quad \Rightarrow \quad u = \mathcal{F}^{-1}\left(\hat{C}_1 e^{-i(k_x{}^2 + k_y{}^2)z}\right) . \tag{5.22}$$

The nonlinear step $u_z = Nu$, i.e.

$$u_z = i(\alpha|u|^2 + \beta|u|^4 + V_{\mathcal{PT}})u \tag{5.23}$$

has the exact solution

$$u = C_2 e^{i(\alpha|u|^2 + \beta|u|^4 + V_{\mathcal{PT}})z} . \tag{5.24}$$

Having found solutions to both parts, the split-step Fourier method can now be employed for the CQNLS equation by using any splitting scheme.

5.3 Linear Stability

Linear stability will be investigated by acquiring and analyzing the linear spectrum and/or by evolving the linearized solitons.

5.3.1 Linear Spectrum

Linear stability spectrum or short, linear spectrum are the eigenvalues of the linear stability operator of a soliton. These eigenvalues give information about the linear stability of a soliton.

Consider the following (2+1)D NLS equation having general type of nonlinearities:

$$
iu_z(x,y,z) + u_{xx}(x,y,z) + u_{yy}(x,y,z) + F(|u(x,y,z)|^2)u(x,y,z)
$$
$$
+ V_{\mathcal{PT}}(x,y)u(x,y,z) = 0 \tag{5.25}
$$

where $F(\cdot) \in \mathbb{R}$ and $F(0) = 0$. As explained before, Eq. (5.25) admits soliton solutions of the form $u(x,y,z) = f(x,y)\,e^{i\mu z}$. Substituting

$$
u_z = i\mu f e^{i\mu z}
$$
$$
u_{xx} = f_{xx}\,e^{i\mu z}
$$
$$
u_{yy} = f_{yy}\,e^{i\mu z} \tag{5.26}
$$
$$
|u|^2 = uu^* = fe^{i\mu z}f^*e^{-i\mu z} = ff^* = |f|^2
$$

in Eq. (5.25) and multiplying by $e^{-i\mu z}$ gives

$$
-\mu f + f_{xx} + f_{yy} + F(|f|^2)f + V_{\mathcal{PT}}f = 0. \tag{5.27}
$$

To analyze the linear stability, the soliton solution is perturbed as follows

$$
u(x,y,z) = \Big[f(x,y) + g(x,y)e^{\sigma z} + h^*(x,y)e^{\sigma^* z} \Big] e^{i\mu z} \tag{5.28}
$$

where g and h are perturbation eigenfunctions and σ is the eigenvalue.

$$
u_z = \Big(\sigma g e^{\sigma z} + \sigma^* h^* e^{\sigma^* z} + i\mu f + i\mu g e^{\sigma z} + i\mu h^* e^{\sigma^* z} \Big) e^{i\mu z}
$$
$$
u_{xx} = \Big(f_{xx} + g_{xx}e^{\sigma z} + h^*_{xx}e^{\sigma^* z} \Big) e^{i\mu z} \tag{5.29}
$$
$$
u_{yy} = \Big(f_{yy} + g_{yy}e^{\sigma z} + h^*_{yy}e^{\sigma^* z} \Big) e^{i\mu z}
$$

$$
|u|^2 = uu^* = \Big(f + g e^{\sigma z} + h^* e^{\sigma^* z} \Big) e^{i\mu z} \Big(f^* + g^* e^{\sigma^* z} + h e^{\sigma z} \Big) e^{-i\mu z}
$$
$$
= ff^* + fg^*e^{\sigma^* z} + fhe^{\sigma z} + f^*ge^{\sigma z} + gg^*e^{(\sigma+\sigma^*)z}
$$
$$
+ ghe^{2\sigma z} + f^*h^*e^{\sigma^* z} + g^*h^*e^{2\sigma^* z} + hh^*e^{(\sigma+\sigma^*)z} \tag{5.30}
$$
$$
\simeq |f|^2 + \Big(g^*e^{\sigma^* z} + he^{\sigma z} \Big) f + \Big(ge^{\sigma z} + h^*e^{\sigma^* z} \Big) f^*
$$

Using linear Taylor expansion $F(x+h) = F(x) + hF'(x) + O(h^2)$,

$$F(|u|^2) = F\left(|f|^2 + \left[\left(g^*e^{\sigma^*z} + he^{\sigma z}\right)f + \left(ge^{\sigma z} + h^*e^{\sigma^*z}\right)f^*\right]\right)$$
$$\simeq F(|f|^2) + \left[\left(g^*e^{\sigma^*z} + he^{\sigma z}\right)f + \left(ge^{\sigma z} + h^*e^{\sigma^*z}\right)f^*\right]F'(|f|^2) .$$

(5.31)

Hence,

$$F(|u|^2)ue^{-i\mu z}$$
$$= F(|f|^2)f + \left[\left(g^*e^{\sigma^*z} + he^{\sigma z}\right)f^2 + \left(ge^{\sigma z} + h^*e^{\sigma^*z}\right)|f|^2\right]F'(|f|^2)$$
$$+ F(|f|^2)ge^{\sigma z}$$
$$+ \left[\left(gg^*e^{(\sigma+\sigma^*)z} + ghe^{2\sigma z}\right)f + \left(g^2e^{2\sigma z} + gh^*e^{(\sigma+\sigma^*)z}\right)f^*\right]F'(|f|^2)$$
$$+ F(|f|^2)h^*e^{\sigma^*z}$$
$$+ \left[\left(g^*h^*e^{2\sigma^*z} + |h|^2e^{(\sigma+\sigma^*)z}\right)f + \left(gh^*e^{(\sigma+\sigma^*)z} + (h^*)^2e^{2\sigma^*z}\right)f^*\right]F'(|f|^2)$$
$$\simeq F(|f|^2)\left[f + ge^{\sigma z} + h^*e^{\sigma^*z}\right]$$
$$+ F'(|f|^2)\left[\left(f^2h + |f|^2g\right)e^{\sigma z} + \left(f^2g^* + |f|^2h^*\right)e^{\sigma^*z}\right] .$$

(5.32)

Substituting Eq. (5.28), (5.29) and (5.32) into Eq. (5.25) gives

$$i\left(\sigma ge^{\sigma z} + \sigma^*h^*e^{\sigma^*z} + i\mu f + i\mu ge^{\sigma z} + i\mu h^*e^{\sigma^*z}\right)e^{i\mu z}$$
$$+ \left(f_{xx} + g_{xx}e^{\sigma z} + h_{xx}^*e^{\sigma^*z}\right)e^{i\mu z}$$
$$+ \left(f_{yy} + g_{yy}e^{\sigma z} + h_{yy}^*e^{\sigma^*z}\right)e^{i\mu z}$$
$$+ \left\{\begin{matrix} F(|f|^2)\left[f + ge^{\sigma z} + h^*e^{\sigma^*z}\right] \\ + F'(|f|^2)\left[\left(f^2h + |f|^2g\right)e^{\sigma z} + \left(f^2g^* + |f|^2h^*\right)e^{\sigma^*z}\right] \end{matrix}\right\}e^{i\mu z}$$
$$+ V_{\mathcal{PT}}\left(f + ge^{\sigma z} + h^*e^{\sigma^*z}\right)e^{i\mu z} = 0 .$$

(5.33)

Grouping the terms and multiplying by $e^{-i\mu z}$ yields

$$\left[-\mu f + f_{xx} + f_{yy} + F(|f|^2)f + V_{\mathcal{PT}}f\right]$$
$$+ \left[i\sigma g - \mu g + g_{xx} + g_{yy} + F(|f|^2)g + \left(f^2h + |f|^2g\right)F'(|f|^2) + V_{\mathcal{PT}}g\right]e^{\sigma z}$$
$$+ \left[i\sigma^*h^* - \mu h^* + h_{xx}^* + h_{yy}^* + F(|f|^2)h^* + \left(f^2g^* + |f|^2h^*\right)F'(|f|^2) + V_{\mathcal{PT}}h^*\right]e^{\sigma^*z}$$
$$= 0 .$$

(5.34)

Here, the first bracket is identically zero as f is a solution (see Eq. (5.27)). For Eq. (5.34) to hold true, the factors of the exponentials must be zero simultaneously. Hence, one has on one hand

$$i\sigma g - \mu g + g_{xx} + g_{yy} + F(|f|^2)g + \left(f^2h + |f|^2g\right)F'(|f|^2) + V_{\mathcal{PT}}g = 0 \qquad (5.35)$$

which can be rewritten as

$$g_{xx} + g_{yy} + \left[F(|f|^2) + F'(|f|^2)|f|^2 - \mu + V_{\mathcal{PT}} \right] g + F'(|f|^2) f^2 h = -i\sigma g \qquad (5.36)$$

and on the other hand

$$i\sigma^* h^* - \mu h^* + h_{xx}^* + h_{yy}^* + F(|f|^2)h^* + \left(f^2 g^* + |f|^2 h^* \right) F'(|f|^2) + V_{\mathcal{PT}} h^* = 0 \quad (5.37)$$

which can be rewritten as

$$h_{xx}^* + h_{yy}^* + \left[F(|f|^2) + F'(|f|^2)|f|^2 - \mu + V_{\mathcal{PT}} \right] h^* + F'(|f|^2) f^2 g^* = -i\sigma^* h^*. \quad (5.38)$$

Taking the conjugate of Eq. (5.38) gives

$$h_{xx} + h_{yy} + \left[F(|f|^2) + F'(|f|^2)|f|^2 - \mu + V_{\mathcal{PT}}^* \right] h + F'(|f|^2)(f^2)^* g = i\sigma h. \quad (5.39)$$

Multiplying Eq. (5.39) by -1 gives

$$-h_{xx} - h_{yy} - \left[F(|f|^2) + F'(|f|^2)|f|^2 - \mu + V_{\mathcal{PT}}^* \right] h - F'(|f|^2)(f^2)^* g = -i\sigma h. \quad (5.40)$$

Writing Eq. (5.36) and (5.40) in matrix form yields

$$i \begin{bmatrix} L_1 & L_2 \\ -L_2{}^* & -L_1{}^* \end{bmatrix} \begin{bmatrix} g \\ h \end{bmatrix} = \sigma \begin{bmatrix} g \\ h \end{bmatrix} \qquad (5.41)$$

where

$$\begin{aligned} L_1 &= \partial_{xx} + \partial_{yy} + F(|f|^2) + F'(|f|^2)|f|^2 - \mu + V_{\mathcal{PT}} \\ L_2 &= F'(|f|^2) f^2 . \end{aligned} \qquad (5.42)$$

For the cubic-quintic nonlinearity,

$$\begin{aligned} F(x) &= \alpha x + \beta x^2 \\ F'(x) &= \alpha + 2\beta x . \end{aligned} \qquad (5.43)$$

Using Eq. (5.43) in Eq. (5.42) yields

$$\begin{aligned} L_1 &= \partial_{xx} + \partial_{yy} + 2\alpha |f|^2 + 3\beta |f|^4 - \mu + V_{\mathcal{PT}} \\ L_2 &= \alpha f^2 + 2\beta f^3 f^* . \end{aligned} \qquad (5.44)$$

For only the cubic nonlinearity, Eq. (5.44) reduces to

$$\begin{aligned} L_1 &= \partial_{xx} + \partial_{yy} + 2\alpha |f|^2 - \mu + V_{\mathcal{PT}} \\ L_2 &= \alpha f^2 \end{aligned} \qquad (5.45)$$

36

by taking $\beta = 0$. For only the quintic nonlinearity, Eq. (5.44) reduces to

$$L_1 = \partial_{xx} + \partial_{yy} + 3\beta |f|^4 - \mu + V_{\mathcal{PT}}$$

$$L_2 = 2\beta f^3 f^*$$

(5.46)

by taking $\alpha = 0$. If the soliton and potential are real, i.e. $f, V_{\mathcal{PT}} \in \mathbb{R}$, Eq. (5.41) becomes

$$i \begin{bmatrix} L_1 & L_2 \\ -L_2 & -L_1 \end{bmatrix} \begin{bmatrix} g \\ h \end{bmatrix} = \sigma \begin{bmatrix} g \\ h \end{bmatrix}$$

(5.47)

where

$$L_1 = \partial_{xx} + \partial_{yy} + 2\alpha f^2 + 3\beta f^4 - \mu + V_{\mathcal{PT}}$$

$$L_2 = \alpha f^2 + 2\beta f^4 \ .$$

(5.48)

Similar analysis can be done for the (1+1)D CQNLS equation, in the absence of the second spatial coordinate y. Furthermore, $V_{\mathcal{PT}}$ can be taken as zero, when working without a potential.

To investigate the linear stability of the lattice solitons in cubic-saturable media, we perturb the solutions to Eq. (1.3) and linearize them in a similar manner to get

$$i \begin{bmatrix} L_1 & L_2 \\ -L_2^* & -L_1^* \end{bmatrix} \begin{bmatrix} g \\ h \end{bmatrix} = \sigma \begin{bmatrix} g \\ h \end{bmatrix}$$

(5.49)

with

$$L_1 = \partial_{xx} + \partial_{yy} + \frac{|f|^2(2 + s|f|^2)}{(1 + s|f|^2)^2} - \mu + V_{\mathcal{PT}}$$

$$L_2 = \frac{f^2}{(1 + s|f|^2)^2} \ .$$

(5.50)

In any case, the eigenvalues σ can be calculated numerically by some eigenvalue algorithm (see [47]). If any of the calculated eigenvalues in the spectrum has a positive real part, then the soliton will blow up as z grows due to the exponential term of the perturbation in Eq. (5.28), in other words the soliton is linearly unstable. If however the spectrum only consists of pure imaginary eigenvalues, the perturbations will only cause oscillations and in this case, one can speak of linear stability [60].

5.3.2 Linear Evolution

To analyze the linear stability, the soliton solution to Eq. (5.25) is perturbed as follows

$$u(x,y,z) = [f(x,y) + \varepsilon g(x,y,z)] e^{i\mu z}$$

(5.51)

37

where $\varepsilon \ll 1$. Henceforth, one has

$$
\begin{aligned}
u_z &= \left[\varepsilon g_z + (f + \varepsilon g) i\mu \right] e^{i\mu z} = \left[i\mu f + \varepsilon (i\mu g + g_z) \right] e^{i\mu z} \\
u_{xx} &= (f_{xx} + \varepsilon g_{xx}) e^{i\mu z} \\
u_{yy} &= (f_{yy} + \varepsilon g_{yy}) e^{i\mu z}
\end{aligned}
\tag{5.52}
$$

and

$$
\begin{aligned}
|u|^2 = uu^* &= (f + \varepsilon g) e^{i\mu z} (f^* + \varepsilon g^*) e^{-i\mu z} \\
&= ff^* + \varepsilon fg^* + \varepsilon f^* g + \varepsilon^2 gg^* \\
&= |f|^2 + \varepsilon (fg^* + f^* g) + O(\varepsilon^2) .
\end{aligned}
\tag{5.53}
$$

Linearizing Eq. (5.53) with respect to ε yields

$$
|u|^2 \cong |f|^2 + \varepsilon (fg^* + f^* g) .
\tag{5.54}
$$

Using linear Taylor expansion $F(x+h) \cong F(x) + hF'(x)$,

$$
\begin{aligned}
F(|u|^2) &= F(|f|^2 + \varepsilon (fg^* + f^* g)) \\
&\cong F(|f|^2) + \varepsilon (fg^* + f^* g) F'(|f|^2) .
\end{aligned}
\tag{5.55}
$$

Substituting Eq. (5.51), (5.52) and (5.55) into Eq. (5.25) gives

$$
\left\{
\begin{aligned}
&-\mu f + \varepsilon(-\mu g + ig_z) + f_{xx} + \varepsilon g_{xx} + f_{yy} + \varepsilon g_{yy} \\
&+ \varepsilon \left[F(|f|^2)g + F'(|f|^2)f^2 g^* + F'(|f|^2)|f|^2 g \right] \\
&+ F(|f|^2)f + V_{\mathcal{PT}} f + \varepsilon V_{\mathcal{PT}} g
\end{aligned}
\right\} e^{i\mu z} = 0 .
\tag{5.56}
$$

Grouping the terms and multiplying by $e^{-i\mu z}$ yields

$$
\begin{aligned}
&\left[-\mu f + f_{xx} + f_{yy} + F(|f|^2)f + V_{\mathcal{PT}} f \right] \\
&+ \varepsilon \left[ig_z - \mu g + g_{xx} + g_{yy} + F(|f|^2)g + F'(|f|^2)f^2 g^* + F'(|f|^2)|f|^2 g + V_{\mathcal{PT}} g \right] = 0 .
\end{aligned}
\tag{5.57}
$$

Here, the first bracket is identically zero as f is a solution (see Eq. (5.27)). For Eq. (5.57) to hold true, the second bracket must be equal to zero, too. Hence, one has

$$
ig_z - \mu g + g_{xx} + g_{yy} + F(|f|^2)g + F'(|f|^2)f^2 g^* + F'(|f|^2)|f|^2 g + V_{\mathcal{PT}} g = 0
\tag{5.58}
$$

which can be rewritten as

$$
g_z = i(g_{xx} + g_{yy}) + i \left[-\mu + F(|f|^2) + F'(|f|^2)|f|^2 + V_{\mathcal{PT}} \right] g + iF'(|f|^2)f^2 g^*
\tag{5.59}
$$

and can be hence split as

$$
\begin{aligned}
&I) \ g_z = i(\partial_{xx} + \partial_{yy})g \\
&II) \ g_z = i \left[-\mu + F(|f|^2) + F'(|f|^2)|f|^2 + V_{\mathcal{PT}} \right] g + iF'(|f|^2)f^2 g^*
\end{aligned}
\tag{5.60}
$$

The first step is solved by means of Fourier transform:

$$g = \mathcal{F}^{-1}\left(\hat{C}_1 e^{-i(k_x^2 + k_y^2)z}\right) \tag{5.61}$$

as explained in Section 5.2. To solve the second step, first consider the equation

$$g_z = Ag + Bg^* \text{ with } g(0) = C_2 . \tag{5.62}$$

Expressing g as the sum of its real and imaginary parts, i.e. $g = \mathrm{Re}(g) + i\,\mathrm{Im}(g)$ and substituting this in Eq. (5.62) results in

$$[\mathrm{Re}(g)]_z + i[\mathrm{Im}(g)]_z = [(A+B)\,\mathrm{Re}(g)] + i\,[(A-B)\,\mathrm{Im}(g)] \tag{5.63}$$

with

$$[\mathrm{Re}(g)]\,(0) = \mathrm{Re}(C_2) \text{ and } [\mathrm{Im}(g)]\,(0) = \mathrm{Im}(C_2) . \tag{5.64}$$

For Eq. (5.63) to hold true, the real and imaginary parts must be equal to each other, respectively. That is, one obtains the following two equations

$$[\mathrm{Re}(g)]_z = (A+B)\,\mathrm{Re}(g) \text{ with } [\mathrm{Re}(g)]\,(0) = \mathrm{Re}(C_2)$$
$$[\mathrm{Im}(g)]_z = (A-B)\,\mathrm{Im}(g) \text{ with } [\mathrm{Im}(g)]\,(0) = \mathrm{Im}(C_2) \tag{5.65}$$

whose solutions are

$$\mathrm{Re}(g) = \mathrm{Re}(C_2)e^{(A+B)z}$$
$$\mathrm{Im}(g) = \mathrm{Im}(C_2)e^{(A-B)z} , \tag{5.66}$$

respectively. Hence, the solution of Eq. (5.62) is given by

$$g = \mathrm{Re}(C_2)e^{(A+B)z} + i\,\mathrm{Im}(C_2)e^{(A-B)z} . \tag{5.67}$$

Using this result, the solution of the second step in Eq. (5.60) is obtained as

$$g = \mathrm{Re}(C_2)e^{i\left[-\mu + F(|f|^2) + F'(|f|^2)(|f|^2 + f^2) + V_{\mathcal{PT}}\right]z}$$
$$+ i\,\mathrm{Im}(C_2)e^{i\left[-\mu + F(|f|^2) + F'(|f|^2)(|f|^2 - f^2) + V_{\mathcal{PT}}\right]z} . \tag{5.68}$$

For the cubic-quintic nonlinearity,

$$F(x) = \alpha x + \beta x^2$$
$$F'(x) = \alpha + 2\beta x . \tag{5.69}$$

Using Eq. (5.69) in Eq. (5.68) yields

$$g = \mathrm{Re}(C_2)e^{i\left[-\mu + \alpha(2|f|^2 + f^2) + 3\beta|f|^4 + 2|f|^2 f^2 + V_{\mathcal{PT}}\right]z}$$
$$+ i\,\mathrm{Im}(C_2)e^{i\left[-\mu + \alpha(2|f|^2 - f^2) + 3\beta|f|^4 - 2|f|^2 f^2 + V_{\mathcal{PT}}\right]z} . \tag{5.70}$$

39

For only the cubic nonlinearity, Eq. (5.70) reduces to

$$g = \text{Re}(C_2) e^{i\left[-\mu+\alpha(2|f|^2+f^2)+2|f|^2f^2+V_{\mathcal{PT}}\right]z} + i\,\text{Im}(C_2) e^{i\left[-\mu+\alpha(2|f|^2-f^2)-2|f|^2f^2+V_{\mathcal{PT}}\right]z}$$

(5.71)

by taking $\beta = 0$. For only the quintic nonlinearity, Eq. (5.70) reduces to

$$g = \text{Re}(C_2) e^{i\left[-\mu+3\beta|f|^4+2|f|^2f^2+V_{\mathcal{PT}}\right]z} + i\,\text{Im}(C_2) e^{i\left[-\mu+3\beta|f|^4-2|f|^2f^2+V_{\mathcal{PT}}\right]z} \quad (5.72)$$

by taking $\alpha = 0$.

In any case, g can be evolved using a splitting scheme. We will use the fourth order split-step scheme given in (5.17) in our analysis. If g stays almost the same during a long distance evolution along the z-direction, one can speak of linear stability of the soliton. If however, the amplitude of g starts to grow continuously leading to a blow up, the soliton is said to be linearly unstable.

6. SOLITONS OF THE (1+1)D CQNLS EQUATION

This chapter deals with the soliton solutions of the (1+1)D CQNLS equation.

6.1 CQNLS without Potential

First, the (1+1)D CQNLS equation is considered without any potential.

6.1.1 Analytical Solutions

Consider the following (1+1)D CQNLS equation:

$$iu_z(x,z) + u_{xx}(x,z) + \alpha|u(x,z)|^2 u(x,z) + \beta|u(x,z)|^4 u(x,z) = 0 . \tag{6.1}$$

To obtain real-valued soliton solutions, the following ansatz is used:

$$u(x,z) = f(x)e^{i\mu z} \text{ where } \lim_{x\to\pm\infty} f(x) = 0 \text{ and } \mu > 0 . \tag{6.2}$$

Substituting

$$u_z = i\mu f e^{i\mu z}$$
$$u_{xx} = f'' e^{i\mu z} \tag{6.3}$$
$$|u|^2 = f e^{i\mu z} f e^{-i\mu z} = f^2$$

into Eq. (6.1) yields

$$\left(-\mu f + f'' + \alpha f^3 + \beta f^5\right) e^{i\mu z} = 0 . \tag{6.4}$$

Multiplying Eq. (6.4) by $2f'e^{-i\mu z}$ gives

$$2f'f'' - 2\mu f f' + 2\alpha f^3 f' + 2\beta f^5 f' = 0 . \tag{6.5}$$

Integrating Eq. (6.5) with respect to x yields

$$(f')^2 - \mu f^2 + \frac{\alpha}{2}f^4 + \frac{\beta}{3}f^6 = C_1 . \tag{6.6}$$

The localization conditions $\lim_{x\to\pm\infty} f(x) = 0$ and $\lim_{x\to\pm\infty} f'(x) = 0$ require the integration constant C_1 to be zero:

$$(f')^2 - \mu f^2 + \frac{\alpha}{2}f^4 + \frac{\beta}{3}f^6 = 0 . \tag{6.7}$$

41

Substituting

$$f(x) = \frac{1}{\sqrt{y(x)}} \quad \text{i.e.} \quad f = y^{-0.5}$$

$$\text{and} \quad f' = -\frac{y^{-1.5}}{2} y' \tag{6.8}$$

into Eq. (6.7) yields

$$\frac{y^{-3}}{4}(y')^2 - \mu y^{-1} + \frac{\alpha}{2} y^{-2} + \frac{\beta}{3} y^{-3} = 0 . \tag{6.9}$$

Multiplying Eq. (6.9) by $4y^3$ gives

$$(y')^2 - 4\mu y^2 + 2\alpha y + \frac{4\beta}{3} = 0 . \tag{6.10}$$

Eq. (6.10) is a separable ODE of first order as follows:

$$\frac{dy}{dx} = \pm\sqrt{4\mu y^2 - 2\alpha y - \frac{4\beta}{3}} . \tag{6.11}$$

Separating the variables x and y, one obtains

$$\pm 2\sqrt{\mu} dx = \frac{1}{\sqrt{y^2 - \frac{\alpha}{2\mu} y - \frac{\beta}{3\mu}}} dy . \tag{6.12}$$

Integrating both sides of Eq. (6.12), i.e.

$$\pm 2\sqrt{\mu} \int dx = \int \frac{1}{\sqrt{y^2 - \frac{\alpha}{2\mu} y - \frac{\beta}{3\mu}}} dy \tag{6.13}$$

results in

$$\pm 2\sqrt{\mu} x + \ln C = \ln \left| \sqrt{y^2 - \frac{\alpha}{2\mu} y - \frac{\beta}{3\mu}} + y - \frac{\alpha}{4\mu} \right| \tag{6.14}$$

considering the auxiliary calculation

$$\int \frac{1}{\sqrt{y^2 - \frac{\alpha}{2\mu} y - \frac{\beta}{3\mu}}} dy = \int \frac{1}{\sqrt{\left(y - \frac{\alpha}{4\mu}\right)^2 - \left(\frac{\alpha^2}{16\mu^2} + \frac{\beta}{3\mu}\right)}} dy$$

$$= \ln \left| \sqrt{\left(y - \frac{\alpha}{4\mu}\right)^2 - \left(\frac{\alpha^2}{16\mu^2} + \frac{\beta}{3\mu}\right)} + \left(y - \frac{\alpha}{4\mu}\right) \right| - \ln C$$

$$= \ln \left| \sqrt{y^2 - \frac{\alpha}{2\mu} y - \frac{\beta}{3\mu}} + y - \frac{\alpha}{4\mu} \right| - \ln C , \tag{6.15}$$

where $\ln C$ is an integration constant. Exponentiating both sides of Eq. (6.14) gives

$$C e^{\pm 2\sqrt{\mu} x} = \sqrt{y^2 - \frac{\alpha}{2\mu} y - \frac{\beta}{3\mu}} + y - \frac{\alpha}{4\mu} . \tag{6.16}$$

42

Squaring Eq. (6.16) yields

$$C^2 e^{\pm 4\sqrt{\mu}x} = y^2 - \frac{\alpha}{2\mu}y - \frac{\beta}{3\mu} + \left(y - \frac{\alpha}{4\mu}\right)^2 + 2\sqrt{y^2 - \frac{\alpha}{2\mu}y - \frac{\beta}{3\mu}}\left(y - \frac{\alpha}{4\mu}\right)$$
$$= 2y^2 - \frac{\alpha}{\mu}y + \frac{\alpha^2}{16\mu^2} - \frac{\beta}{3\mu} + \sqrt{y^2 - \frac{\alpha}{2\mu}y - \frac{\beta}{3\mu}}\left(2y - \frac{\alpha}{2\mu}\right) .$$

(6.17)

Multiplying Eq. (6.16) by $\frac{\alpha}{2\mu}$ gives

$$\frac{\alpha}{2\mu}Ce^{\pm 2\sqrt{\mu}x} = \frac{\alpha}{2\mu}\sqrt{y^2 - \frac{\alpha}{2\mu}y - \frac{\beta}{3\mu}} + \frac{\alpha}{2\mu}y - \frac{\alpha^2}{8\mu^2} .$$

(6.18)

Adding Eq. (6.17) and (6.18) side by side, one obtains

$$C^2 e^{\pm 4\sqrt{\mu}x} + \frac{\alpha}{2\mu}Ce^{\pm 2\sqrt{\mu}x} = 2y^2 - \frac{\alpha}{2\mu}y - \frac{\alpha^2}{16\mu^2} - \frac{\beta}{3\mu} + 2y\sqrt{y^2 - \frac{\alpha}{2\mu}y - \frac{\beta}{3\mu}} .$$

(6.19)

After regrouping Eq. (6.19), one gets

$$C^2 e^{\pm 4\sqrt{\mu}x} + \frac{\alpha}{2\mu}Ce^{\pm 2\sqrt{\mu}x} + \frac{\alpha^2}{16\mu^2} + \frac{\beta}{3\mu} = 2y\left(y - \frac{\alpha}{4\mu} + \sqrt{y^2 - \frac{\alpha}{2\mu}y - \frac{\beta}{3\mu}}\right)$$

(6.20)

and after substituting Eq. (6.16) in here, one obtains

$$C^2 e^{\pm 4\sqrt{\mu}x} + \frac{\alpha}{2\mu}Ce^{\pm 2\sqrt{\mu}x} + \frac{\alpha^2}{16\mu^2} + \frac{\beta}{3\mu} = 2y\, Ce^{\pm 2\sqrt{\mu}x} .$$

(6.21)

Solving for y yields

$$y = \frac{1}{2}Ce^{\pm 2\sqrt{\mu}x} + \left(\frac{\alpha^2}{32\mu^2} + \frac{\beta}{6\mu}\right)C^{-1}e^{\mp 2\sqrt{\mu}x} + \frac{\alpha}{4\mu} .$$

(6.22)

Substituting Eq. (6.22) back in Eq. (6.8), one obtains

$$f = \frac{1}{\sqrt{\frac{1}{2}Ce^{\pm 2\sqrt{\mu}x} + \left(\frac{\alpha^2}{32\mu^2} + \frac{\beta}{6\mu}\right)C^{-1}e^{\mp 2\sqrt{\mu}x} + \frac{\alpha}{4\mu}}} .$$

(6.23)

The localization condition $0 = \lim\limits_{x\to\pm\infty} f(x) = \frac{1}{\sqrt{\frac{1}{2}Ce^{\pm 2\sqrt{\mu}x} + \frac{\alpha}{4\mu}}}$ requires the integration constant C to be positive:

$$C > 0 .$$

(6.24)

Under the condition in Eq. (6.24), the localization condition $0 = \lim\limits_{x\to\mp\infty} f(x) = \frac{1}{\sqrt{\left(\frac{\alpha^2}{32\mu^2} + \frac{\beta}{6\mu}\right)C^{-1}e^{\mp 2\sqrt{\mu}x} + \frac{\alpha}{4\mu}}}$ requires

$$\alpha^2 + \frac{16}{3}\beta\mu > 0 ,$$

(6.25)

43

which also implies that α and β cannot be zero at the same time:

$$(\alpha, \beta) \neq (0, 0) \,. \tag{6.26}$$

Considering Eq. (6.26) and combining the conditions on μ in Eq. (6.2) and (6.25) yield

$$\begin{aligned} 0 < \mu \qquad\qquad &, \text{if} \quad \beta \geqslant 0 \\ 0 < \mu < \frac{3\alpha^2}{16|\beta|} \quad &, \text{if} \quad \beta < 0 \end{aligned} \tag{6.27}$$

given that α is non-zero. If $\alpha = 0$, β and μ must be positive. For convenience, the coefficients of the exponential terms in Eq. (6.23) can be set equal to each other:

$$\frac{1}{2} C = \left(\frac{\alpha^2}{32\mu^2} + \frac{\beta}{6\mu} \right) C^{-1} \,. \tag{6.28}$$

Solving for C yields

$$C = \frac{\sqrt{\alpha^2 + \frac{16}{3}\beta\mu}}{4\mu} \,. \tag{6.29}$$

Note that this choice of C is compatible with Eq. (6.24) and (6.25). Substituting Eq. (6.29) in Eq. (6.23) yields

$$\begin{aligned} f &= \frac{1}{\sqrt{\left(\frac{\sqrt{\alpha^2 + \frac{16}{3}\beta\mu}}{4\mu} \right) \left(\frac{e^{\pm 2\sqrt{\mu}x} + e^{\mp 2\sqrt{\mu}x}}{2} \right) + \frac{\alpha}{4\mu}}} \\ &= \frac{2\sqrt{\mu}}{\sqrt{\alpha + \left(\sqrt{\alpha^2 + \frac{16}{3}\beta\mu} \right) \cosh(2\sqrt{\mu}x)}} \,. \end{aligned} \tag{6.30}$$

Hence, an exact solution of Eq. (6.1) is

$$u(x, z) = \frac{2\sqrt{\mu}}{\sqrt{\alpha + \left(\sqrt{\alpha^2 + \frac{16}{3}\beta\mu} \right) \cosh(2\sqrt{\mu}x)}} \, e^{i\mu z} \tag{6.31}$$

(cf. [47]).

As it can be seen from Eq. (6.30), the existence of a real soliton solution depends on the values of the coefficient of the cubic nonlinearity α, the coefficient of the quintic nonlinearity β and the propagation constant μ. Is the coefficient of nonlinearity positive, then there is a so-called self-focusing nonlinearity. Is the coefficient of nonlinearity negative, then there is a so-called self-defocusing nonlinearity. The

44

coefficients α and β may be negative, zero or positive, so there are 9 different cases to investigate. The propagation constant μ will be considered positive as set up in Eq. (6.2).

1) Self-defocusing cubic, self-defocusing quintic case:

In this case, $\alpha<0$ and $\beta<0$. The condition in Eq. (6.25) becomes $\alpha^2 - \frac{16}{3}|\beta|\mu > 0$ and holds true if $\mu < \frac{3\alpha^2}{16|\beta|}$. However, since $\beta < 0$ and $\cosh(2\sqrt{\mu}x) \geqslant 1$, $\left(\sqrt{\alpha^2 + \frac{16}{3}\beta\mu}\right)\cosh(2\sqrt{\mu}x) < |\alpha|$ for small values of x. For instance for $x = 0$, $\alpha + \left(\sqrt{\alpha^2 + \frac{16}{3}\beta\mu}\right)\cosh(2\sqrt{\mu}x) = -|\alpha| + \sqrt{\alpha^2 + \frac{16}{3}\beta\mu} < 0$. That is, there exists no real soliton solution for positive μ values.

2) Self-defocusing cubic case:

In this case, $\alpha < 0$ and $\beta = 0$. So, Eq. (6.30) becomes

$$f = \frac{2\sqrt{\mu}}{\sqrt{-|\alpha| + |\alpha|\cosh(2\sqrt{\mu}x)}} = \frac{2\sqrt{\mu}}{\sqrt{|\alpha|\left(\cosh(2\sqrt{\mu}x) - 1\right)}} . \qquad (6.32)$$

Since $\alpha \neq 0$ and $\cosh(2\sqrt{\mu}x) \geqslant 1$, f looks like a soliton except at $x = 0$ where it tends to infinity. Hence, no real soliton solution exists in this case.

3) Self-defocusing cubic, self-focusing quintic case:

In this case, $\alpha < 0$ and $\beta > 0$. Since $\beta > 0$, the condition in Eq. (6.30) holds true. Moreover, since $\beta > 0$ and $\cosh(2\sqrt{\mu}x) \geqslant 1$, $\left(\sqrt{\alpha^2 + \frac{16}{3}\beta\mu}\right)\cosh(2\sqrt{\mu}x) > |\alpha|$. That is, there exist real soliton solutions for all positive μ values.

4) Self-defocusing quintic case:

In this case, $\alpha = 0$ and $\beta < 0$. Since $\beta < 0$, the condition in Eq. (6.30) never holds true. That is, there exists no real soliton solution for positive μ values.

5) Linear case:

In this case, $\alpha = 0$ and $\beta = 0$. So, Eq. (6.7) becomes

$$(f')^2 = \mu f^2 . \qquad (6.33)$$

After taking the square root of both sides, the following linear ODE of first order is obtained

$$f' = \pm\sqrt{\mu}f , \qquad (6.34)$$

45

whose solutions are

$$f = \tilde{C}e^{\pm\sqrt{\mu}x} \,. \tag{6.35}$$

The localization condition $0 = \lim_{x\to\pm\infty} f(x) = \tilde{C}e^{\pm\sqrt{\mu}x}$ requires the integration constant $\tilde{C}$ to be zero. So, the linear case has the trivial zero solution, which is obviously not a soliton.

6) Self-focusing quintic case:

In this case, $\alpha = 0$ and $\beta > 0$. So, Eq. (6.30) becomes

$$f = \sqrt{\frac{\sqrt{3\mu}}{\sqrt{\beta}\cosh(2\sqrt{\mu}x)}} \,. \tag{6.36}$$

Since $\beta > 0$ and $\cosh(2\sqrt{\mu}x) \geqslant 1$, there exist real soliton solutions for all positive μ values.

7) Self-focusing cubic, self-defocusing quintic case:

In this case, $\alpha > 0$ and $\beta < 0$. As in the self-defocusing cubic, self-defocusing quintic case, the condition in Eq. (6.30) holds true if $\mu < \frac{3\alpha^2}{16|\beta|}$. Given this and since $\alpha > 0$ and $\cosh(2\sqrt{\mu}x) \geqslant 1$, $\alpha + \left(\sqrt{\alpha^2 + \frac{16}{3}\beta\mu}\right)\cosh(2\sqrt{\mu}x) > 0$. That is, there exist real soliton solutions for $0 < \mu < \frac{3\alpha^2}{16|\beta|}$.

8) Self-focusing cubic case:

In this case, $\alpha > 0$ and $\beta = 0$. So, Eq. (6.30) becomes

$$f = \frac{2\sqrt{\mu}}{\sqrt{|\alpha| + |\alpha|\cosh(2\sqrt{\mu}x)}} = \frac{2\sqrt{\mu}}{\sqrt{|\alpha|\left(\cosh(2\sqrt{\mu}x)+1\right)}} \,. \tag{6.37}$$

Since $\alpha \neq 0$ and $\cosh(2\sqrt{\mu}x) \geqslant 1$, there exist real soliton solutions for all positive μ values.

9) Self-focusing cubic, self-focusing quintic case:

In this case, $\alpha > 0$ and $\beta > 0$. Since $\beta > 0$, the condition in Eq. (6.30) holds true. Moreover, since $\alpha > 0$ and $\cosh(2\sqrt{\mu}x) \geqslant 1$, $\alpha + \left(\sqrt{\alpha^2 + \frac{16}{3}\beta\mu}\right)\cosh(2\sqrt{\mu}x) > 0$. That is, there exist real soliton solutions for all positive μ values.

The results of these 9 cases are summarized in Figure 6.1.

Figure 6.1 : Existence of analytical solutions of the (1+1)D CQNLS equation without any potential.

6.1.2 Numerical Solutions

Solutions are also obtained numerically using Spectral Renormalization Method. Figure 6.2 represents selected solitons in different media, namely in:

(a) self-defocusing cubic, self-focusing quintic

(b) self-focusing quintic

(c) self-focusing cubic, self-defocusing quintic

(d) self-focusing cubic

(e) self-focusing cubic, self-focusing quintic

media. No soliton could be obtained for the other cases, as expected. The red numbers by the peak of solitons in Figure 6.2 mark their maximum amplitudes.

It is to be noted that the numerical solutions are in perfect agreement with the analytical ones. This validates our numerical method and is very important for the cases where an analytical solution does not exist.

6.2 CQNLS with a $\mathcal{PT}$-Symmetric Potential

Now, the (1+1)D CQNLS equation is considered with a $\mathcal{PT}$-symmetric potential.
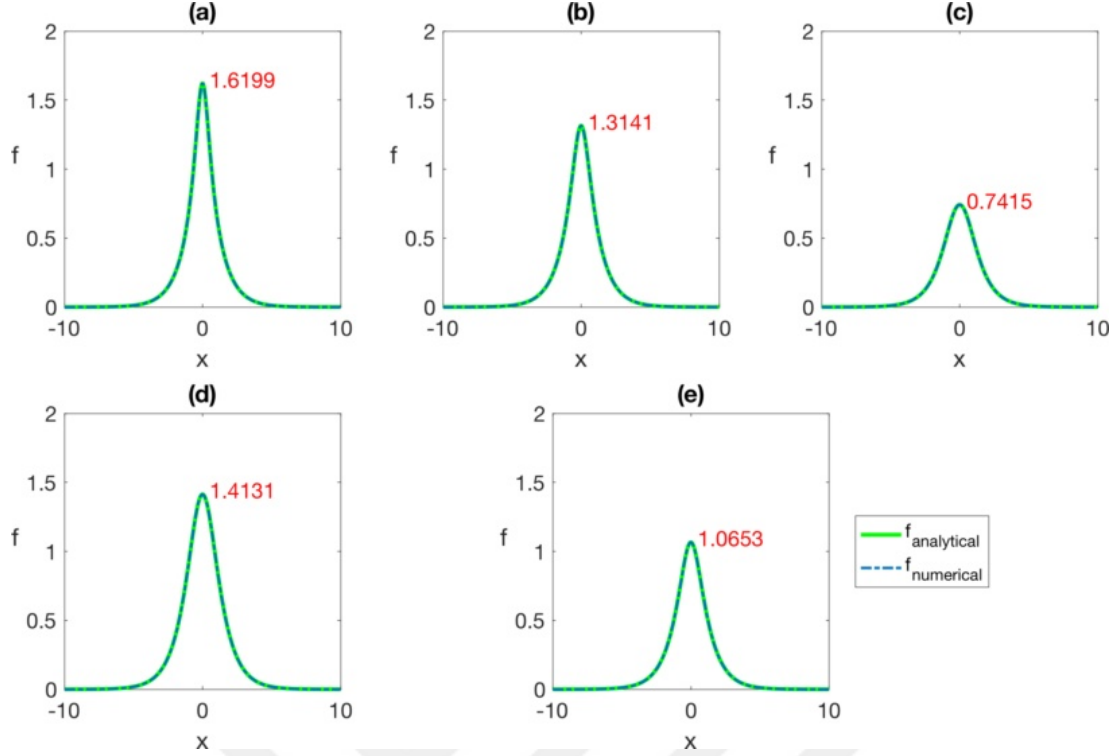
Figure 6.2 : Numerical solutions ($f_{numerical}$) of the (1+1)D CQNLS equation without any potential in comparison with the corresponding analytical solutions ($f_{analytical}$) in different media: (a) $\alpha = -1, \beta = 1$, (b) $\alpha = 0, \beta = 1$, (c) $\alpha = 4, \beta = -1$, (d) $\alpha = 1, \beta = 0$, (e) $\alpha = 1, \beta = 1$.

6.2.1 Analytical Solutions

Consider the following (1+1)D CQNLS equation with a $\mathcal{PT}$-symmetric potential:

$$
iu_z(x,z) + u_{xx}(x,z) + \alpha|u(x,z)|^2 u(x,z) + \beta|u(x,z)|^4 u(x,z)
$$
$$
+ [V(x) + iW(x)]u(x,z) = 0 . \tag{6.38}
$$

Here, $V(x)$ is an even, real-valued function and $W(x)$ is an odd, real-valued function by the definition of $\mathcal{PT}$-symmetry. Clearly, $u(x,z) = 0$ is a trivial solution of Eq. (6.38). To obtain non-zero solutions, set $u(x,z) \neq 0$. Dividing Eq. (6.38) by $u(x,z)$ yields

$$
i\frac{u_z}{u} + \frac{u_{xx}}{u} + \alpha|u|^2 + \beta|u|^4 + V + iW = 0 . \tag{6.39}
$$

To obtain stationary solutions, the following ansatz is used:

$$
u(x,z) = f(x)\, e^{i[\mu z + g(x)]} \tag{6.40}
$$

where $f(x)$ and $g(x)$ are real-valued functions different than zero function. Substituting this along with

$$
\begin{aligned}
u_z &= i\mu f e^{i(\mu z + g)} = i\mu u \\
u_{xx} &= \left[f'' + 2if'g' + ifg'' - f(g')^2 \right] e^{i(\mu z + g)} \\
|u|^2 &= f e^{i(\mu z + g)} f e^{-i(\mu z + g)} = f^2
\end{aligned} \tag{6.41}
$$

48

into Eq. (6.39) yields

$$\left[-\mu + \frac{f''}{f} - (g')^2 + \alpha f^2 + \beta f^4 + V \right] + i\left[\frac{2f'g'}{f} + g'' + W \right] = 0 \ . \tag{6.42}$$

To obtain soliton solutions, the following ansatz is used

$$f(x) = f_0 \operatorname{sech}^p(x) \quad \text{where} \quad f_0 \in \mathbb{R}\backslash\{0\} \text{ and } p \in \mathbb{Z} \ . \tag{6.43}$$

Substituting

$$f' = f_0 p \operatorname{sech}^{p-1}(x)\left(-\operatorname{sech}(x)\tanh(x)\right) = f\left(-p\tanh(x)\right)$$

$$f'' = f'\left(-p\tanh(x)\right) + f\left(-p\operatorname{sech}^2(x)\right) = f\left[p^2 - (p^2 + p)\operatorname{sech}^2(x)\right] \tag{6.44}$$

into Eq. (6.42) yields

$$\left[-\mu + p^2 - (p^2 + p)\operatorname{sech}^2(x) - (g')^2 + \alpha f_0^2 \operatorname{sech}^{2p}(x) + \beta f_0^4 \operatorname{sech}^{4p}(x) + V \right]$$
$$+ i\left[-2p\tanh(x)g' + g'' + W \right] = 0 \ . \tag{6.45}$$

Using the following ansatz

$$g'(x) = g_0 \operatorname{sech}^q(x) \quad \text{where} \quad g_0 \in \mathbb{R}\backslash\{0\} \text{ and } q \in \mathbb{Z} \tag{6.46}$$

and substituting it along with

$$g'' = g_0 q \operatorname{sech}^{q-1}(x)\left(-\operatorname{sech}(x)\tanh(x)\right) = -g_0 q \operatorname{sech}^q(x)\tanh(x) \tag{6.47}$$

into the complex part of Eq. (6.45) gives

$$-(2p + q)g_0 \operatorname{sech}^q(x)\tanh(x) + W = 0 \ . \tag{6.48}$$

Hence, the complex part of the $\mathcal{PT}$-symmetric potential is to be taken as

$$W(x) = W_0 \operatorname{sech}^q(x)\tanh(x) \quad \text{with} \quad W_0 = (2p + q)g_0 \ . \tag{6.49}$$

W(x) is indeed an odd function as

$$W(-x) = W_0 \operatorname{sech}^q(-x)\tanh(-x) = W_0 \operatorname{sech}^q(x)\left(-\tanh(x)\right) = -W(x) \ . \tag{6.50}$$

Substituting Eq. (6.46) into the real part of Eq. (6.45) gives

$$-\mu + p^2 - (p^2 + p)\operatorname{sech}^2(x) - g_0^2 \operatorname{sech}^{2q}(x)$$
$$+ \alpha f_0^2 \operatorname{sech}^{2p}(x) + \beta f_0^4 \operatorname{sech}^{4p}(x) + V = 0 \ . \tag{6.51}$$

Hence, the real part of the $\mathcal{PT}$-symmetric potential can be taken as

$$V(x) = V_0 + V_1 \operatorname{sech}^{4p}(x) + V_2 \operatorname{sech}^{2p}(x) + V_3 \operatorname{sech}^{2q}(x) + V_4 \operatorname{sech}^2(x) \tag{6.52}$$

49

with

$$V_0 = \mu - p^2$$

$$V_1 = -\beta f_0{}^4$$

$$V_2 = -\alpha f_0{}^2 \qquad (6.53)$$

$$V_3 = g_0{}^2$$

$$V_4 = p(p+1) \, .$$

For simplicity, set $\mu = p^2$ to get rid of the coefficient V_0. $V(x)$ is indeed an even function as

$$V(-x) = V_1 \text{sech}^{4p}(-x) + V_2 \text{sech}^{2p}(-x) + V_3 \text{sech}^{2q}(-x) + V_4 \text{sech}^2(-x)$$
$$= V_1 \text{sech}^{4p}(x) + V_2 \text{sech}^{2p}(x) + V_3 \text{sech}^{2q}(x) + V_4 \text{sech}^2(x) = V(x) \, . \qquad (6.54)$$

In conclusion, the general soliton solution of Eq. (6.38) with

$$V(x) = -\beta f_0{}^4 \text{sech}^{4p}(x) - \alpha f_0{}^2 \text{sech}^{2p}(x) + g_0{}^2 \text{sech}^{2q}(x) + p(p+1)\text{sech}^2(x)$$
$$W(x) = (2p+q)g_0 \text{sech}^q(x)\tanh(x) \qquad (6.55)$$

is given as

$$u(x,z) = f_0 \text{sech}^p(x) \, e^{i\left[p^2 z + g_0 \int \text{sech}^q(x) \, dx\right]} \, . \qquad (6.56)$$

Now, $V(x)$ can be simplified by equating the powers of $\text{sech}(x)$. The four powers $4p$, $2p$, $2q$ and 2 can be equated in ${}_4C_4 + {}_4C_3 + \frac{4C_2}{2} = 1 + 4 + 3 = 8$ different ways:

1) $\{4p = 2p = 2q = 2\} \Rightarrow \emptyset$:

This case is not possible.

2) $\{4p \, , \, 2p = 2q = 2\} \Rightarrow p = q = 1$:

$$V(x) = \left(-\alpha f_0{}^2 + g_0{}^2 + 2\right) \text{sech}^2(x) + \left(-\beta f_0{}^4\right) \text{sech}^4(x)$$
$$W(x) = 3g_0 \text{sech}(x)\tanh(x) \qquad (6.57)$$
$$u(x,z) = f_0 \text{sech}(x) e^{i[z + g_0 \arctan(\sinh(x))]}$$

3) $\{2p \, , \, 4p = 2q = 2\} \Rightarrow p = \frac{1}{2}, \, q = 1$:

$$V(x) = \left(-\alpha f_0{}^2\right) \text{sech}(x) + \left(-\beta f_0{}^4 + g_0{}^2 + \frac{3}{4}\right) \text{sech}^2(x)$$
$$W(x) = 2g_0 \text{sech}(x)\tanh(x) \qquad (6.58)$$
$$u(x,z) = f_0 \sqrt{\text{sech}(x)} e^{i\left[\frac{z}{4} + g_0 \arctan(\sinh(x))\right]}$$

4) $\{2q \, , \, 4p = 2p = 2\} \Rightarrow \emptyset$:

50

This case is not possible.

5) $\{2\,,\,4p = 2p = 2q\} \Rightarrow p = q = 0$:

$$V(x) = \left(-\beta f_0{}^4 - \alpha f_0{}^2 + g_0{}^2\right)$$
$$W(x) = 0 \tag{6.59}$$
$$u(x,z) = u(x) = f_0 e^{ig_0 x}$$

This case is of no interest as the solution is not a function of z anymore.

6) $\{4p = 2p,\,2q = 2\} \Rightarrow p = 0,\,q = 1$:

$$V(x) = \left(-\beta f_0{}^4 - \alpha f_0{}^2\right) + \left(g_0{}^2\right)\text{sech}^2(x)$$
$$W(x) = g_0\text{sech}(x)\tanh(x) \tag{6.60}$$
$$u(x,z) = u(x) = f_0 e^{ig_0 \arctan(\sinh(x))}$$

This case is of no interest as the solution is not a function of z anymore.

7) $\{4p = 2q,\,2p = 2\} \Rightarrow p = 1,\,q = 2$:

$$V(x) = \left(-\alpha f_0{}^2 + 2\right)\text{sech}^2(x) + \left(-\beta f_0{}^4 + g_0{}^2\right)\text{sech}^4(x)$$
$$W(x) = 4g_0\text{sech}^2(x)\tanh(x) \tag{6.61}$$
$$u(x,z) = f_0\text{sech}(x)e^{i[z+g_0\tanh(x)]}$$

8) $\{4p = 2,\,2p = 2q\} \Rightarrow p = q = \frac{1}{2}$:

$$V(x) = \left(-\alpha f_0{}^2 + g_0{}^2\right)\text{sech}(x) + \left(-\beta f_0{}^4 + \frac{3}{4}\right)\text{sech}^2(x)$$
$$W(x) = \frac{3}{2}g_0\sqrt{\text{sech}(x)}\tanh(x) \tag{6.62}$$
$$u(x,z) = f_0\sqrt{\text{sech}(x)}\exp\left(i\left[\frac{z}{4} + g_0\int\sqrt{\text{sech}(x)}\,dx\right]\right)$$

In this case, the solution contains an elliptic integral.

We will consider the $\mathcal{PT}$-symmetric potential in the second case for $\alpha \neq 0$:

$$V(x) = V_0\text{sech}^2(x) + V_1\text{sech}^4(x)$$
$$W(x) = W_0\text{sech}(x)\tanh(x) \tag{6.63}$$

where

$$V_0 = -\alpha f_0{}^2 + g_0{}^2 + 2$$
$$V_1 = -\beta f_0{}^4 = -\beta\left(\frac{18 - 9V_0 + W_0{}^2}{9\alpha}\right)^2 \tag{6.64}$$
$$W_0 = 3g_0\,.$$

51

This choice turns out to give the potential in Eq. (3.10) along with the exact solution to Eq. (6.38). It follows from Eq. (6.64) that

$$f_0 = \sqrt{\frac{2 - V_0 + \frac{W_0^2}{9}}{\alpha}}$$

$$g_0 = \frac{W_0}{3}$$

(6.65)

and hence the exact solution is obtained as

$$u(x,z) = \sqrt{\frac{2 - V_0 + \frac{W_0^2}{9}}{\alpha}} \operatorname{sech}(x) \exp\left(i \left[z + \frac{W_0}{3} \arctan(\sinh(x)) \right] \right) .$$

(6.66)

For only cubic nonlinearity, i.e. if $\beta = 0$, Eq. (6.63) reduces to Eq. (3.12):

$$V(x) = V_0 \operatorname{sech}^2(x) \quad , \quad W(x) = W_0 \operatorname{sech}(x) \tanh(x) .$$

(6.67)

6.2.2 Numerical Solutions

Numerical solutions to Eq. (6.38) with the $\mathcal{PT}$-symmetric potential in Eq. (3.10) are sought by means of the Spectral Renormalization Method. The propagation constant is fixed to $\mu = 1$ by the choice of the potential. To investigate different potentials, we let the potential depths V_0 and W_0 vary between 0 and 7.

For the numerical results in self-focusing cubic, self-defocusing quintic media, we set $\alpha = 1$, $\beta = -1$ and let the potential depths V_0 and W_0 vary between 0 and 5.

A typical field profile of an obtained soliton is shown in Figure 6.3. One can see the real parts of the soliton obtained numerically and analytically in the self-focusing cubic, self-defocusing quintic case for $V_0 = 0.7$ and $W_0 = 0.3$ in Figure 6.3(a), their complex parts in Figure 6.3(b) and phases in Figure 6.3(c). Hereon, one can observe that the numerical solution coincides with the analytical solution.

All the numerically obtained solitons are shown in Figure 6.4(a) where the stars represent solitons corresponding to λ_1 in the Spectral Renormalization Method (see Eq. (4.6)) whereas the pluses represent solitons corresponding to λ_2. One can notice that solitons corresponding to different λ's are disjoint; i.e. there are no bistable solitons. The dashed line is the threshold for f_0 to be real (see Eq. (6.65)); in self-focusing cubic media, solitons may exist below it (and indeed, they do).

For the numerical results in self-focusing cubic, self-focusing quintic media, we set $\alpha = \beta = 1$ and let the potential depths V_0 and W_0 vary between 0 and 4.
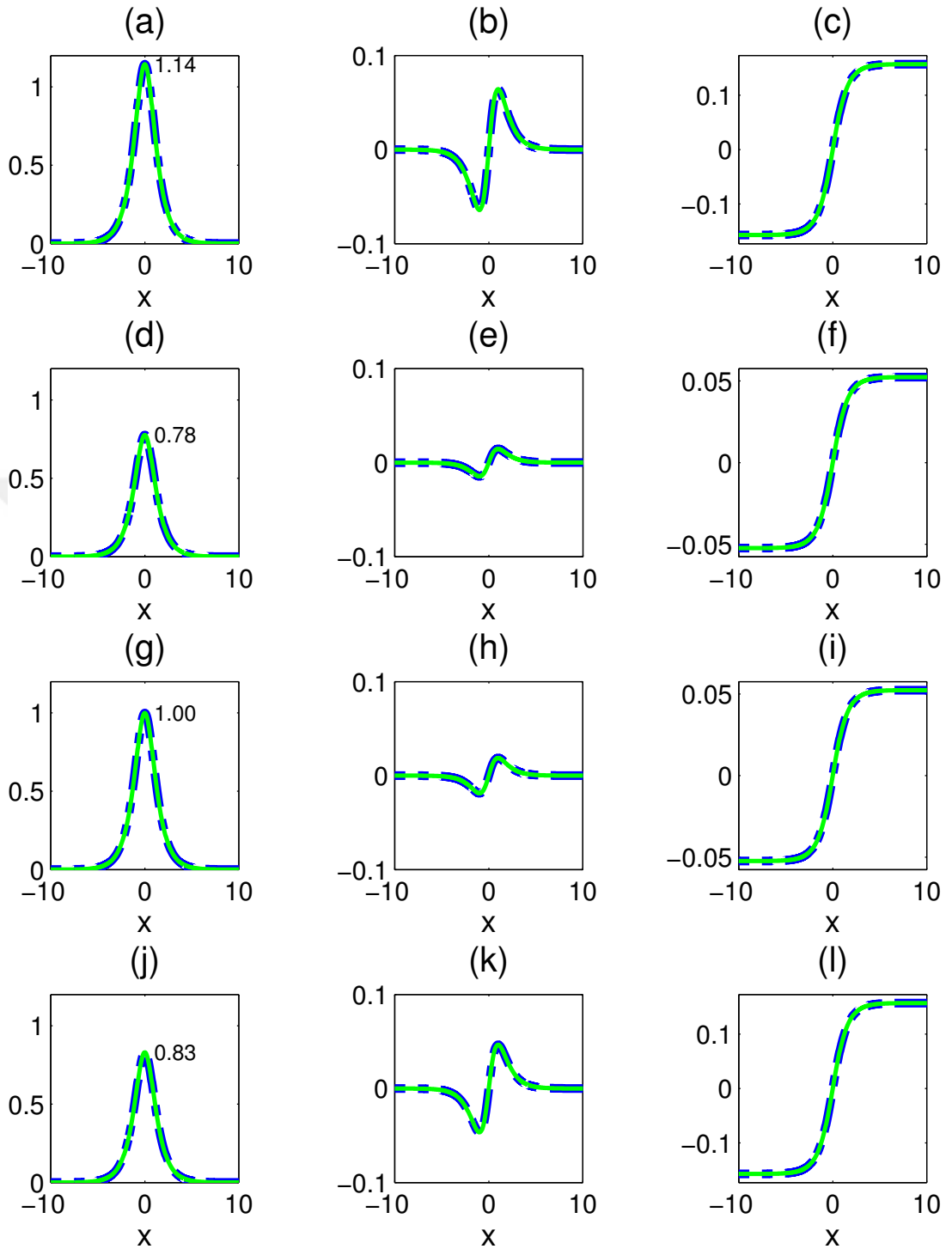
Figure 6.3 : (a) Real part, (b) complex part and (c) phase of the soliton obtained for $\alpha = 1, \beta = -1, V_0 = 0.7, W_0 = 0.3$. (d) Real part, (e) complex part and (f) phase of the soliton obtained for $\alpha = \beta = 1, V_0 = 1.4, W_0 = 0.1$. (g) Real part, (h) complex part and (i) phase of the soliton obtained for $\alpha = \beta = -1, V_0 = 3, W_0 = 0.1$. (j) Real part, (k) complex part and (l) phase of the soliton obtained for $\alpha = -1, \beta = 1, V_0 = 2.7, W_0 = 0.3$. In all cases, numerically obtained soliton is plotted with a dashed blue line whereas analytically obtained soliton is plotted with a green line.

53
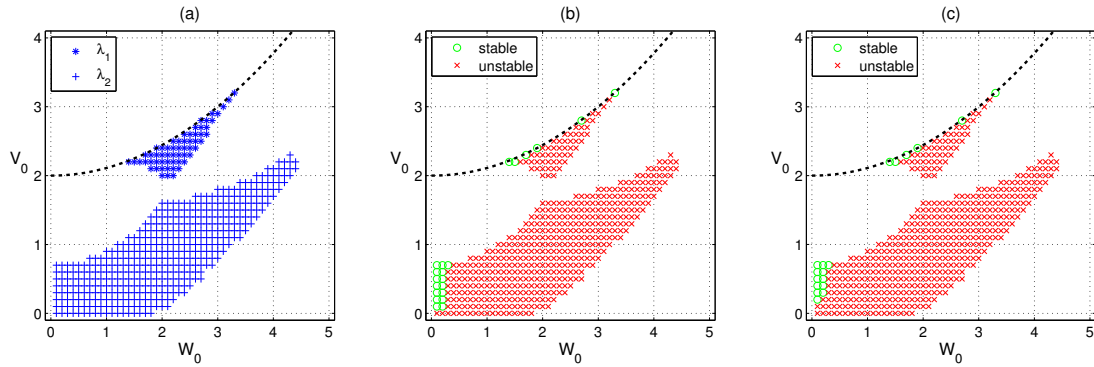
Figure 6.4 : (a) Numerically obtained solitons of the (1+1)D CQNLS equation with a $\mathcal{PT}$-symmetric potential for varying potential depths in the self-focusing cubic, self-defocusing quintic case ($\alpha = 1$, $\beta = -1$), (b) Numerically obtained, nonlinearly stable (marked as green circles) and nonlinearly unstable (marked as red crosses) solitons, (c) Analytically obtained, nonlinearly stable (marked as green circles) and nonlinearly unstable (marked as red crosses) solitons.
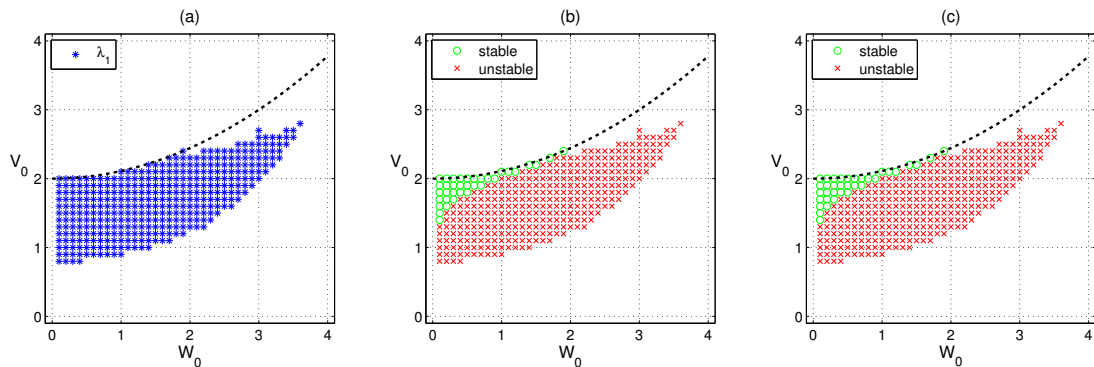
Figure 6.5 : (a) Numerically obtained solitons of the (1+1)D CQNLS equation with a $\mathcal{PT}$-symmetric potential for varying potential depths in the self-focusing cubic, self-focusing quintic case ($\alpha = \beta = 1$), (b) Numerically obtained, nonlinearly stable (marked as green circles) and nonlinearly unstable (marked as red crosses) solitons, (c) Analytically obtained, nonlinearly stable (marked as green circles) and nonlinearly unstable (marked as red crosses) solitons.

54
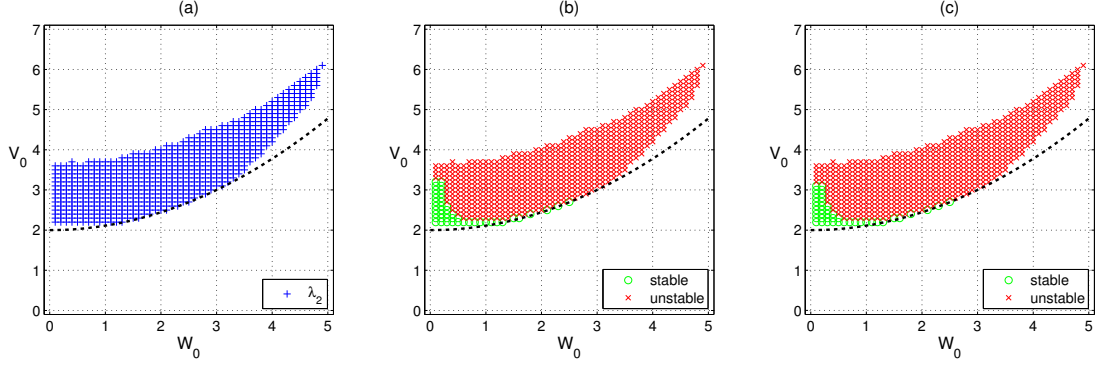
Figure 6.6 : (a) Numerically obtained solitons of the (1+1)D CQNLS equation with a $\mathcal{PT}$-symmetric potential for varying potential depths in the self-defocusing cubic, self-defocusing quintic case ($\alpha = \beta = -1$), (b) Numerically obtained, nonlinearly stable (marked as green circles) and nonlinearly unstable (marked as red crosses) solitons, (c) Analytically obtained, nonlinearly stable (marked as green circles) and nonlinearly unstable (marked as red crosses) solitons.

A typical field profile of an obtained soliton is shown in Figure 6.3. One can see the real parts of the soliton obtained numerically and analytically in the self-focusing cubic, self-focusing quintic case for $V_0 = 1.4$ and $W_0 = 0.1$ in Figure 6.3(d), their complex parts in Figure 6.3(e) and phases in Figure 6.3(f). Hereon, one can observe that the numerical solution coincides with the analytical solution.

All the numerically obtained solitons are shown in Figure 6.5(a) where the stars represent solitons corresponding to λ_1. Like in the self-focusing cubic, self-defocusing quintic case, solitons exist below the dashed line. One can notice that no soliton corresponding to λ_2 is found. It is also remarkable that there exists no soliton solution if the potential is pure imaginary (i.e. when $V_0 = 0$).

For the numerical results in self-defocusing cubic, self-defocusing quintic media, we set $\alpha = \beta = -1$ and let the potential depths V_0 and W_0 vary between 0 and 7.

A typical field profile of an obtained soliton is shown in Figure 6.3. One can see the real parts of the soliton obtained numerically and analytically in the self-defocusing cubic, self-defocusing quintic case for $V_0 = 3$ and $W_0 = 0.1$ in Figure 6.3(g), their complex parts in Figure 6.3(h) and phases in Figure 6.3(i). Hereon, one can observe that the numerical solution coincides with the analytical solution.

All the numerically obtained solitons are shown in Figure 6.6(a) where the pluses represent solitons corresponding to λ_2. The dashed line is the threshold for f_0 to be
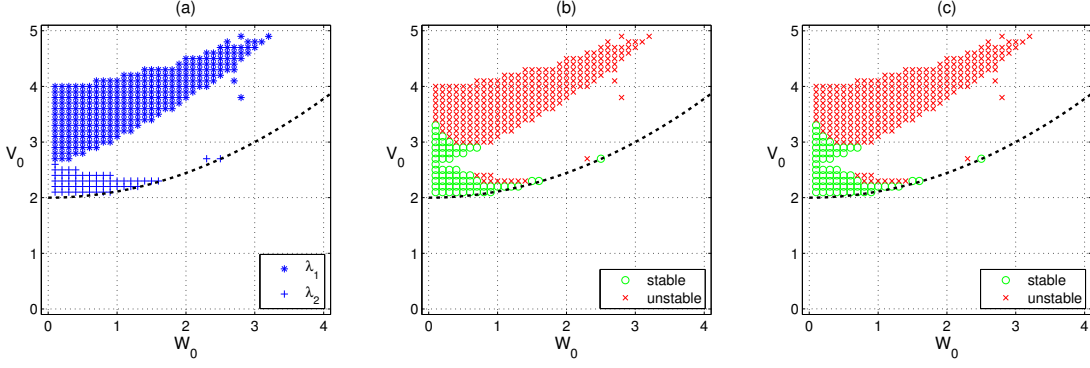
Figure 6.7 : Numerically obtained solitons of the (1+1)D CQNLS equation with a $\mathcal{PT}$-symmetric potential for varying potential depths in the self-defocusing cubic, self-focusing quintic case ($\alpha = -1$, $\beta = 1$), (b) Numerically obtained, nonlinearly stable (marked as green circles) and nonlinearly unstable (marked as red crosses) solitons, (c) Analytically obtained, nonlinearly stable (marked as green circles) and nonlinearly unstable (marked as red crosses) solitons.

real; in self-defocusing cubic media, solitons may exist above it (and indeed, they do). One can notice that no soliton corresponding to λ_1 is found.

For the numerical results in self-defocusing cubic, self-focusing quintic media, we set $\alpha = -1$, $\beta = 1$ and let the potential depths V_0 and W_0 vary between 0 and 5.

A typical field profile of an obtained soliton is shown in Figure 6.3. One can see the real parts of the soliton obtained numerically and analytically in the self-defocusing cubic, self-focusing quintic case for $V_0 = 2.7$ and $W_0 = 0.3$ in Figure 6.3(j), their complex parts in Figure 6.3(k) and phases in Figure 6.3(l). Hereon, one can observe that the numerical solution coincides with the analytical solution.

All the numerically obtained solitons are shown in Figure 6.7 where the stars represent solitons corresponding to λ_1 whereas the pluses represent solitons corresponding to λ_2. One can notice that solitons corresponding to different λ's are disjoint; i.e. there are no bistable solitons. Like in the self-defocusing cubic, self-defocusing quintic case, solitons exist above the dashed line.

6.2.3 Nonlinear Stability

A soliton should preserve its shape, location and maximum amplitude during direct simulations in order to be considered as nonlinearly stable. To study their nonlinear stability, obtained solitons are computed over a long distance. For this purpose,

split-step Fourier method is employed to advance in z. The solitons are then plotted from $z = 0$ to $z = 100$ at each integer value of z.

The results of the nonlinear stability analysis of the numerically and analytically obtained solitons in self-focusing cubic, self-defocusing quintic media ($\alpha = 1$, $\beta = -1$) are shown in Figure 6.4(b) and 6.4(c) respectively, where the circles represent stable solitons whereas the crosses represent unstable ones. The dotted line is again the threshold for f_0 to be real. It can be seen that the numerical findings are in good agreement with the analytical results, that the majority of the solitons are unstable and that stable solitons are predominantly obtained either for smaller values of W_0 or close to the threshold curve.

Nonlinear stability and instability regions of the numerically and analytically obtained solitons in self-focusing cubic, self-focusing quintic media ($\alpha = \beta = 1$) are given in Figure 6.5(b) and 6.5(c) respectively, where the circles represent stable solitons whereas the crosses represent unstable ones. It can be seen that the numerical findings are in good agreement with the analytical results, that the majority of the solitons are unstable and that stable solitons are predominantly obtained either for smaller values of W_0 or close to the threshold curve.

In Figure 6.8, a nonlinearly unstable soliton is shown. It is observed that the maximum amplitude increases during the evolution which leads to nonlinear instability.

Nonlinear stability and instability regions of the numerically and analytically obtained solitons in self-defocusing cubic, self-defocusing quintic media ($\alpha = \beta = -1$) are given in Figure 6.6(b) and 6.6(c) respectively, where the circles represent stable solitons whereas the crosses represent unstable ones. It can be seen that the numerical findings are in good agreement with the analytical results, that the majority of the solitons are unstable and that stable solitons are predominantly obtained either for smaller values of W_0 or close to the threshold curve.

In Figure 6.9, a nonlinearly stable soliton is depicted. It can be seen that the soliton conserves its shape and maximum amplitude during the evolution.

The results of the nonlinear stability analysis of the numerically and analytically obtained solitons in self-defocusing cubic, self-focusing quintic media ($\alpha = -1$, $\beta = 1$) are shown in Figure 6.7(b) and 6.7(c) respectively, where the circles represent stable
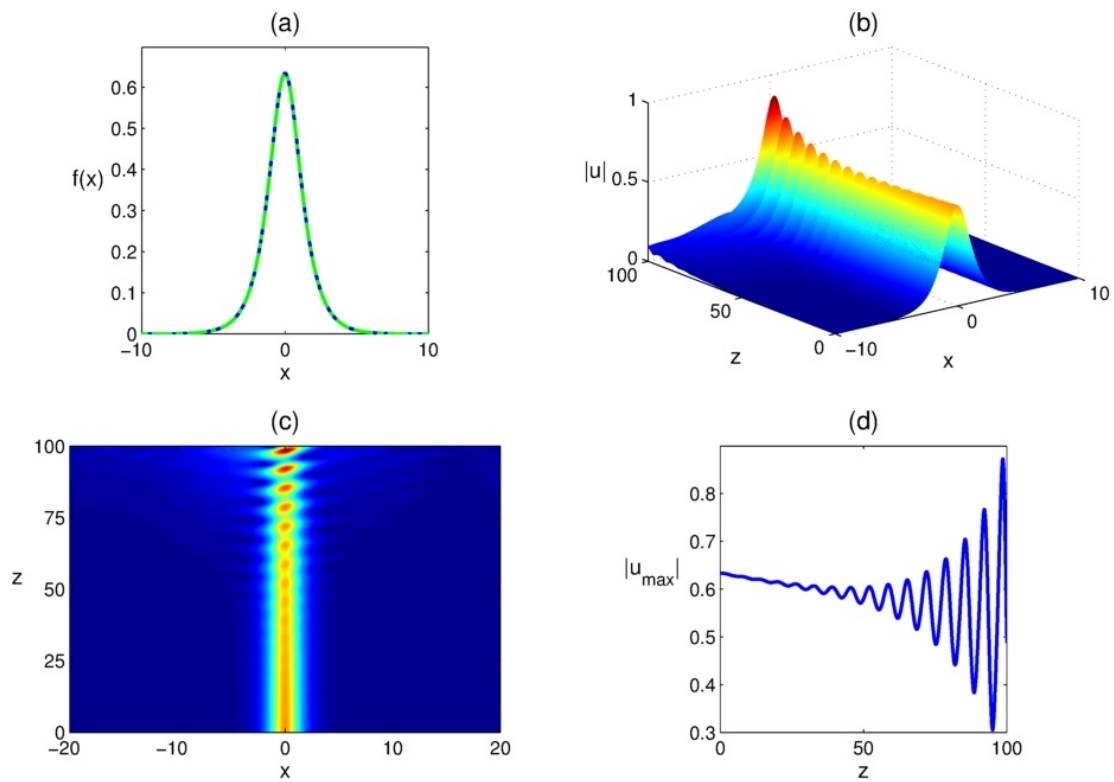
Figure 6.8 : (a) Numerically obtained soliton of the (1+1)D CQNLS equation with a $\mathcal{PT}$-symmetric potential for $V_0 = 2$ and $W_0 = 1.9$ in the self-focusing cubic, self-focusing quintic case ($\alpha = \beta = 1$), (b) Nonlinear evolution of the soliton, (c) View from top, (d) Maximum amplitude as a function of the propagation distance z.
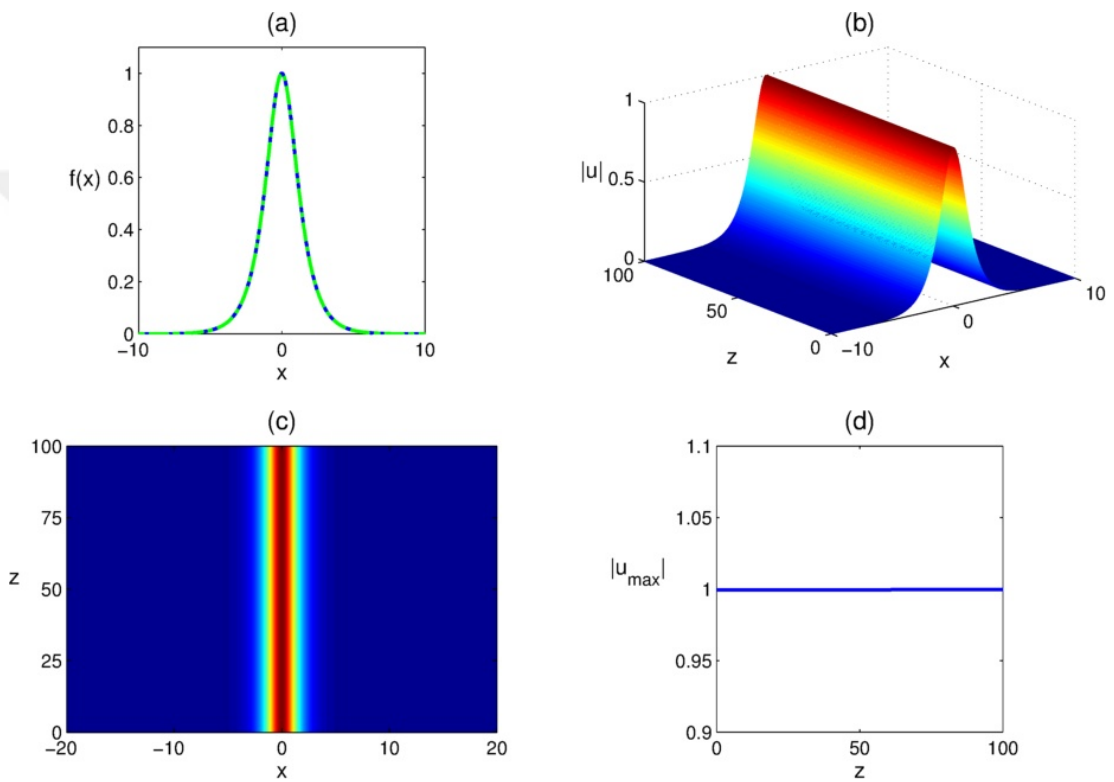
Figure 6.9 : (a) Numerically obtained soliton of the (1+1)D CQNLS equation with a $\mathcal{PT}$-symmetric potential for $V_0 = 3$ and $W_0 = 0.1$ in the self-defocusing cubic, self-defocusing quintic case ($\alpha = \beta = -1$), (b) Nonlinear evolution of the soliton, (c) View from top, (d) Maximum amplitude as a function of the propagation distance z.
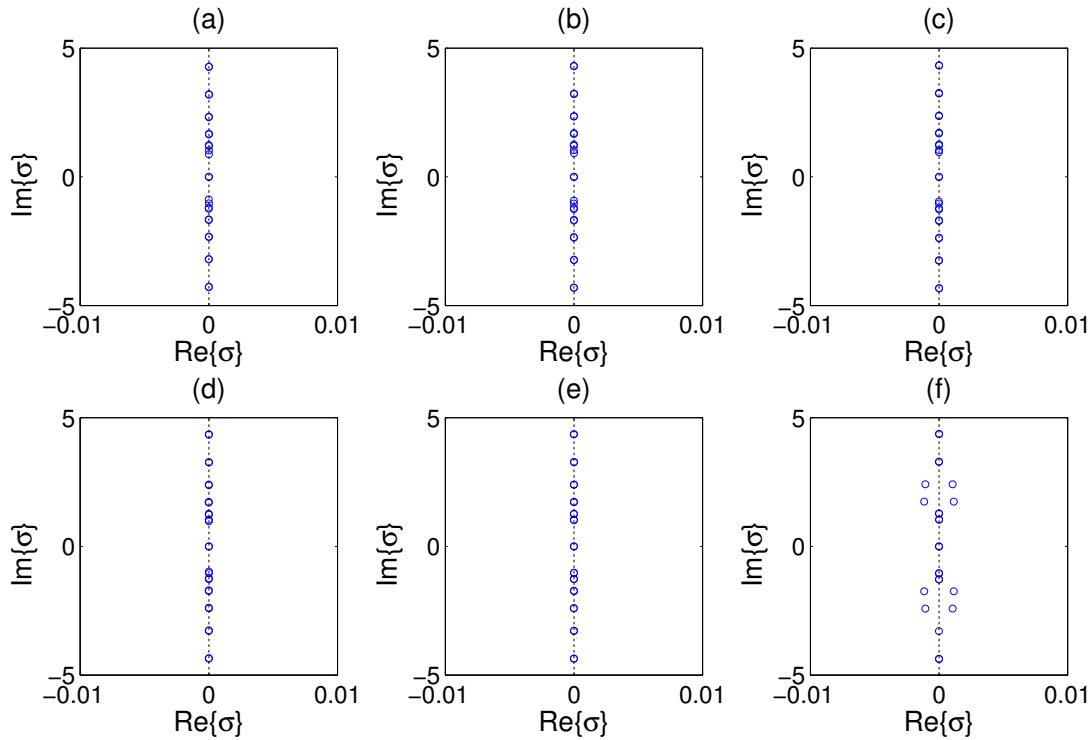
Figure 6.10 : Linear spectrum of the numerically obtained solitons of the (1+1)D CQNLS equation with a $\mathcal{PT}$-symmetric potential for $V_0 = 1$ and $W_0 = 0.1$ in the self-focusing cubic case (a) $\alpha = 1$, $\beta = 0$ and self-focusing cubic, self-defocusing quintic cases: (b) $\alpha = 1$, $\beta = -0.2$, (c) $\alpha = 1$, $\beta = -0.4$, (d) $\alpha = 1$, $\beta = -0.6$, (e) $\alpha = 1$, $\beta = -0.8$, (f) $\alpha = 1$, $\beta = -1$.

solitons whereas the crosses represent unstable ones. It can be seen that the numerical findings are in good agreement with the analytical results, that the majority of the solitons are unstable and that stable solitons are predominantly obtained either for smaller values of W_0 or close to the threshold curve.

6.2.4 Linear Stability

In order to observe the effect of the quintic term on the soliton stability, linear spectra of the solitons are investigated starting with solely the cubic nonlinearity and extending it by gradually decreasing β, the coefficient in front of the self-defocusing quintic term. As it can be concluded from Figure 6.10, decreasing the value of β while keeping the other parameters the same, has a negative effect on soliton stability in self-focusing cubic, self-defocusing quintic media. In the case where $\alpha = 1$ and $\beta = -1$, there are unstable eigenvalues (see Figure 6.10(f)) which lead the soliton to blow-up; an indicator for linear instability.
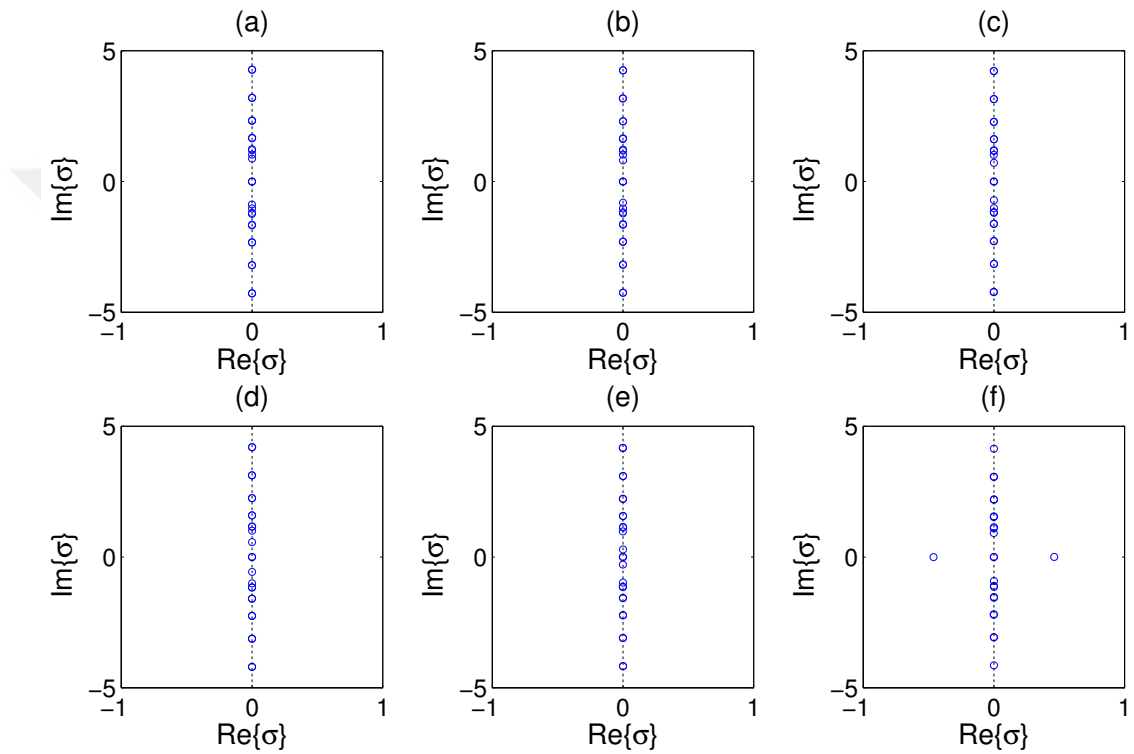
Figure 6.11 : Linear spectrum of the numerically obtained solitons of the (1+1)D CQNLS equation with a $\mathcal{PT}$-symmetric potential for $V_0 = 1$ and $W_0 = 0.1$ in the self-focusing cubic case (a) $\alpha = 1$, $\beta = 0$ and self-focusing cubic, self-focusing quintic cases: (b) $\alpha = 1$, $\beta = 0.2$, (c) $\alpha = 1$, $\beta = 0.4$, (d) $\alpha = 1$, $\beta = 0.6$, (e) $\alpha = 1$, $\beta = 0.8$, (f) $\alpha = 1$, $\beta = 1$.
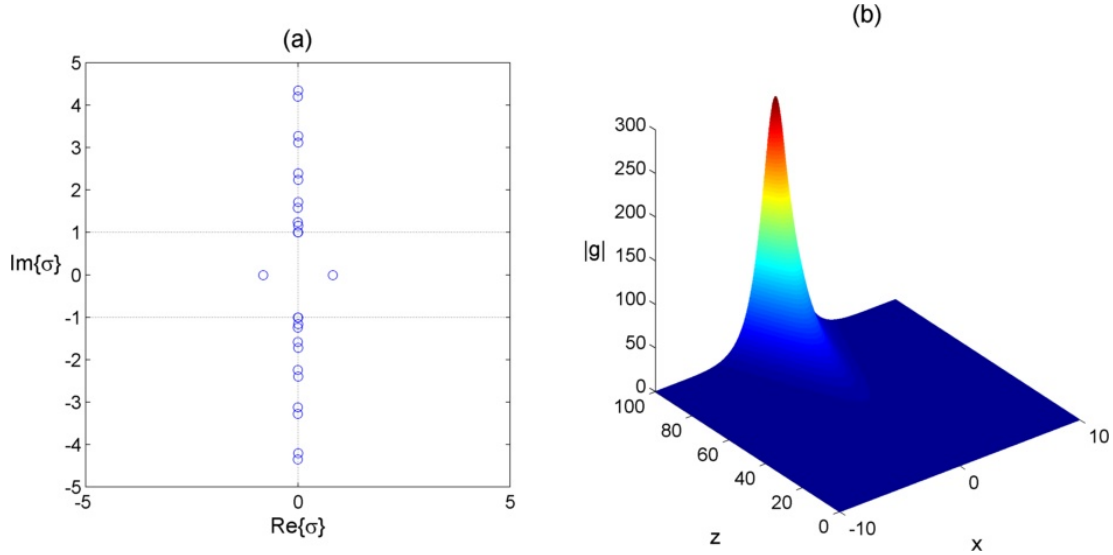
Figure 6.12 : (a) Linear spectrum of the numerically obtained soliton of the (1+1)D CQNLS equation with a $\mathcal{PT}$-symmetric potential for $V_0 = 3.6$ and $W_0 = 0.1$ in the self-defocusing cubic, self-focusing quintic case ($\alpha = -1$, $\beta = 1$), (b) Linear evolution of the soliton.

In order to further observe the effect of the quintic term on the soliton stability, linear spectra of the solitons are investigated starting with solely the cubic nonlinearity and extending it by gradually increasing β, the coefficient in front of the self-focusing quintic term. As it can be concluded from Figure 6.11, increasing the value of β while keeping the other parameters the same, has a negative effect on soliton stability in self-focusing cubic, self-focusing quintic media. Due to the existence of eigenvalues with non-zero real parts in their linear spectra, all solitons considered in this medium ($\alpha = \beta = 1$) are found to be linearly unstable.

Due to eigenvalues with non-zero real parts in their linear spectra and instant growth in their amplitudes during linear evolution, all solitons considered in self-defocusing cubic, self-defocusing quintic media ($\alpha = \beta = -1$) are found to be linearly unstable.

In Figure 6.12, a linearly unstable soliton is plotted. It can be clearly seen that two eigenvalues with non-zero real parts exist in the linear spectrum (a) and the maximum amplitude of the soliton increases instantly during the evolution which indicates blow-up (b). On the other hand, Figure 6.13 points out the linear instability of the same soliton but this time obtained analytically. The other solitons considered in self-defocusing cubic, self-focusing quintic media ($\alpha = -1$, $\beta = 1$) are also found to be linearly unstable.
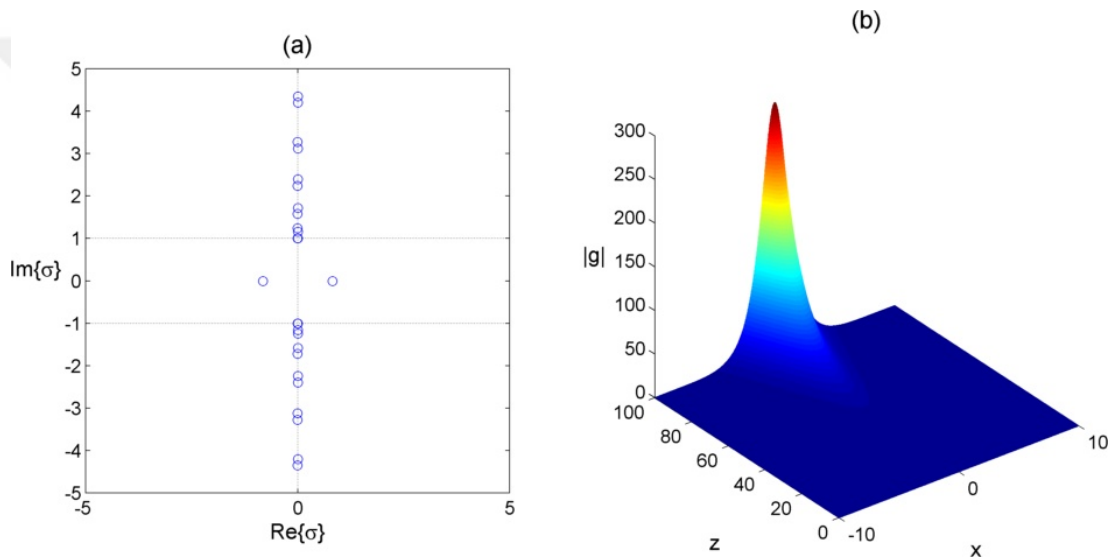
Figure 6.13 : (a) Linear spectrum of the analytically obtained soliton of the (1+1)D CQNLS equation with a $\mathcal{PT}$-symmetric potential for $V_0 = 3.6$ and $W_0 = 0.1$ in the self-defocusing cubic, self-focusing quintic case $(\alpha = -1,\ \beta = 1)$, (b) Linear evolution of the soliton.

7. SOLITONS OF THE (2+1)D CQNLS EQUATION

In this chapter, the problem is extended to (2+1)D, where there are not so many results published in the literature, especially for the quintic case.

7.1 CQNLS without Potential

Consider the following (2+1)D CQNLS equation without any potential:

$$u_z(x,y,z) + u_{xx}(x,y,z) + u_{yy}(x,y,z) + \alpha|u(x,y,z)|^2 u(x,y,z) + \beta|u(x,y,z)|^4 u(x,y,z) = 0 .$$
(7.1)

Analytical and numerical solutions to its (1+1)D form were shown in Section 6.1.

7.1.1 Numerical Solutions

As Eq. (7.1) does not admit analytical solutions, numerical solutions to Eq. (7.1) are sought by means of the Spectral Renormalization Method. The values for the parameters are set as $\alpha, \beta \in \{-1,\ 0,\ 1\}$ and $\mu \leqslant 4$.

No soliton is obtained in the

- self-defocusing cubic, self-defocusing quintic medium ($\alpha = \beta = -1$),

- self-defocusing cubic medium ($\alpha = -1$, $\beta = 0$),

- self-defocusing quintic medium ($\alpha = 0$, $\beta = -1$),

- linear medium ($\alpha = \beta = 0$) and

- self-focusing cubic, self-defocusing quintic medium ($\alpha = 1$, $\beta = -1$)

as it was the case in (1+1)D.

For the other media, i.e.

- self-defocusing cubic, self-focusing quintic medium ($\alpha = -1$, $\beta = 1$),
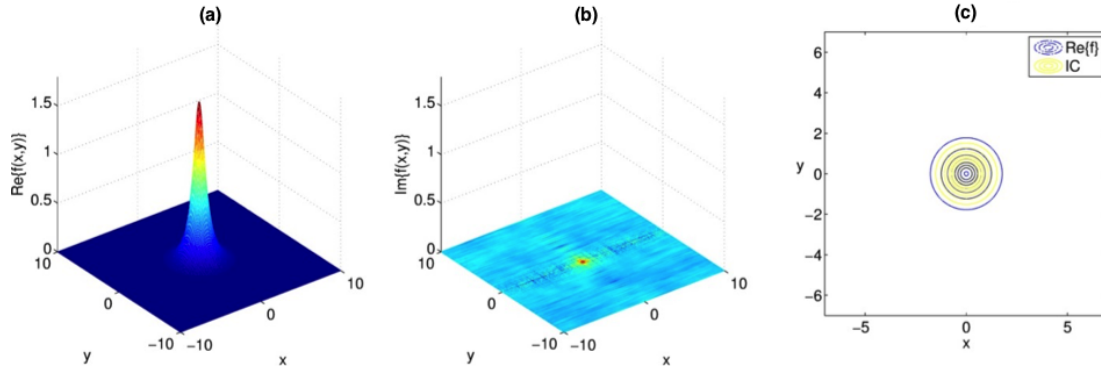
Figure 7.1 : (a) Real and (b) imaginary parts of the soliton obtained numerically for CQNLS equation with $\alpha = \beta = 1$ and (c) its contour plot along with the initial condition (IC).

- self-focusing quintic medium ($\alpha = 0$, $\beta = 1$),

- self-focusing cubic medium ($\alpha = 1$, $\beta = 0$) and

- self-focusing cubic, self-focusing quintic medium ($\alpha = \beta = 1$),

solitons are obtained for all the values of μ.

An example for those solitons is given in Figure 7.1. The soliton obtained in the self-focusing cubic, self-focusing quintic case for $\mu = 1$ is plotted in Figure 7.1(a). As it can be seen from Figure 7.1(b), the obtained soliton is real. In Figure 7.1(c), the contour plots of the initial condition (IC) and the soliton are given.

The results for (2+1)D CQNLS equation are in good agreement with those for (1+1)D CQNLS equation.

7.2 CQNLS with a Periodic Potential

In this section, a periodic potential is added to the system on the ground of its positive effect on existence and stability of the solitons.

7.2.1 Numerical Solutions

The solution to the CQNLS equation with the periodic potential in Eq. (3.1) for $N = 4$ is again found using spectral methods. Solitons are obtained for varying μ and V_0 values only when there is a self-focusing cubic and/or quintic nonlinearity in the equation as expected from the previous results.
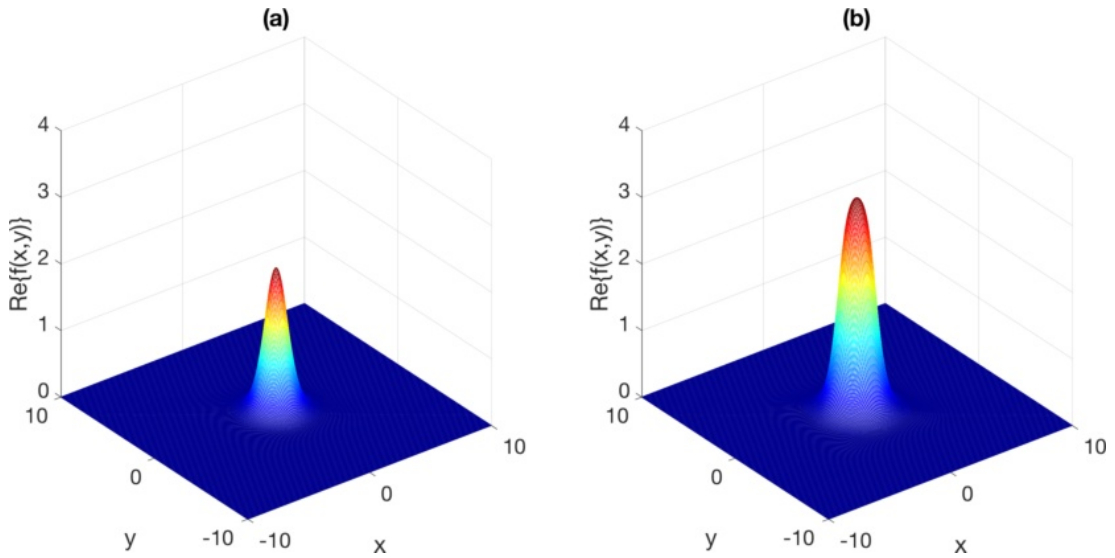
**Figure 7.2** : Bistable solitons of the CQNLS equation with a periodic potential obtained for $\mu = 3$ and $V_0 = 4$.
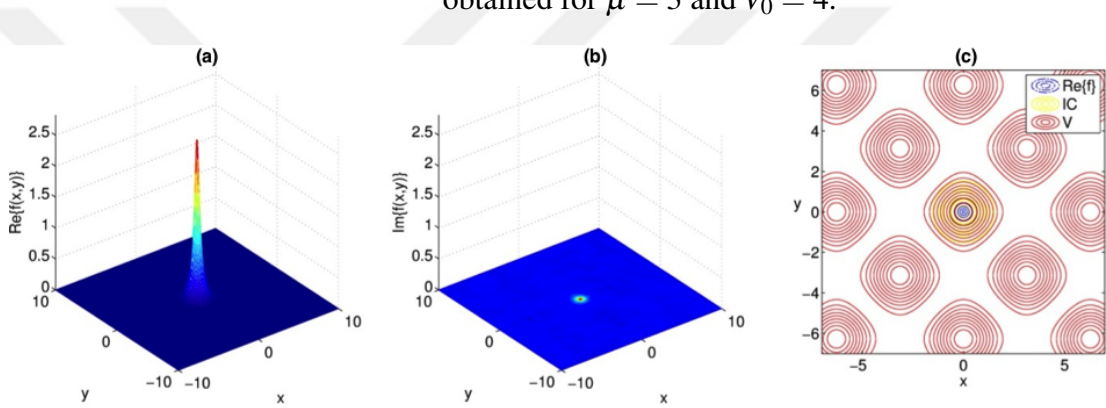
Figure 7.3 : (a) Real and (b) imaginary parts of the soliton obtained numerically for CQNLS equation with $\alpha = 0, \beta = 1, V_0 = 1, \mu = 4$ and (c) its contour plot along with the initial condition (IC) and periodic potential (V).

One remarkable result is the existence of soliton pairs in the self-focusing cubic, self-defocusing quintic case ($\alpha = 1, \beta = -0.1$). There exist two different solitons for some propagation constants μ at the potential depth $V_0 = 4$, namely for $\mu \in [2.8; 3]$ for the periodic potential. In other words, there are pairs of solitons having different powers for the same propagation constants. An example of these soliton pairs is given in Figure 7.2. This arises, yet not always, due to the dual choice of λ in the spectral method. The soliton corresponding to λ_1, shown in Figure 7.2(a), has a maximum amplitude of magnitude 2.1496 and a power of magnitude 9.0736 whereas the soliton corresponding to λ_2, shown in Figure 7.2(b), has a maximum amplitude of magnitude 3.1999 and a power of magnitude 40.4428. In the literature, such pairs are referred to as bistable solitons.

Another thing to be noticed is solitons starting to get narrower and taller after a while although their gap regions seem semi-infinite in the self-focusing cubic, self-focusing quintic case ($\alpha = \beta = 1$) and self-focusing quintic case ($\alpha = 0$, $\beta = 1$) for instance, which brings up the question of stability. An example of such a narrow soliton is given in Figure 7.3. The soliton obtained in the self-focusing quintic case for $V_0 = 1$ and $\mu = 4$ is plotted in Figure 7.3(a). One can directly notice how spindly the soliton is. As it can be seen in Figure 7.3(b), the obtained soliton has no imaginary part. The contour plots of the initial condition, periodic potential and soliton are given in Figure 7.3(c).

7.3 CQNLS with a $\mathcal{PT}$-Symmetric Potential

This section is the extension of Section 6.2 to (2+1)D.

7.3.1 Analytical Solutions

Consider the following (2+1)D CQNLS equation with a $\mathcal{PT}$-symmetric potential:

$$
\begin{aligned}
& iu_z(x,y,z) + u_{xx}(x,y,z) + u_{yy}(x,y,z) + \alpha|u(x,y,z)|^2 u(x,y,z) \\
& + \beta|u(x,y,z)|^4 u(x,y,z) + [V(x,y) + iW(x,y)]\, u(x,y,z) = 0 \ .
\end{aligned}
\tag{7.2}
$$

The idea is to generalize the solution in Eq. (6.66) to (2+1)D as follows

$$
u(x,y,z) = f_0 \text{sech}(x)\text{sech}(y)\, e^{i\{\mu z + g_0[\arctan(\sinh(x)) + \arctan(\sinh(y))]\}}
\tag{7.3}
$$

[61]. Writing Eq. (7.3) in Eq. (7.2) yields

$$
\begin{bmatrix} -\mu + 2 - (2 + g_0^2)\left(\text{sech}^2(x) + \text{sech}^2(y)\right) \\ +\alpha f_0^2\text{sech}^2(x)\text{sech}^2(y) \\ +\beta f_0^4\text{sech}^4(x)\text{sech}^4(y) + V \end{bmatrix} + i \begin{bmatrix} -3g_0\text{sech}(x)\tanh(x) \\ -3g_0\text{sech}(y)\tanh(y) \\ +W \end{bmatrix} = 0.
\tag{7.4}
$$

Setting real and complex parts of Eq. (7.4) equal to zero gives

$$
\begin{aligned}
V &= (2 + g_0^2)\left[\text{sech}^2(x) + \text{sech}^2(y)\right] \\
&\quad - \alpha f_0^2\text{sech}^2(x)\text{sech}^2(y) - \beta f_0^4\text{sech}^4(x)\text{sech}^4(y) \\
W &= 3g_0\left[\text{sech}(x)\tanh(x) + \text{sech}(y)\tanh(y)\right] \\
\mu &= 2 \ .
\end{aligned}
\tag{7.5}
$$

By defining

$$
V_2 = 2 + \frac{W_0^2}{9}
\tag{7.6}
$$

and using the same coefficients in Eq. (6.64), the potential is obtained as follows:

$$V(x,y) = (V_0 - V_2)\text{sech}^2(x)\text{sech}^2(y) + V_1\text{sech}^4(x)\text{sech}^4(y)$$

$$+ V_2 \left[\text{sech}^2(x) + \text{sech}^2(y)\right] \tag{7.7}$$

$$W(x,y) = W_0 \left[\text{sech}(x)\tanh(x) + \text{sech}(y)\tanh(y)\right] .$$

It can be easily seen that $V(x,y)$ is an even function and $W(x,y)$ is an odd function. That is, $V(x,y) + iW(x,y)$ is indeed the $\mathcal{PT}$-symmetric potential given in Eq. (3.11).

As a result, exact fundamental soliton solutions to Eq. (7.2) are obtained in the form of

$$u(x,y,z) = \sqrt{\frac{2 - V_0 + \frac{W_0^2}{9}}{\alpha}} \text{sech}(x)\,\text{sech}(y)$$

$$\exp\left(i\left\{2z + \frac{W_0}{3}\left[\arctan(\sinh(x)) + \arctan(\sinh(y))\right]\right\}\right) \tag{7.8}$$

by choosing suitable values for f_0 and g_0.

7.3.2 Numerical Solutions

Numerical solutions to Eq. (7.2) with the $\mathcal{PT}$-symmetric potential in Eq. (3.11) are sought by means of the Spectral Renormalization Method. The propagation constant is fixed to $\mu = 2$ by the choice of the potential. To investigate different potentials, we let the potential depths V_0 and W_0 vary between 0 and 6.

We start the exact and numerical analysis by considering self-focusing cubic and self-defocusing quintic medium. Figure 7.4 features the typical field profile of an obtained soliton. The real part of the numerically obtained soliton in the self-focusing cubic, self-defocusing quintic case for $V_0 = 0.1$ and $W_0 = 0.5$ is plotted in Figure 7.4(a) and its complex part in Figure 7.4(d). The analytical solution depicted in Figure 7.4(b) and 7.4(e), coincides with the numerical solution. This can be seen from their superposed cross sections in Figure 7.4(c) and 7.4(f).

For the numerical results in self-focusing cubic, self-defocusing quintic media, we fix $\alpha = 1$, $\beta = -1$ and vary the potential depths V_0 and W_0 between 0 and 4. Obtained solitons are marked in Figure 7.5(a), where stars indicate the ones obtained using the first root λ_1 in the fixed point iteration and pluses indicate the ones obtained using the second root λ_2. Recall that solitons in self-focusing cubic media may only exist below the dotted curve that depicts the case $f_0 = 0$.
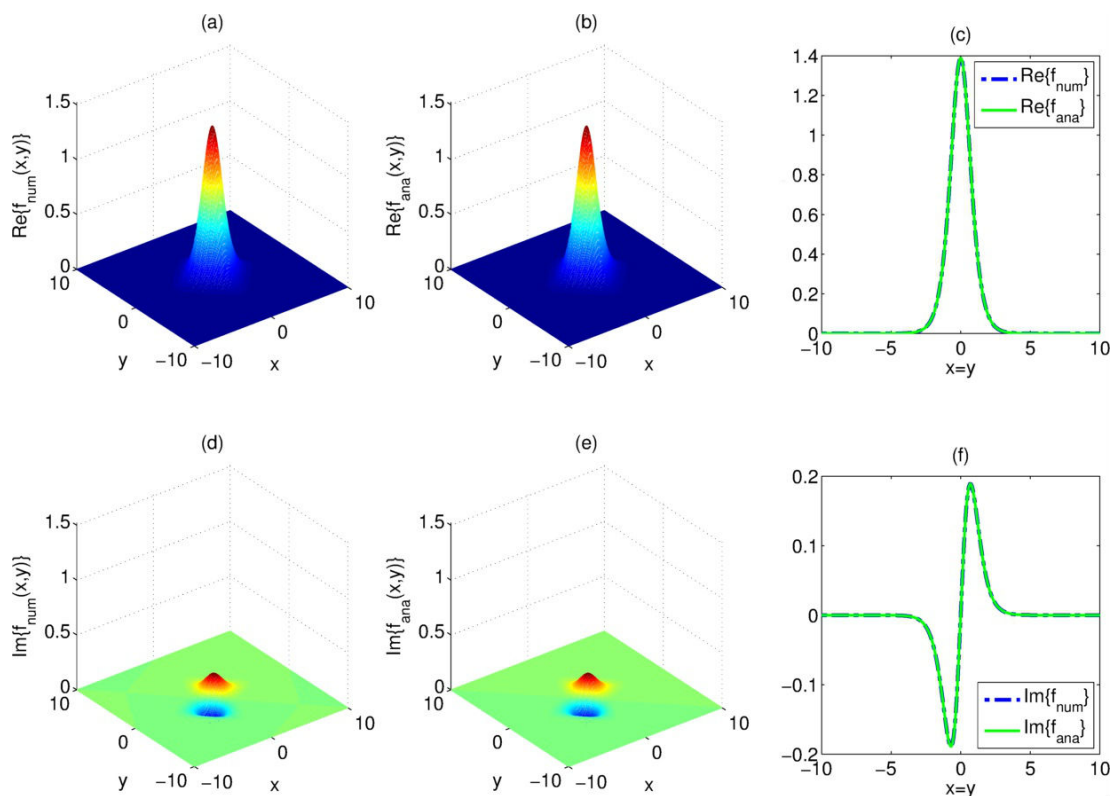
Figure 7.4 : Real parts of the solitons obtained numerically (a), analytically (b) and their superposed cross sections (c) for $\alpha = 1, \beta = -1, V_0 = 0.1, W_0 = 0.5$. Complex parts of the solitons obtained numerically (d), analytically (e) and their superposed cross sections (f) for the same case.
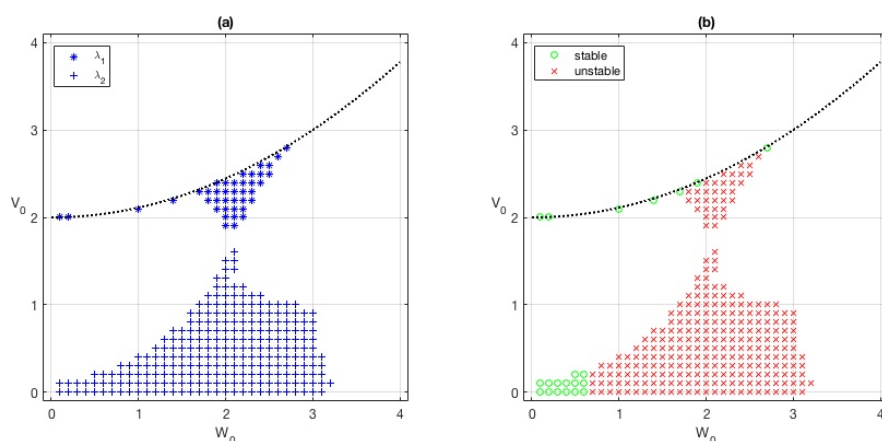
Figure 7.5 : (a) Numerically obtained solitons for $\alpha = 1$, $\beta = -1$ and varying potential depths, (b) Analytically obtained, nonlinearly stable (marked as green circles) and nonlinearly unstable (marked as red crosses) solitons.
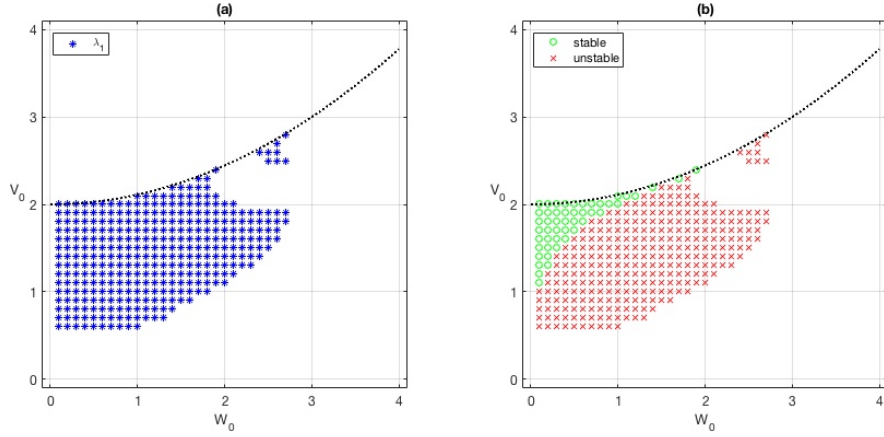
Figure 7.6 : (a) Numerically obtained solitons for $\alpha = \beta = 1$ and varying potential depths, (b) Analytically obtained, nonlinearly stable (marked as green circles) and nonlinearly unstable (marked as red crosses) solitons.
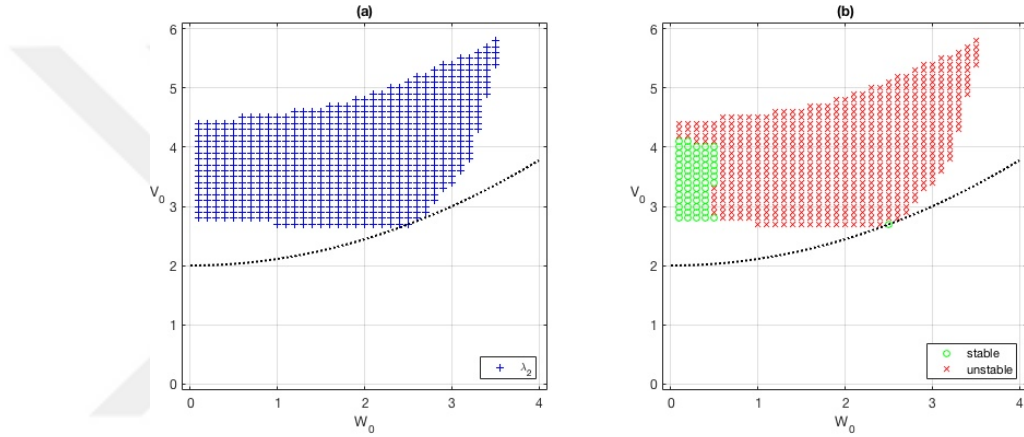
Figure 7.7 : (a) Numerically obtained solitons for $\alpha = \beta = -1$ and varying potential depths, (b) Analytically obtained, nonlinearly stable (marked as green circles) and nonlinearly unstable (marked as red crosses) solitons.

For the numerical results in self-focusing cubic, self-focusing quintic media, we fix $\alpha = \beta = 1$ and vary the potential depths V_0 and W_0 between 0 and 4. Obtained solitons are marked in Figure 7.6(a) with stars. Note that the second root λ_2 in the fixed point iteration does not yield any soliton in this case and there exists no solitons in case of a pure imaginary potential, i.e. if $V_0 = 0$.

For the numerical results in self-defocusing cubic, self-defocusing quintic media, we fix $\alpha = \beta = -1$ and vary the potential depths V_0 and W_0 between 0 and 6. Obtained solitons are marked in Figure 7.7(a) with pluses. Recall that solitons in self-defocusing cubic media may only exist above the dotted curve that depicts the case $f_0 = 0$. Note that the first root λ_1 in the fixed point iteration does not yield any soliton in this case.

For the numerical results in self-defocusing cubic, self-focusing quintic media, we fix $\alpha = -1$, $\beta = 1$ and vary the potential depths V_0 and W_0 between 0 and 5. Obtained
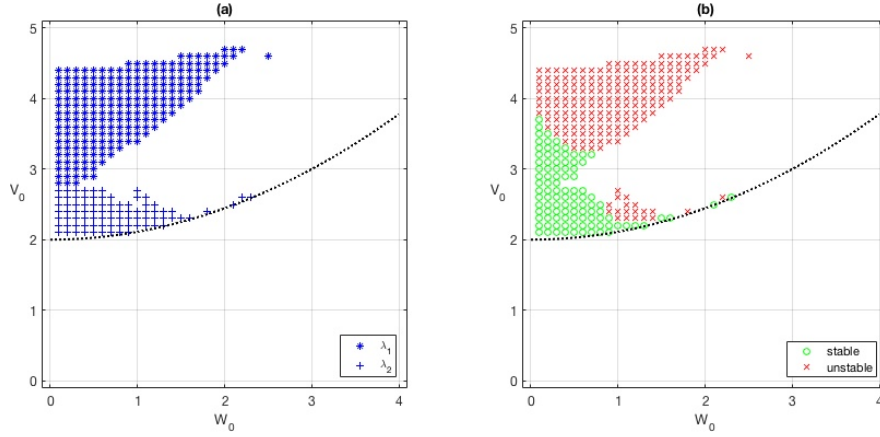
Figure 7.8 : (a) Numerically obtained solitons for $\alpha = -1$, $\beta = 1$ and varying potential depths, (b) Analytically obtained, nonlinearly stable (marked as green circles) and nonlinearly unstable (marked as red crosses) solitons.

solitons are marked in Figure 7.8(a), where stars indicate the ones obtained using the first root λ_1 in the fixed point iteration and pluses indicate the ones obtained using the second root λ_2.

7.3.3 Nonlinear Stability

Regarding the nonlinear stability of the obtained solitons in self-focusing cubic, self-defocusing quintic media ($\alpha = 1$, $\beta = -1$), circles in Figure 7.5(b) map stable solitons whereas the crosses map unstable ones. It can be observed that most solitons are unstable and that stable solitons are mainly obtained for smaller W_0 values or close to the threshold curve.

Regarding the nonlinear stability of the obtained solitons in self-focusing cubic, self-focusing quintic media ($\alpha = \beta = 1$), circles in Figure 7.6(b) map stable solitons whereas the crosses map unstable ones. It can be observed that most solitons are unstable and that stable solitons are mainly obtained close to the threshold curve.

A nonlinearly unstable soliton in self-focusing cubic, self-focusing quintic media is depicted in Figure 7.9. It is observed that neither the maximum amplitude nor the shape is conserved during the evolution; the blow-up can be clearly seen in Figure 7.9(b) around $z = 71$.

Regarding the nonlinear stability of the obtained solitons in self-defocusing cubic, self-defocusing quintic media ($\alpha = \beta = -1$), circles in Figure 7.7(b) map stable

72

z=0 z=20 z=40 z=60 z=71

(b)

$|u_{max}|$

z
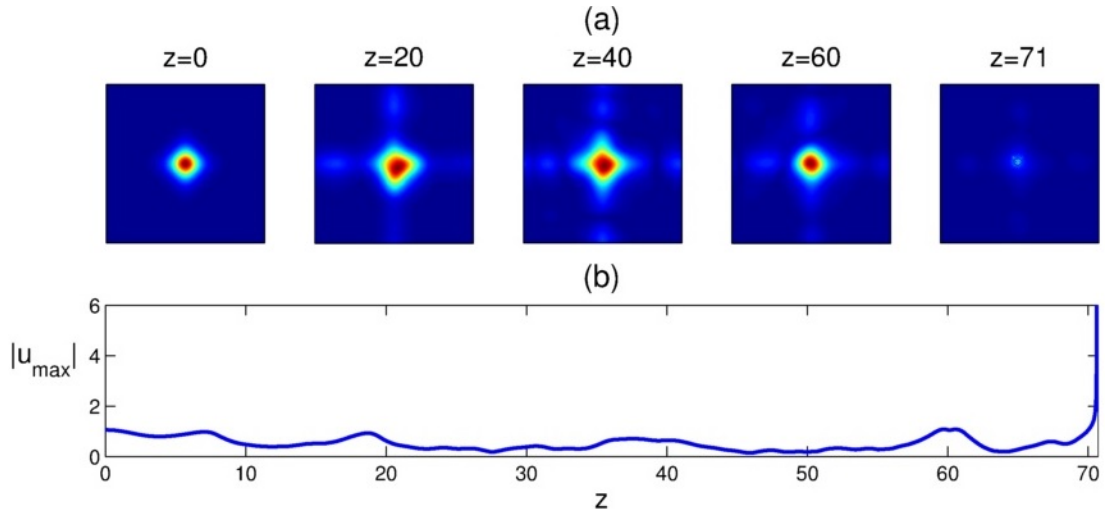
Figure 7.9 : (a) Nonlinear evolution of the numerically obtained soliton for $V_0 = 1$, $W_0 = 1$ and $\alpha = \beta = 1$ (view from top), (b) Maximum amplitude as a function of the propagation distance z.

(a)

z=0 z=25 z=50 z=75 z=100

(b)

$|u_{max}|$

z
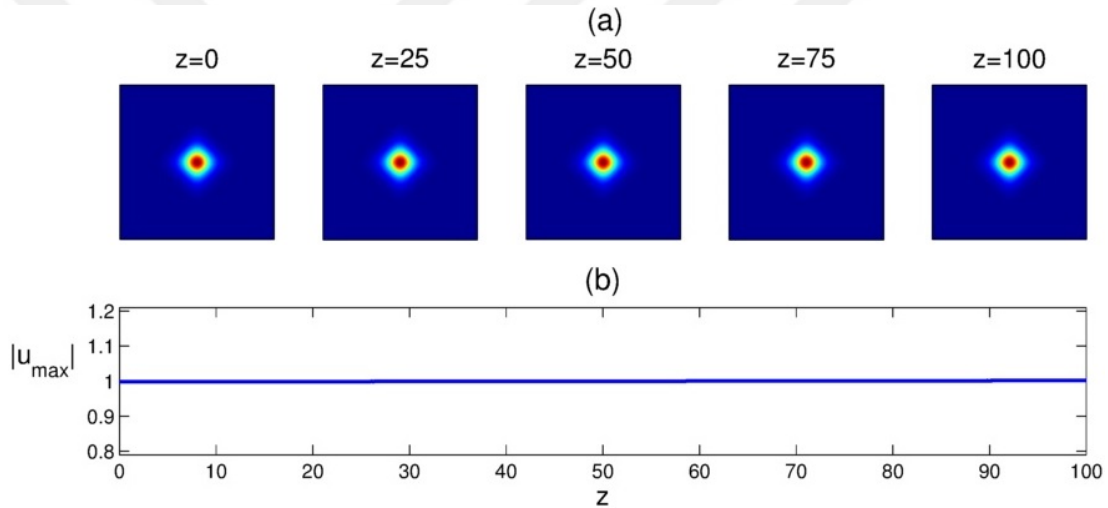
Figure 7.10 : (a) Nonlinear evolution of the numerically obtained soliton for $V_0 = 3$, $W_0 = 0.1$ and $\alpha = \beta = -1$ (view from top), (b) Maximum amplitude as a function of the propagation distance z.

solitons whereas the crosses map unstable ones. It can be observed that most solitons are unstable and that stable solitons are mainly obtained for smaller values of W_0.

A nonlinearly stable soliton in self-defocusing cubic, self-defocusing quintic media is depicted in Figure 7.10. It is observed that both the maximum amplitude and the shape are conserved during the evolution.

Regarding the nonlinear stability of the obtained solitons in self-defocusing cubic, self-focusing quintic media ($\alpha = -1$, $\beta = 1$), circles in Figure 7.8(b) map stable
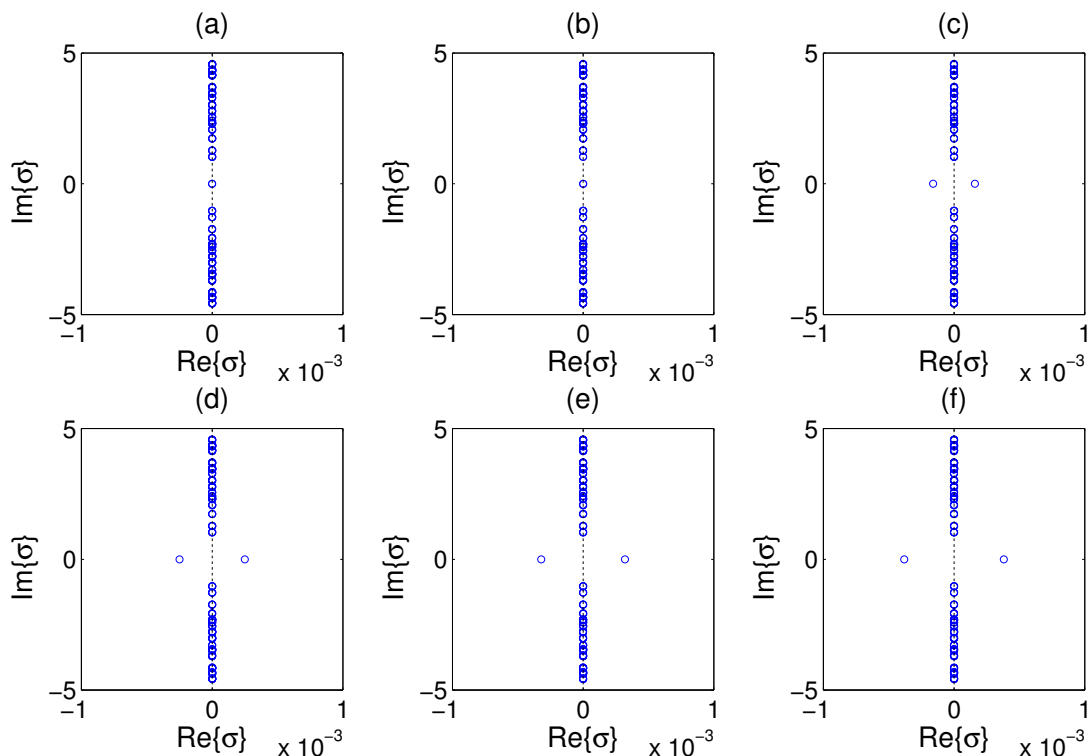
Figure 7.11 : Linear spectrum of the numerically obtained solitons for $V_0 = 2$, $W_0 = 0.1$, $\alpha = 1$ and (a) $\beta = -5$, (b) $\beta = -3$, (c) $\beta = -1$, (d) $\beta = 1$, (e) $\beta = 3$, (f) $\beta = 5$.

solitons whereas the crosses map unstable ones. It can be observed that most solitons are unstable and that stable solitons are mainly obtained for smaller values of W_0.

7.3.4 Linear Stability

To find out the impact of the quintic term on the soliton stability, linear spectra of the solitons are acquired by gradually increasing β, the coefficient of the quintic term. As Figure 7.11 reveals, increasing the value of β without changing the other parameters, influences soliton stability in self-focusing cubic media adversely. The eigenvalues with positive real parts in Figure 7.11(c) thru (f) will cause these solitons to blow up.

Linear spectra of all solitons in self-defocusing cubic, self-defocusing quintic media ($\alpha = \beta = -1$) contain eigenvalues with non-zero real parts, hence obtained solitons are linearly unstable.

Similar to the previous case, linear spectra of all solitons in self-defocusing cubic, self-focusing quintic media ($\alpha = -1$, $\beta = 1$) also contain eigenvalues with non-zero

real parts. Hence, we can say that the obtained solitons in self-defocusing cubic media are linearly unstable.

7.3.5 Power Analysis

Soliton power is defined as

$$P = \int\limits_{-\infty}^{\infty} \int\limits_{-\infty}^{\infty} |u(x,y,z)|^2 dx dy \tag{7.9}$$

[62]. In the presence of a dissipative potential, the mass of the particle does not remain constant and the total power of the soliton evolves according to the equation

$$\frac{d}{dz} \int\limits_{-\infty}^{\infty} \int\limits_{-\infty}^{\infty} |u|^2 dx dy = 2 \int\limits_{-\infty}^{\infty} \int\limits_{-\infty}^{\infty} W(x,y)|u|^2 dx dy . \tag{7.10}$$

Here, Eq. (7.10) turns out to be zero, meaning that the power is not varying with the propagation distance z. In fact, for the solitons given by Eq. (7.8), the power is explicitly obtained as

$$P = f_0^2 \int\limits_{-\infty}^{\infty} \operatorname{sech}^2(x)dx \int\limits_{-\infty}^{\infty} \operatorname{sech}^2(y)dy = 4f_0^2 = \frac{4}{\alpha}\left(2 - V_0 + \frac{W_0^2}{9}\right) . \tag{7.11}$$

It is to be noted that the power is a positive quantity and independent of parameter β, the coefficient of the quintic term. As the power is also independent of z, a stable soliton's power stays constant during evolution.

7.4 CQNLS with a $\mathcal{PT}$-Symmetric Potential with Defects

In this section, we consider the CQNLS in self-focusing cubic, self focusing quintic media as a model by setting the values $\alpha = \beta = \mu = 1$, $W_0 = 0.1$ and letting V_0 vary between 0 and 4.

7.4.1 Numerical Solutions

For the potential depth $V_0 = 1$, the obtained solitons are depicted in Figure 7.12, 7.13 and 7.14 on the lattice without defect, with positive defect and with negative defect, respectively. The cross sections of the solitons are plotted with green curves in the (b) and (d) parts of these figures whereas the blue curves depict the corresponding potentials. It can be seen that ceteris paribus, the positive defect decreases the amplitude of the soliton whereas the negative defect increases it.
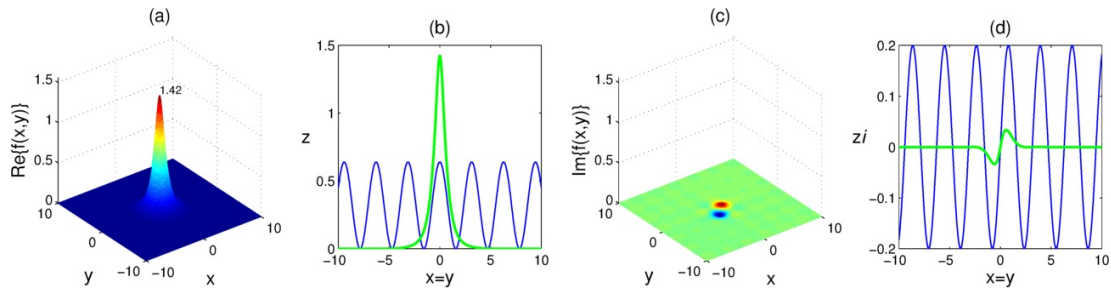
Figure 7.12 : (a) Real part, (b) Cross section of the real part, (c) Imaginary part, (d) Cross section of the imaginary part of the obtained soliton with $V_0 = 1$ on the lattice without defect.
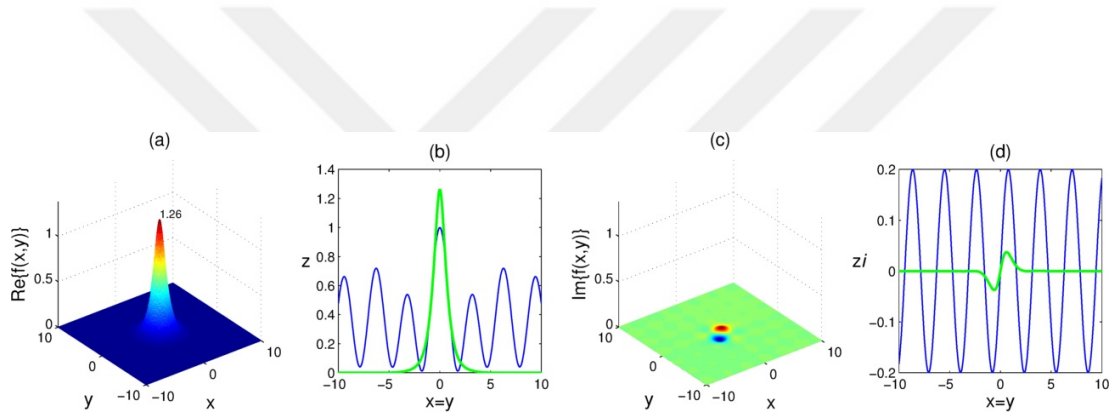
Figure 7.13 : (a) Real part, (b) Cross section of the real part, (c) Imaginary part, (d) Cross section of the imaginary part of the obtained soliton with $V_0 = 1$ on the lattice with positive defect.
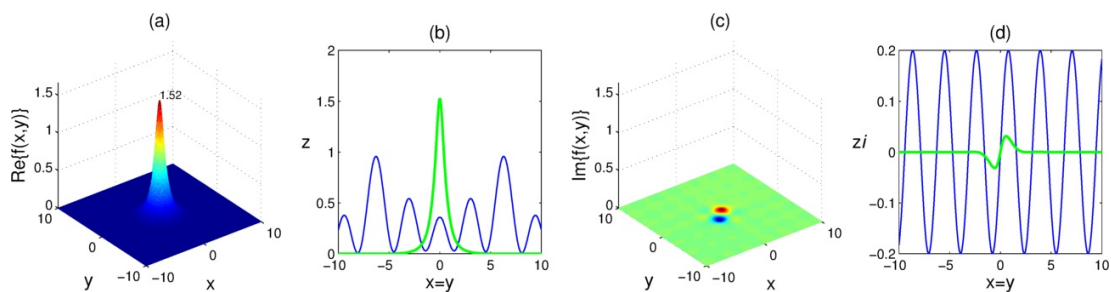

Figure 7.14 : (a) Real part, (b) Cross section of the real part, (c) Imaginary part, (d) Cross section of the imaginary part of the obtained soliton with $V_0 = 1$ on the lattice with negative defect.
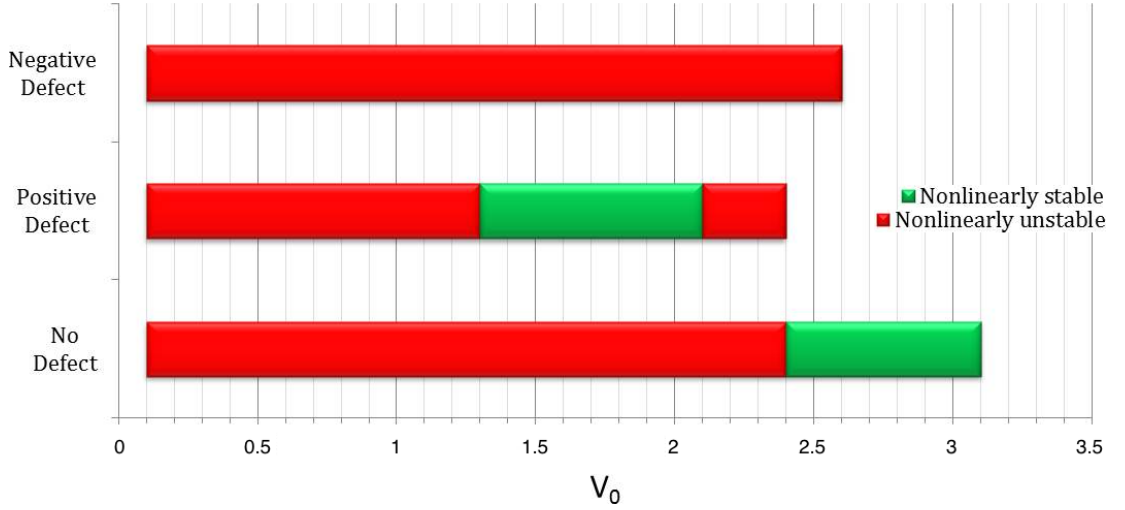
Figure 7.15 : Numerically obtained solitons of the (2+1)D CQNLS equation with a
$\mathcal{PT}$-symmetric potential with and without defects for varying potential
depths V_0 in the self-focusing cubic, self-focusing quintic case
$(\alpha = \beta = 1)$ for $\mu = 1$ and $W_0 = 1$.

7.4.2 Nonlinear Stability

The results of the nonlinear stability analysis of the numerically obtained solitons are
summarized in Figure 7.15, where the color green represents stable solitons whereas
the color red represents unstable ones. It can be seen that adding a defect to the lattice
narrows down the existence region of the solitons and that the negative defect makes
all the solitons nonlinearly unstable in this medium while one can obtain nonlinearly
stable solitons with the positive defect, for different values of the potential depth V_0.

In Figure 7.16, a nonlinearly stable soliton is depicted. It can be seen that the
soliton conserves its shape and maximum amplitude during the evolution unlike the
nonlinearly unstable soliton shown in Figure 7.17, during whose evolution neither the
maximum amplitude nor the shape is conserved.

7.4.3 Linear Stability

The linear stability of the obtained solitons are investigated by the linear spectrum
analysis and all of them are found to be linearly unstable. The linear spectra of the
solitons given in Figure 7.12, 7.13 and 7.14 are plotted in Figure 7.18. Although these
solitons are all unstable due to the positive real eigenvalues in their linear spectra, it
can be noted that the value of the unstable eigenvalue is smaller with the positive defect
and greater with the negative defect compared to the value of the unstable eigenvalue
without the defect in this medium.

(a)

z=0   z=5   z=10   z=15   z=20   z=25   z=30

(b)
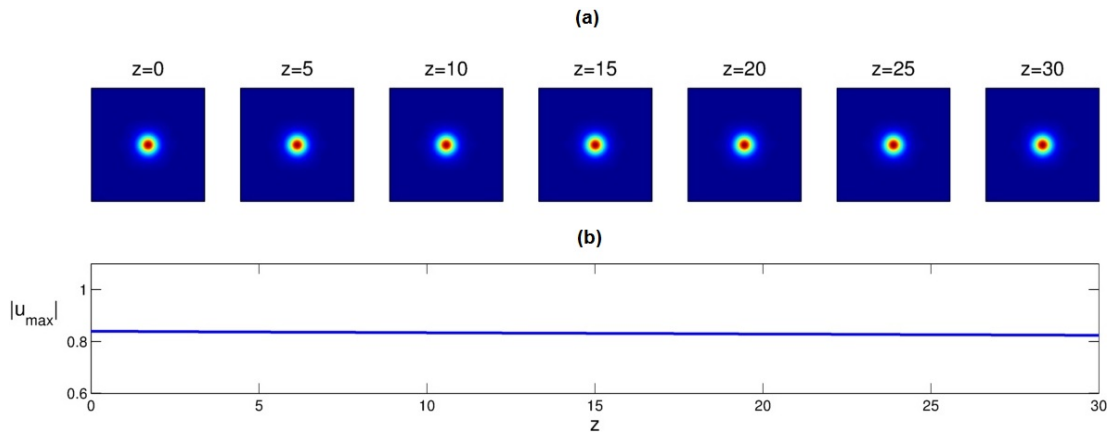
Figure 7.16 : (a) Nonlinear evolution of the numerically obtained soliton of the (2+1)D CQNLS equation with a $\mathcal{PT}$-symmetric potential with positive defect for $V_0 = 2$ and $W_0 = 0.1$ in the self-defocusing cubic, self-focusing quintic case $(\alpha = \beta = 1)$ (view from top), (b) Maximum amplitude as a function of the propagation distance z.

z=0   z=5   z=10   z=15   z=20   z=25   z=30
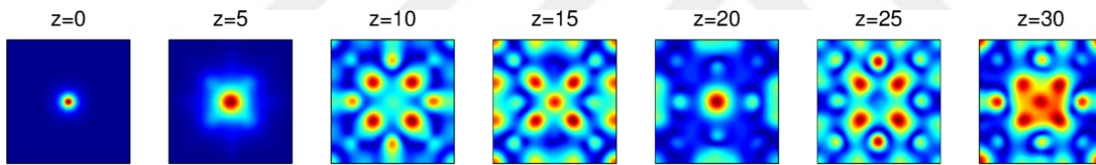
**Figure 7.17** : Nonlinear evolution of the numerically obtained soliton of the (2+1)D CQNLS equation with a $\mathcal{PT}$-symmetric potential with negative defect for $V_0 = 2$ and $W_0 = 0.1$ in the self-defocusing cubic, self-focusing quintic case $(\alpha = \beta = 1)$ (view from top).
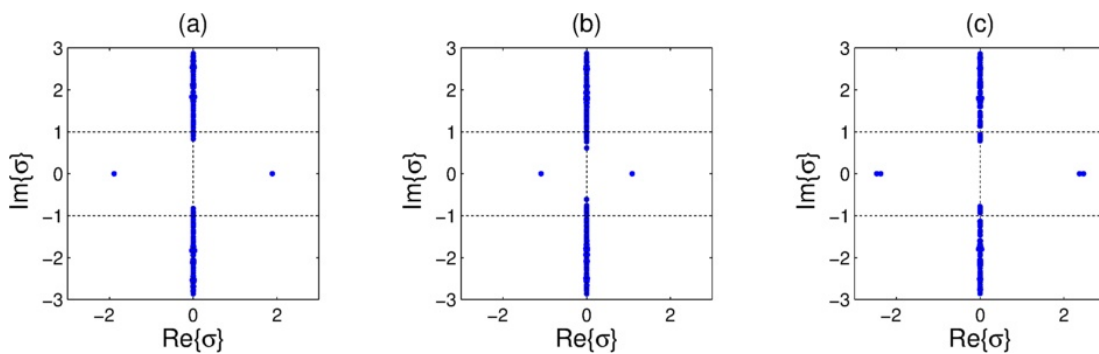
Figure 7.18 : Linear spectrum of the solitons given in (a) Figure 7.12, (b) Figure 7.13 and (c) Figure 7.14.

78

8. SOLITONS OF THE (2+1)D CUBIC-SATURABLE NLS EQUATION

8.1 Cubic-Saturable NLS with a $\mathcal{PT}$-Symmetric Potential with Defects

In this section, we present graphs and existence regimes of numerically obtained solitons of Eq. (1.3) in various saturable media and their stability properties for different potentials given in Section 3.3.

8.1.1 Numerical Solutions

For the numerical results, we let the propagation constant μ vary between 0 and 10 while changing the value of the saturation coefficient s between 0 and 1.

Typical field profiles of obtained solitons are shown in Figure 8.1 for different potentials. In the presence of a positive defect, the maximum amplitude of a soliton is smaller and in the presence of a negative defect, the maximum amplitude of a soliton is greater in comparison to the potential without defect.

All the solitons obtained numerically by means of the Pseudo-Spectral Renormalization Method explained in Section 4.2 are marked in Figure 8.2 by stars where the blue lines are the gap boundries for the potential without defect ($\delta = 0$), the green lines for the potential with positive defect (θ^+, $\delta = 1$) and the red lines for the potential with negative defect (θ^-, $\delta = 1$). The gap region of the solitons under the potential without defect is bigger than the gap regions of the solitons under the potential with defects, as expected. It can be also seen that more solitons are obtained whenever there is no saturation ($s = 0$) and no soliton could be obtained if the saturation coefficient $s > 0.5$.

8.1.2 Nonlinear Stability

In Figure 8.3, a nonlinearly unstable soliton is shown. It can be clearly seen that the soliton conserves neither its shape nor its maximum amplitude during evolution. This is also true for other gap solitons on the $\mathcal{PT}$-symmetric potential with or without defect if there is no saturation. In saturable media on the other hand, obtained solitons
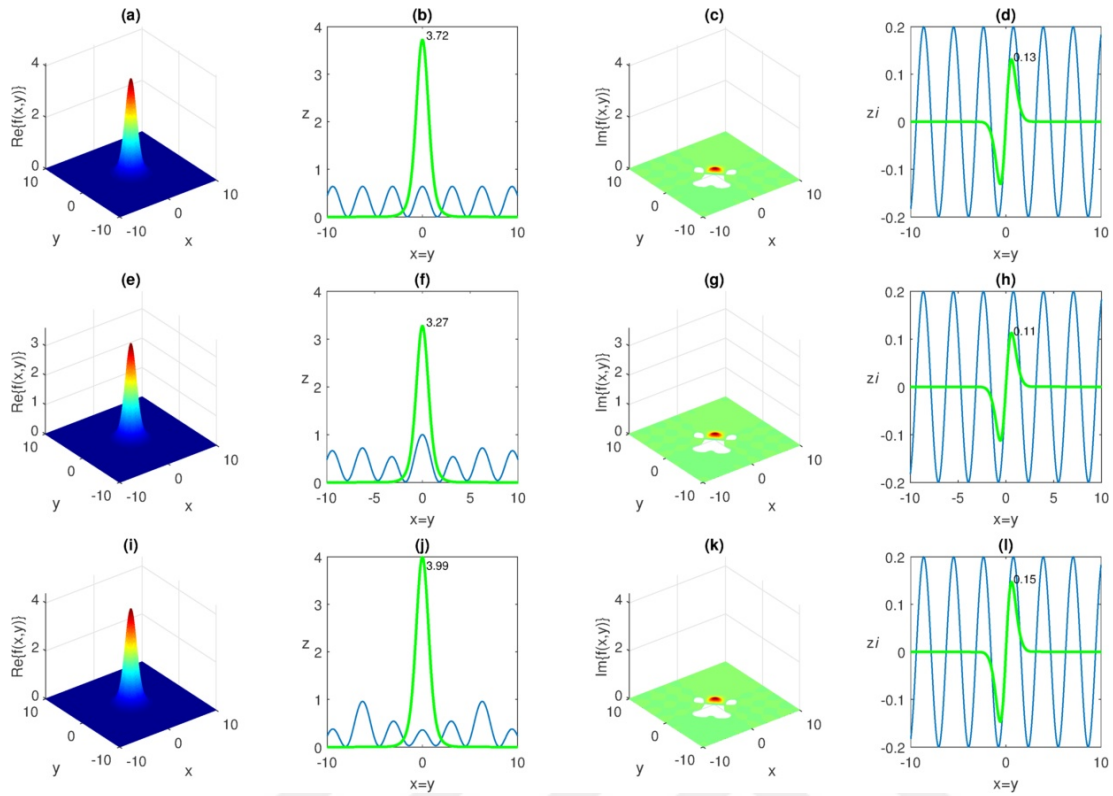
Figure 8.1 : Real parts of the numerically obtained solitons (a, e, i) and their diagonal cross sections superposed on the potential (b, f, j), imaginary parts of the numerically obtained solitons (c, g, k) and their diagonal cross sections superposed on the potential (d, h, l) where $s = 0.2$, $\mu = 1.9$ and the potential has no defect, positive defect and negative defect, respectively.
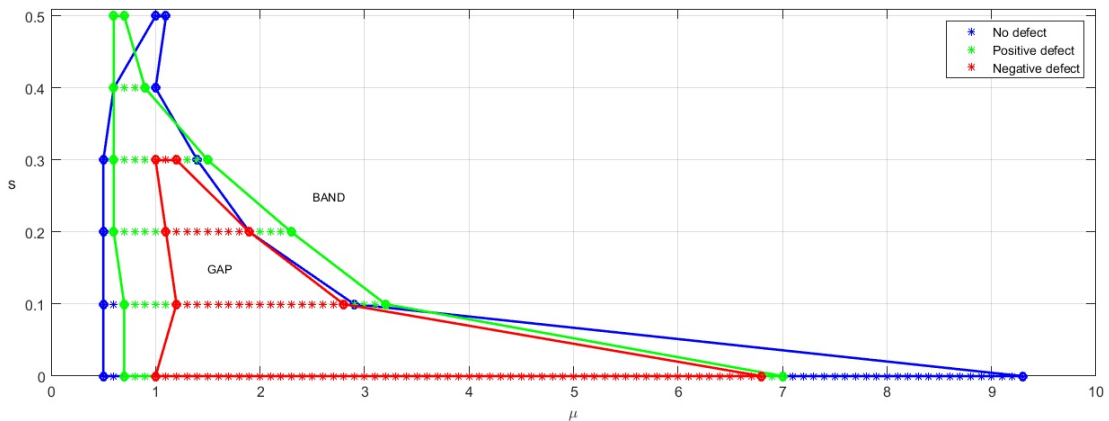
Figure 8.2 : Band-gap regions for the numerically obtained solitons of the (2+1)D cubic-saturable NLS equation with a $\mathcal{PT}$-symmetric potential without defect (blue), with positive defect (green) and with negative defect (red).
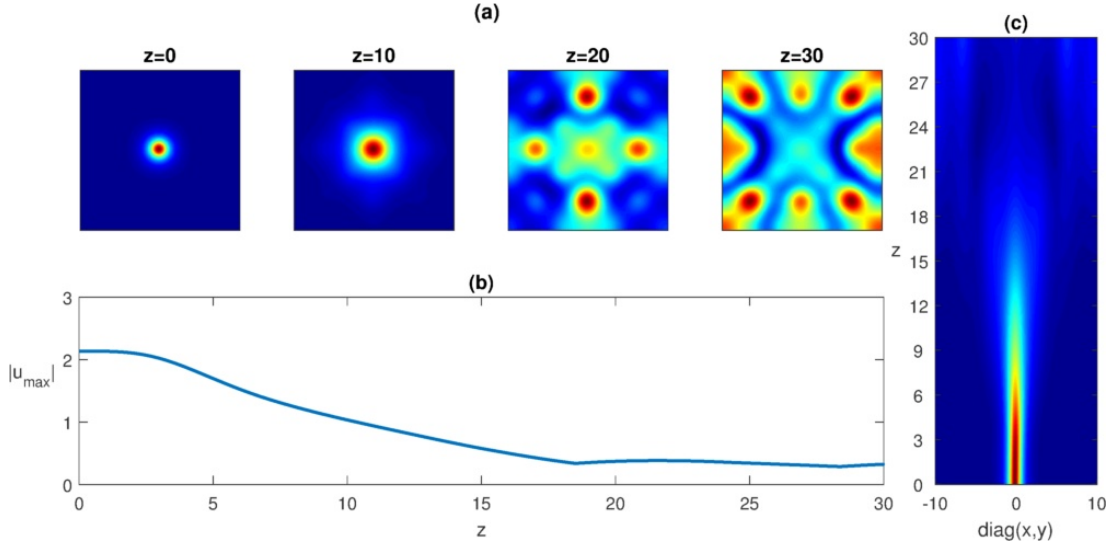
Figure 8.3 : Nonlinear evolution of the soliton obtained for $s = 0$, $\mu = 1.1$ and with a $\mathcal{PT}$-symmetric potential with negative defect: (a, c) View from top, (b) Maximum amplitude as a function of the propagation distance z.

are nonlinearly stable. An example of a nonlinearly stable soliton is depicted in Figure 8.4 where the soliton's shape is well-conserved during evolution.

8.1.3 Power Analysis

Soliton power defined in Section 7.3.5, can also be utilized in determining a soliton's stability. A necessary condition for the soliton solution $u(x,y,z) = f(x,y)e^{i\mu z}$ to be stable is that its power increases with increasing propagation constant, i.e.

$$\frac{dP}{d\mu} > 0 \,, \tag{8.1}$$

also known as the slope condition [35]. Furthermore, a necessary condition for collapse in the 2D cubic NLS equation is that the power of the soliton exceeds the critical power $P_c \approx 11.7$ [38].

The powers of the obtained solitons are plotted versus their propagation constants. As it can be seen in Figure 8.5, the slope condition is satisfied in all the cases. It is remarkable that the power graphs asymptotically approach the critical power for increasing values of μ when there is no saturation (see Figure 8.5(a-c)).

8.1.4 Linear Stability

Now that the slope condition is satisfied and the critical power is not exceeded, one may expect stable solitons. However, the linear spectrum analysis reveals the opposite.

81
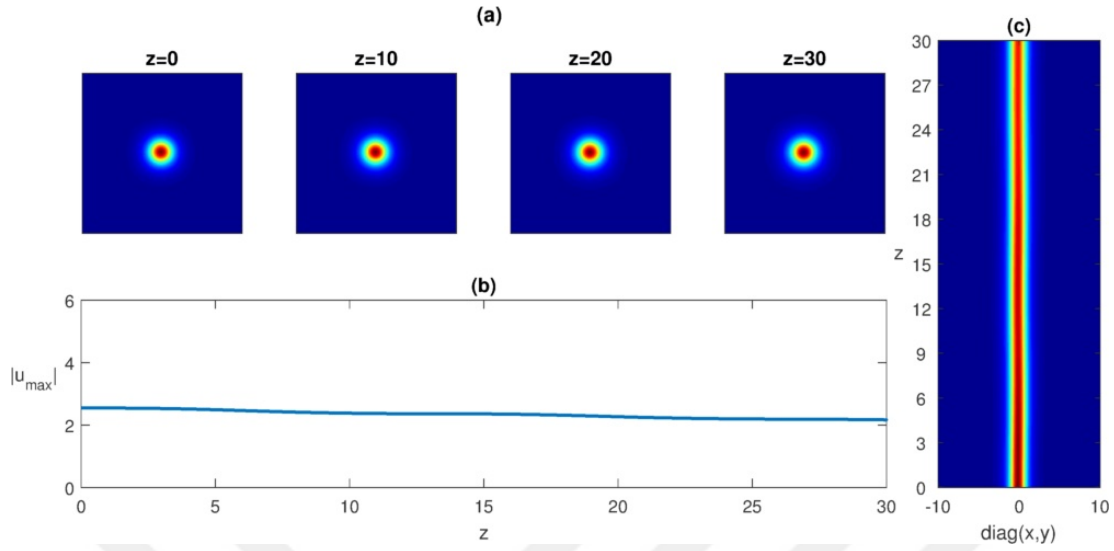
Figure 8.4 : Nonlinear evolution of the soliton obtained for $s = 0.2$, $\mu = 1.1$ and with a $\mathcal{PT}$-symmetric potential with negative defect: (a, c) View from top, (b) Maximum amplitude as a function of the propagation distance z.
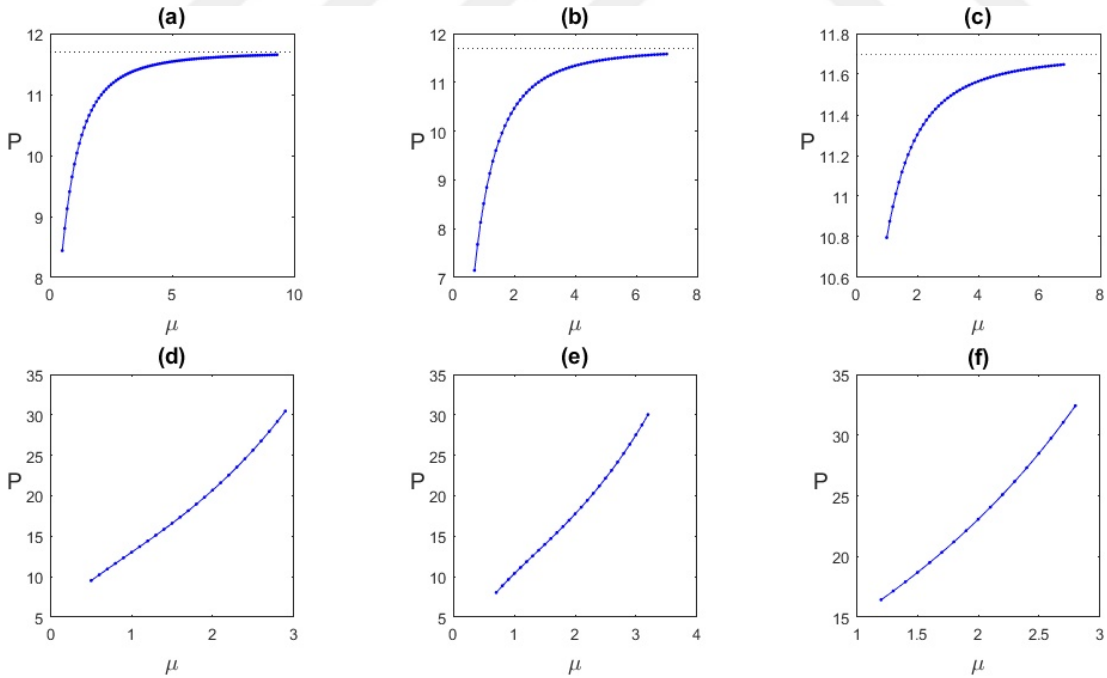
Figure 8.5 : Power as a function of propagation constant for the numerically obtained solitons: (a) $s = 0$, no defect; (b) $s = 0$, positive defect; (c) $s = 0$, negative defect; (d) $s = 0.1$, no defect; (e) $s = 0.1$, positive defect; (f) $s = 0.1$, negative defect.
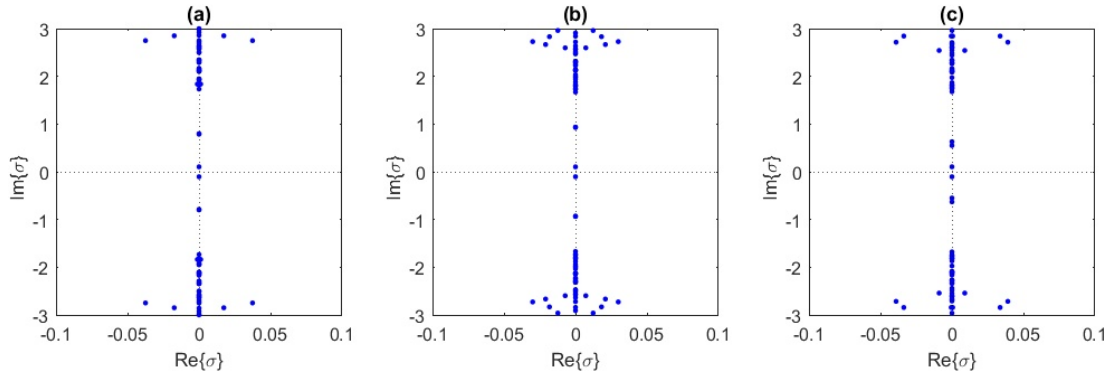
Figure 8.6 : Linear spectrum of the solitons obtained for $s = 0.2$, $\mu = 1.9$ and with a $\mathcal{PT}$-symmetric potential (a) without defect , (b) with positive defect and (c) with negative defect.

Due to eigenvalues with non-zero real parts in their linear spectra, solitons considered in Figure 8.6 and all the other gap solitons are found to be linearly unstable. The presence or absence of a defect in the lattice does not really affect the linear stability. However, the presence of saturation in the medium drastically lowers $\max\left(\mathrm{Re}\{\sigma\}\right)$, i.e. contributes towards linear stability.

9. CONCLUSIONS AND RECOMMENDATIONS

The purpose of the study regarding (1+1)D CQNLS equation with $\mathcal{PT}$-symmetric potential was to investigate the existence and stability properties of solitons of the (1+1)D CQNLS equation with a $\mathcal{PT}$-symmetric potential. Firstly, the solutions are obtained numerically by means of the Spectral Renormalization Method for various potential depths and in different self-focusing / defocusing cubic-quintic media. It is shown that the numerical and the analytical results are in good agreement. No bistable soliton is found in the investigated cases. The linear and nonlinear stability properties of the numerically and analytically obtained solitons are investigated by means of linear spectrum analysis and by direct simulations. Stability and instability regions of the solitons are depicted and it is observed that stable solitons are predominantly obtained either for smaller values of W_0 or close to the threshold curve.

In the work regarding (2+1)D CQNLS equation with $\mathcal{PT}$-symmetric potential, two-dimensional optical solitons of the CQNLS equation with a $\mathcal{PT}$-symmetric potential along with their stability properties are examined. Primarily, exact soliton solutions are calculated for the chosen $\mathcal{PT}$-symmetric potential. Then, solitons are numerically obtained using our modified Spectral Renormalization Method for various potential depths and in different self-focusing / defocusing cubic-quintic media. For various potentials and media, analytical and numerical results regarding the existence and stability of the fundamental solitons are computed and these are in accord. In any of the four media investigated in this study, no bistable soliton is observed. Linear spectrum analysis and direct simulations are employed to discover the stable and unstable solitons. The results show that most solitons are unstable. However, stable solitons could be obtained when the depth of the complex part of the $\mathcal{PT}$-symmetric potential is small. An important finding is that increasing the value of the coefficient of the quintic term destabilizes solitons in self-focusing cubic media. Moreover, for all the investigated cases, numerically obtained soliton powers match up with the exact values and nonlinearly stable solitons' powers stay constant during evolution as expected.

To sum up the study regarding (2+1)D CQNLS equation with $\mathcal{PT}$-symmetric potential possessing defects, a defect in the $\mathcal{PT}$-symmetric lattice reduces the gap width, a negative defect causes the solitons to become nonlinearly unstable and all obtained solitons are linearly unstable independently of the defect, in self-focusing cubic, self-focusing quintic media.

The purpose of the study regarding (2+1)D cubic-saturable NLS equation with $\mathcal{PT}$-symmetric potential possessing defects, was to investigate the existence and stability properties of solitons of the (2+1)D cubic-saturable NLS equation with $\mathcal{PT}$-symmetric potentials with different types of defects. Solitons are obtained numerically by means of the Pseudo-Spectral Renormalization Method for various values of the propagation constant and in different saturable media. It is observed that increasing the saturation or adding defects to the potential narrows down the gap width. The linear and nonlinear stability properties of the numerically obtained solitons are investigated by linear spectrum and direct simulations, respectively. Although the slope condition is satisfied, the solitons are found to be linearly unstable. On the other hand, solitons are found to be nonlinearly stable if there is saturation in the medium. All in all, a defect in the $\mathcal{PT}$-symmetric lattice reduces the gap width whereas saturation has a positive effect on the soliton stability.

As a future study, existence and stability properties of dipole and vortex solitons might be investigated.

REFERENCES

[1] **Kivshar, Y.S. and Agrawal, G.P.** (2003). *Optical Solitons: From Fibers to Photonic Crystals*, Academic Press.

[2] **Dauxois, T. and Peyrard, M.** (2006). *Physics of Solitons*, Cambridge University Press.

[3] **Christodoulides, D.N., Lederer, F. and Silberberg, Y.** (2003). Discretizing light behaviour in linear and nonlinear waveguide lattices, *Nature*, *424*, 817–823.

[4] **Musslimani, Z.H., Makris, K.G., El-Ganainy, R. and Christodoulides, D.N.** (2008). Optical solitons in $\mathcal{PT}$ periodic potentials, *Physical Review Letters*, *100*, 030402.

[5] **Nath, D., Roy, B. and Roychoudhury, R.** (2015). $\mathcal{PT}$ symmetric nonlinear optical lattice: Analytical solutions, *Chaos, Solitons and Fractals*, *81*, 91–97.

[6] **Ahmed, Z.** (2001). Real and complex discrete eigenvalues in an exactly solvable one-dimensional complex $\mathcal{PT}$-invariant potential, *Physics Letters A*, *282*, 343–348.

[7] **Boudebsa, G., Cherukulappuratha, S., Leblonda, H., Trolesb, J., Smektalab, F. and Sancheza, F.** (2003). Experimental and theoretical study of higher-order nonlinearities in chalcogenide glasses, *Optics Communications*, *219*, 427–433.

[8] **Zegadlo, K.B., Wasak, T., Malomed, B.A., Karpierz, M.A. and Trippenbach, M.** (2014). Stabilization of solitons under competing nonlinearities by external potentials, *Chaos: An Interdisciplinary Journal of Nonlinear Science*, *24*, 043136.

[9] **Genoud, F., Malomed, B.A. and Weishäupl, R.M.** (2016). Stable NLS solitons in a cubic–quintic medium with a delta-function potential, *Nonlinear Analysis: Theory, Methods and Applications*, *133*, 28–50.

[10] **Burlak, G. and Malomed, B.A.** (2013). Stability boundary and collisions of two-dimensional solitons in $\mathcal{PT}$-symmetric couplers with the cubic-quintic nonlinearity, *Physical Review E*, *88*, 062904.

[11] **Göksel, İ., Bakırtaş, İ. and Antar, N.** (2015). Nonlinear lattice solitons in saturable media, *Applied Mathematics and Information Sciences*, *9*, 377–385.

[12] **Göksel, İ.**, **Antar, N. and Bakırtaş, İ.** (2015). Solitons of (1+1)D cubic-quintic nonlinear Schrödinger equation with $\mathcal{PT}$-symmetric potentials, *Optics Communications*, *354*, 277–285.

[13] **Ge, L.**, **Shen, M.**, **Zang, T.**, **Ma, C. and Dai, L.** (2015). Stability of optical solitons in parity-time-symmetric optical lattices with competing cubic and quintic nonlinearities, *Physical Review E*, *91*, 023203.

[14] **Hu, S. and Chen, H.** (2014). The optical properties of two-dimensional Scarff parity–time symmetric potentials, *Physics Letters A*, *378*, 3079–3083.

[15] **Bağcı, M.**, **Bakırtaş, İ. and Antar, N.** (2015). Fundamental solitons in parity-time symmetric lattice with a vacancy defect, *Optics Communications*, *356*, 472–481.

[16] **Conte, R. and Chow, K.W.** (2008). Doubly periodic waves of a discrete nonlinear Schrödinger system with saturable nonlinearity, *Journal of Nonlinear Mathematical Physics*, *15*, 398–409.

[17] **Calvo, G.F.**, **Belmonte-Beitia, J. and Pérez-García, V.M.** (2009). Exact bright and dark spatial soliton solutions in saturable nonlinear media, *Chaos, Solitons and Fractals*, *41*, 1791–1798.

[18] **Göksel, İ.**, (2011). Nonlinear lattice solitons in saturable media, Master's thesis, İTÜ, Istanbul, Turkey.

[19] **Lomdahl, P.S.** (1984). *What is a soliton?*, Los Alamos Science.

[20] **Senechal, M.** (2006). What is a quasicrystal?, *Notices to the American Mathematical Society*, *53*(8), 886–887.

[21] **Freedman, B.**, **Bartal, G.**, **Segev, M.**, **Lifshitz, R.**, **Christodoulides, D.N. and Fleischer, J.** (2006). Wave and defect dynamics in nonlinear photonic quasicrystals, *Nature*, *440*, 1166–1169.

[22] **Myint-U, T.** (1987). *Partial Differential Equations for Scientists and Engineers*, Prentice-Hall.

[23] **Berge, L.** (1998). Wave collapse in physics: principles and applications to light and plasma waves, *Physics Reports*, *303*, 259–370.

[24] **Kelley, P.L.** (1965). Self-focusing of optical beams, *Physical Review Letters*, *15*, 1005–1008.

[25] **Fibich, G. and Papanicolaou, G.C.** (1998). A modulation method for self-focusing in the perturbed critical nonlinear Schrödinger equation, *Physical Letters A*, *239*, 167–173.

[26] **Fibich, G. and Papanicolaou, G.C.** (1999). Self-focusing in the perturbed and unperturbed nonlinear Schrödinger equation in critical dimension, *SIAM Journal on Applied Mathematics*, *60*, 183–240.

[27] **Bağcı, M.**, (2010). Fundamental solitons in complex two dimensional lattices, Master's thesis, İTÜ, Istanbul, Turkey.

[28] **Segev, M. and Stegeman, G.I.** (1999). Optical spatial solitons and their interactions: universality and diversity, *Science*, *286*, 1518–1523.

[29] **Ablowitz, M.J. and Horikis, T.P.** Nonlinear waves in optical media, *Journal of Computational and Applied Mathematics*, *234*, 1896–1903.

[30] **Yang, J.** (2004). Stability of vortex solitons in a photorefractive optical lattice, *New Journal of Physics*, *6*(47), 1–12.

[31] **Akhmediev, N.N.**, **Soto-Crespo, J.M. and Wright, E.M.** (1992). Recurrence and azimuthal-symmetry breaking of a cylindrical Gaussian beam in a saturable self-focusing medium, *Physical Review A*, *45*, 3168.

[32] **Edmundson, D.E. and Enns, R.H.** (1995). Particlelike nature of colliding three-dimensional optical solitons, *Physical Review A*, *51*, 2491–2498.

[33] **Petviashvili, V.I.** (1976). Equation of an extraordinary soliton, *Soviet Journal of Plasma Physics*, *2*, 257–258.

[34] **Ablowitz, M.J. and Musslimani, Z.H.** (2005). Spectral renormalization method for computing self-localized solutions to nonlinear systems, *Optics Letters*, *30*, 2140–2142.

[35] **Vakhitov, N.G. and Kolokolov, A.A.** (1973). Stationary solutions of the wave equation in a medium with nonlinearity saturation, *Radiophysics and Quantum Electronics*, *16*, 783–789.

[36] **Weinstein, M.I.** (1985). Modulational stability of ground states of nonlinear Schrödinger equations, *SIAM Journal on Mathematical Analysis*, *16*, 472–491.

[37] **Rose, H.A. and Weinstein, M.I.** (1988). On the bound states of the nonlinear Schrödinger equation with a linear potential, *Physica D*, *30*, 207–218.

[38] **Weinstein, M.I.** (1983). Nonlinear Schrödinger equation and sharp interpolation estimates, *Communications in Mathematical Physics*, *87*, 567–576.

[39] **Sivan, Y.**, **Fibich, G.**, **Ilan, B. and Weinstein, M.I.** (2008). Qualitative and quantitative analysis of stability and instability dynamics of positive lattice solitons, *Physical Review E*, *78*, 046602.

[40] **Cagnon, L.** (1989). Exact travelling-wave solutions for optical models based on the nonlinear cubic-quintic Schrödinger equation, *Journal of the Optical Society of America A*, *6*, 1477–1483.

[41] **Peyrard, M. and Dauxois, T.** (2004). *Physique des Solitons*, EDP Sciences.

[42] **Scott, A.** (2003). *Nonlinear Science*, Oxford University Press.

[43] **Whitham, G.B.** (1974). *Linear and Nonlinear Waves*, Wiley.

[44] **Abdullaev, F.K.**, **Kartashov, Y.V.**, **Konotop, V.V. and Zezyulin, D.A.** (2011). Solitons in $\mathcal{PT}$-symmetric nonlinear lattices, *Physical Review A*, *83*, 041805(R).

[45] **Maxwell, J.** (1873). *A Treatise on Electricity and Magnetism*, Clarendon Press.

[46] **Laine, T.** (2000). Electromagnetic wave propagation in nonlinear Kerr media, *Ph.D. thesis*, KTH, Stockholm, Sweden.

[47] **Yang, J.** (2010). *Nonlinear Waves in Integrable and Nonintegrable Systems*, SIAM Society for Industrial and Applied Mathematics.

[48] **Ablowitz, M.J.** (2011). *Nonlinear Dispersive Waves Asymptotic Analysis and Solitons*, Cambridge University Press.

[49] **Bender, C.M. and Boettcher, S.** (1998). Real spectra in non-Hermitian Hamiltonians having $\mathcal{PT}$-symmetry, *Physical Review Letters*, *80*, 5243–5246.

[50] **Bender, C.M., Boettcher, S. and Meisinger, P.N.** (1999). PT-symmetric quantum mechanics, *Journal of Mathematical Physics*, *40*, 2201–2229.

[51] **Bender, C.M.** (2007). Making sense of non-Hermitian Hamiltonians, *Reports on Progress in Physics*, *70*, 947–1018.

[52] **Makris, K.G., El-Ganainy, R., Christodoulides, D.N. and Musslimani, Z.H.** (2010). $\mathcal{PT}$-symmetric optical lattices, *Physical Review A*, *81*, 063807.

[53] **Khare, A., Al-Marzoug, S.M. and Bahlouli, H.** (2012). Solitons in PT-symmetric potential with competing nonlinearity, *Physics Letters A*, *376*, 2880–2886.

[54] **Bagchi, B. and Quesne, C.** (2010). An update on $\mathcal{PT}$-symmetric complexified Scarf II potential, spectral singularities and some remarks on the rationally-extended supersymmetric partners, *Journal of Physics A: Mathematical and Theoretical*, *43*, 305301.

[55] **Ablowitz, M.J., Ilan, B., Schonbrun, E. and Piestun, R.** (2006). Solitons in two-dimensional lattices possessing defects, dislocations, and quasicrystal structures, *Physical Review E*, *74*, 035601(R).

[56] **Antar, N.** (2014). Pseudospectral renormalization method for solitons in quasicrystal lattice with the cubic-quintic nonlinearity, *Journal of Applied Mathematics*, *2014*, 848153.

[57] **Strang, G.** (1968). On the construction and comparison of difference schemes, *SIAM Journal on Numerical Analysis*, *5*, 506–517.

[58] **Rossmann, W.** (2002). *Lie Groups – An Introduction Through Linear Groups*, Oxford Science Publications.

[59] **Washburn, B.** (2002). Numerical solutions to the nonlinear Schrödinger equation, *Ph.D. thesis*, Georgia Tech, Atlanta, GA, USA.

[60] **Nixon, S., Ge, L. and Yang, J.** (2012). Stability analysis for solitons in $\mathcal{PT}$-symmetric optical lattices, *Physical Review A*, *85*, 023822.

[61] **Musslimani, Z.H.**, **Makris, K.G.**, **El-Ganainy, R. and Christodoulides, D.N.** (2008). Analytical solutions to a class of nonlinear Schrödinger equations with $\mathcal{PT}$-like potentials, *Journal of Physics A: Mathematical and Theoretical*, *41*, 244019.

[62] **Bağcı, M.**, **Bakırtaş, İ. and Antar, N.** (2014). Vortex and dipole solitons in lattices possessing defects and dislocations, *Optics Communications*, *331*, 204–218.

CURRICULUM VITAE

Name Surname: İzzet GÖKSEL

Place and Date of Birth: Şişli, 23 May 1985

E-Mail: gokseli@itu.edu.tr

EDUCATION:

- **B.Sc.:** 2009, Istanbul Technical University, Faculty of Science and Letters, Mathematical Engineering

- **B.Sc.:** 2010, Istanbul Technical University, Faculty of Electrics and Electronics, Computer Engineering

- **M.Sc.:** 2011, Istanbul Technical University, Graduate School of Science, Engineering and Technology, Mathematical Engineering

PROFESSIONAL EXPERIENCE AND REWARDS:

- 2006-2007 : Student Assistant at the Department of Mathematics at Istanbul Technical University.

- 2008-2009 : Lecture Assistant at the Department of Mathematics at Istanbul Technical University.

- 2010-2017 : Research Assistant at the Department of Mathematics at Istanbul Technical University.

- 2013-cont. : Sworn Translator in German, English and French at Istanbul Courthouse.

- 2014-cont. : Expert in Mathematical Engineering, Maths, Computer Engineering and Computer Programming at Istanbul Courthouse.

- 2016-2017 : Visiting Scholar, Lecturer, Junior Specialist at the Department of Applied Mathematics at University of California, Merced (USA).

- 2017-cont. : Engineer at the Faculty of Science and Letters at Istanbul Technical University.

- 2009 : Best graduate of Mathematical Engineering (B.Sc.) at Istanbul Technical University.

- 2011 : Best graduate of Mathematical Engineering (M.Sc.) at Istanbul Technical University.

PUBLICATIONS, PRESENTATIONS AND PATENTS ON THE THESIS:

- **Göksel, İ.**, Antar, N., Bakırtaş, İ., 2015. Solitons of (1+1)D Cubic-Quintic Nonlinear Schrödinger Equation with $\mathcal{PT}$-Symmetric Potentials, *Optics Communications*, 354, 277-285.

- **Göksel, İ.**, Bakırtaş, İ., Antar, N., 2013. Solitons of Cubic-Quintic Nonlinear Schrödinger Equation with Various External Potentials. *Nonlinear Waves–Theory and Applications*, June 12-15, 2013 Beijing, China.

- **Göksel, İ.**, Bakırtaş, İ., Antar, N., 2013. Kübik-Kuintik NLS Denkleminin Soliton Çözümleri. *XVIII. Ulusal Mekanik Kongresi*, August 26-30, 2013 Manisa, Turkey.

- **Göksel, İ.**, Antar, N., Bakırtaş, İ., 2014. Solitons of Cubic-Quintic Nonlinear Schrödinger Equation with PT-Symmetric Potentials. *International Conference on Advances in Applied Mathematics and Mathematical Physics*, August 19-21, 2014 Istanbul, Turkey.

- **Göksel, İ.**, Antar, N., Bakırtaş, İ., 2015. Vortex and Dipole Solitons in PT-Symmetric Lattices with Positive and Negative Defects. *Nonlinear Evolution Equations and Dynamical Systems 2015*, May 24-31, 2015 Cagliari, Sardinia, Italy.

- **Göksel, İ.**, Antar, N., Bakırtaş, İ., 2015. Odaklanan Kubik, Odaklanan Kuintik Ortamda PT-Simetrisine Sahip Kafesler Üzerinde NLS Denkleminin Temel Soliton Çözümleri. *XIX. Ulusal Mekanik Kongresi*, August 24-28, 2015 Trabzon, Turkey.

- **Göksel, İ.**, Bakırtaş, İ., 2015. Odaklanan Kubik, Odaktan Sapan Kuintik Ortamda PT-Simetrisine Sahip Kafesler Üzerinde NLS Denkleminin Temel Soliton Çözümleri. *XIX. Ulusal Mekanik Kongresi*, August 24-28, 2015 Trabzon, Turkey.

OTHER PUBLICATIONS, PRESENTATIONS AND PATENTS:

- **Göksel, İ.**, Bakırtaş, İ., Antar, N., 2015. Nonlinear Lattice Solitons in Saturable Media, *Applied Mathematics & Information Sciences*, 9(1), 377-385.

- Yüksel, B., Oktuğ, S., Karabulut Kurt, G., **Göksel, İ.**, 2010. An Empirical Study on The Effect of Mobility of GSM Telephone Traffic. *IEEE 21st International Symposium on Personal, Indoor and Mobile Radio Communications*, September 26-30, 2010 Istanbul, Turkey.

- **Göksel, İ.**, Bakırtaş, İ., Antar, N., 2011. Doyurulabilir Ortamlarda Doğrusal Olmayan Kafes Solitonları. *XVII. Ulusal Mekanik Kongresi*, September 05-09, 2011 Elazig, Turkey.

- **Göksel, İ.**, Bakırtaş, İ., Antar, N., 2012. Nonlinear Lattice Solitons in Saturable Media. *Nonlinear Evolution Equations and Dynamical Systems 2012*, July 08-15, 2012 Kolymbari, Crete, Greece.

- **Göksel, İ.**, 2016. Wave Solutions of the Sine-Gordon Equation. *First Annual Central Valley SIAM Regional Conference*, April 29, 2016 Merced, California, USA.